Predicting underwater noise generated by offshore piling at large distances

by

Thomas Franciscus Stijntjes

to obtain the degree of Master of Science in Offshore and Dredging Engineering
at the Delft University of Technology,
to be defended publicly on Wednesday April 25, 2018 at 14:30.

Student number: 4084721
Project duration: May 17, 2017 – April 25, 2018
Thesis committee:

Prof. dr. ir. A. Metrikine,	TU Delft, chairman
Dr. ir. A. Tsouvalas,	TU Delft
Dr. ir. F. Pisanò,	TU Delft
Ir. O. Sainz Avila,	Royal Boskalis Westminster N.V.

TU Delft Delft University of Technology

Boskalis

Abstract

The demand for renewable energy has caused a large increase in the construction of offshore wind farms. As the industry is evolving, wind generators are becoming larger and are being installed further offshore and in deeper waters. This causes the foundations of the generators to increase in size. Currently monopile foundations represent 80% of all installed foundation types in Europe and they will remain the preferred choice of substructure in the near future. The installation of these monopiles consists of an impact hammer that applies a series of blows to the top of the pile, effectively hammering the pile into the soil. Each strike results into strong impulsive noise that is emitted into the underwater environment and can be detected tens of kilometers away. Consequently, offshore pile driving has become a strictly regulated construction process, imposing limits on the sound levels.

To acquire insight in the physics of noise generation and act responsibly to mitigate the radiated sound if necessary, studies simulating the piling of the monopile are performed prior to installation. For this, various models exist. In most cases the water and soil are described as linear acoustic fluids. The acoustic representation of the water region can indeed be a reasonable approximation of reality, but the behavior of the soil is much more complex. Most of the energy introduced by the hammer enters the soil region and only a small percentage is radiated into the fluid. It is possible that energy re-radiates back into the water column via leaky interface waves that travel along the seabed-water interface. These waves can only be captured by the soil if it can support shear waves, which it cannot if it is described with an equivalent fluid approximation. To account for these aspects the modelling of the soil should be approximated by a viscoelastic medium. The model created by Tsouvalas and Metrikine uses this approximating of the soil and will be used in this study. The Elastic Medium Model in question was created as part of the PhD dissertation of Apostolos Tsouvalas.

This graduation thesis aims to investigate the possibility to use the Elastic Medium Model for accurate noise predictions for the far-field. The model was created for research purposes and focuses on the near-field, where it is very accurate. However, the model has some mathematical and computational constraints that make it unable to calculate the noise levels at locations far from the pile, where the noise level restrictions are imposed, at 750 meters from the source to be exact. The maximum distance within which the model provides time traces of the various physical quantities is about 150 meters, although this value depends on the soil properties and the location of interest.

To expand the range, linear interpolation was applied to increase the resolution of the response spectra for locations far from the pile. However, the oscillatory nature of the Hankel function is the reason why this was unsuccessful. Alternatively, it was shown that by alternate use of the model, it is possible to create accurate time traces for the far-field. At locations far from the pile the setup of the model becomes important as waves reflecting from the lower boundary appear. This is unphysical in the manner the case study was setup, but do imply that waves reflecting from soil interfaces can have an impact. It was concluded that the sound levels are mainly determined by the radiated waves traveling through the water layer and that the influence of the waves traveling through the soil is limited. The results were validated with data from the Veja Mate project, which led to the conclusion that the model can perform accurate predictions of the sound levels. Although it was shown that the Scholte wave can travel up to large distances, the contribution to the sound levels is minor. It should be noted that the attenuation factor for the shear wave in the soil is still a large unknown and further study should be done to accurately represent the soil layering and its contribution to the sound levels and their effect on marine life.

Preface

"All models are wrong, some are useful"
George Box

I found the quote above to be particularly relevant. We tend to be very confident when having a model to back-up our findings, however reality ends up defying and surprising us time and time again. Therefore, the results from models should be taken with a grain of salt. The model in this graduation study is a valuable tool, but without asking it the right question, we will not get the desired results.

I can now proudly say, that I have contributed to the understanding and the development of an acoustic model predicting underwater noise generated by offshore piling, a highly relevant topic, where still a lot has to be discovered. To help me reach this achievement I was supported by various knowledgeable, inspiring and enthusiastic mentors, namely Oscar, Apostolos and Andrei. I would like to thank each of them, starting with Oscar, who always had a moment to spare to answer my questions or think of some new solutions. I always enjoyed working with you and really appreciate your contribution to my graduation struggle. Next I would like to thank Apostolos, who I could depend on when I needed some explaining regarding his state of the art Elastic Medium Model and who pushed me to always be thorough. At last, but certainly not least, I would like to thank Andrei for guiding me and your smart comments during each meeting always kept me on my toes.

Finally, I want to acknowledge the great support I have received from my parents, girlfriend, close friends and family. I have always experienced your support and want to thank you for believing in me and trusting me. I have experienced my time studying as a great adventure and had the time of my life. I am well aware that this is mostly thanks to you.

T.F. Stijntjes
Delft, January 2013

Nomenclature

α	Plane-wave attenuation
δ	Loss tangent
λ	Wavelength
μPa	Micro Pascal(s)
ω	Angular frequency
ADD	Acoustic Deterrent Devices
$B(OH)_3$	Boric acid
BSH	Federal Maritime and Hydrographic Agency, Germany
Btu	British thermal unit
c	Sound speed
$C-PODs$	Continuous porpoise detectors
D	Depth
d	Diameter
dB	Decibel(s)
EIA	U.S. Energy Information Administration
EMM	Elastic Medium Model
EU	European Union
EUR	Euro
f	Frequency
$GRLWEAP$	Goble Rausche Liking Wave Equation Analysis Program
GW	Gigawatt
$GWEC$	Global Wind Energy Council
Hz	Hertz
I	Intensity
i	Imaginary number
IEA	International Energy Agency
$ITAP$	Institut fur Technische und Angewandte Physik
k	Wave number
kHz	Kilohertz
kJ	Kilo Joule(s)
km	Kilometer(s)
L_{peak}	Peak Sound Pressure Level
m	Meter(s)
$MgSO_4$	Magnesium sulphate
MMO	Marine Mammel Observer
MW	Megawatt
MWh	Megawatt hour(s)
Np	Nepers
Pa	Pascal(s)
re	Reference
rms	Root mean square
s	Second(s)
SEL	Sound Exposure Level
$sonar$	Sound Navigation And Ranging
SPL	Sound Pressure Level
TWh	Terawatt hour(s)

Contents

1

Introduction

This chapter will provide an introduction for this graduation thesis. It will highlight the problem, state the research question and elaborate on the structure of the report.

1.1. Problem statement

The demand for renewable energy has caused a large increase in the construction of offshore wind farms. Offshore wind energy has rapidly expanded and is playing an increasingly important role in the energy market. As the industry is evolving, wind generators are becoming larger and are being installed further offshore and in deeper waters.

This causes the foundations of the generators to increase in size. There are multiple foundations available for offshore wind generators (Byrne and Houlsby, 2003), namely: monopiles, tripods, jackets, suction caissons and gravity-based foundations. The choice for the foundation type depends on a large number of parameters such as water depth, soil conditions and the sea state at location. In general the monopile is the preferred foundation for water depths up to 50 meters (WindEurope, 2018b). The size of the monopile has been increasing as mentioned above, the largest monopiles installed to date have a diameter of 8 meters and a total length of 80 meters. The installation of such a monopile, often several tens of meters into the soil, is done by an impact hammer that is placed on the head of the pile, while it is kept in upright position. The impact hammer applies a large number of blows to the pile, causing the pile to be driven into the soil.

This process can require hundreds to thousands of strikes and severals hours to fully install one pile. Each blow produces high sound levels that propagate into the underwater sea environment. These sound levels can be detected tens of kilometers away from the construction site (Bailey et al., 2010). Numerous studies have investigated the noise emissions and their effects on marine life (Thomsen et al., 2006; Bailey et al., 2010; Damian and Merck, 2014). The extent of damage that is possible from the strong impulsive sound can vary from light behavioral disturbances to strong avoidance of the construction site and in extreme cases even permanent hearing impairment is possible. The high noise levels generated by marine piling have drawn the attention of regulatory bodies and environmental organizations in several nations. An overview of the regulations of each nation can be found in *Underwater Noise. Social Cost Benefit Analysis* (RoyalHaskoningDHV, 2015). The German Federal government adopts certain sound level criteria. These have been set to 160 $dBre1\mu Pa^2$ for the sound exposure level (SEL) and to 190 $dB1\mu Pa^2$ for the sound peak pressure level. Both these restrictions apply at 750 meters from the location of the pile.

To meet these restrictions the industry has developed a variety of noise mitigation methods to reduce the impulsive noise (Nehls et al., 2007); big bubble curtains, hydro sound dampers, noise mitigation screens and a cofferdams. The noise mitigation systems focus on blocking

the primary path of the propagation noise. This is the path where the noise radiates directly into the fluid layer. However the secondary noise path, where the noise re-radiates into the fluid layer from the soil layer, is mostly left unaffected. The mitigation methods mentioned above are expensive and can drive the price of the total installation cost of an offshore wind farm foundation. New techniques to install the monopile with less noise production are being investigated within the industry, such as Blue Piling (Fistuca, 2016), vibro-drill technology (GMBWorks, 2018) that uses vibrations at the tip of the pile for installation and screw piles that screw piles into the soil (Engineering and Physical Sciences Research Council, 2018). Unfortunately these techniques are still in early stages of development.

To be able to make accurate preparations as to what noise mitigation methods will have to be used during a installation of an offshore wind park's foundation piles, it is important to have a good understanding of the character and the level of the radiated sound. Therefore, the focus in this study is on the prediction of the noise that is generated by marine piling.

1.2. Noise prediction models

Underwater noise in deep oceans has been studied and documented thoroughly. Formidable development was achieved in this field during the second World War and the the Cold War. The reason for the thorough research was the development of powerful sonars for detecting and locating military targets and submarines. In shallow waters (depths up to 200 meters) the prediction of sound propagation is more complicated. The surface, volume and soil properties are all important, spatially varying, time varying (the oceanographic parameters) and often not known in sufficient detail and accuracy to permit long-range predictions (Jensen et al., 2011). Additionally, in shallow water, sound propagations is largely affected by multiple reflections, refractions and scattering of sound waves at the sea surface and the sea bed. Theoretically and experimentally the acoustics of shallow water have been thoroughly investigated. Yet, the accumulation of the theory and measurements has failed to give the quantitative understanding required for accurate prediction of long-range propagation in shallow water. For all the reasons mentioned, the modelling of underwater sound propagation in shallow water has always been, and still remains, quite a challenge. Further complexity is added by the addition of the monopile and the pile driving process. This creates a system that consists of three interrelated domains; the water environment, the soil region and the pile. To correctly model this situation it is important to understand all the individual components as well as the way in which they interact with each other.

The first to develop a detailed numerical model that can be used for the prediction of underwater noise produced by pile driving were Reinhall and Dahl (2011). The model was based on the finite element method for predicting the noise levels in the vicinity of the structure. For predictions at larger distances a sound propagation model was adopted. The division between near- and far-field was a necessity due to the computational restrictions imposed by the finite element model. The water and soil were described as linear acoustic fluids, were the wave speeds in the water region and the soil domain were assumed to be different. Similar models that use the same approach as Reinhall and Dahl (2011) have been created worldwide (Lippert and Lippert, 2012; Lippert et al., 2013; Zampolli et al., 2013) and are considered as the state-of-the-art for pile driving noise predictions. The acoustic representation of the water region can indeed be a reasonable approximation of reality, but the behaviour of the soil is much more complex and cannot be captured accurately by the equivalent acoustic description. First, the majority of the energy introduced by the hammer into the pile enters the soil region and only a small percentage is radiated in the form of pressure waves into the fluid. Therefore, the description of the soil should be able to account for the presence of shear waves. Second, pile driving generates waves that travel along the seabed-water interface. These waveforms cannot be captured by an equivalent fluid approximation. Third, without a proper description of the soil, the amount of energy that re-radiates back into the water column cannot be predicted accurately. To account for these three aspects the modelling of the soil should be approximated by a viscoelastic medium. The model created

by Tsouvalas and Metrikine (2014) uses this approximation of the soil and will be used in this study. The Elastic Medium Model in question was created as part of the PhD thesis of Apostolos Tsouvalas (2015).

1.3. Problem definition

This graduation thesis aims to investigate the possibility to use the Elastic Medium Model of Tsouvalas and Metrikine for accurate noise predictions in the far-field. The model was created for research purposes and focuses on the near-field, where it is very accurate. However the model has some mathematical and computational constraints that make it unable to exactly calculate the noise levels at locations far from the pile. The maximum distance within which the model provides time traces of the various physical quantities is about 150 meters, although this value depends on the soil properties and the location of interest.

The following research question was set:

"What has to be done to increase the range for which the Elastic Medium Model can predict accurate time traces of the various physical quantities?"

In order to answer the main research question, the following subquestions were set:

1. What introduces the time window limitation of the original model?
2. How can the limitation be overcome?
3. What are the main phenomena contributing to the sound levels at large distances?

This study aims to contribute to the understanding of underwater noise propagation in shallow water and to the process of developing reliable and practical prediction models.

1.4. Thesis outline

Chapter 2 provides a thorough literature study, granting insight in the prospects of offshore wind, the installation process of offshore wind generators and an introduction in ocean acoustics. Chapter 3 and 4 will elaborate on the Elastic Medium Model created by Tsouvalas and Metrikine (2014) and the system parameters of the location that will be analyzed. Chapter 5 will exist of the theoretical principles used, that form the basis of the alterations that will be made in order to extend the range of the model. Chapter 6 will be used to discuss the results and the validation of these results with the real world data that is available from the Veja Mate project. Additionally, a parametric study will be performed in chapter 7 to increase insight in the model's output and sensitivity. Finally ending with the conclusion and recommendations in chapter 8.

2

Literature study

This chapter provides a framework for this thesis. It will elaborate on various aspects related to offshore wind energy. Starting with a brief introduction on the global energy demand and production, followed by European energy statistics and trends and how offshore wind production is becoming of greater importance. Finally, there will be a short explanation of the installation process of the foundations for offshore wind generators and a brief introduction in ocean acoustics.

2.1. Energy demand

The U.S. Energy Information Administration yearly releases an International Energy Outlook (EIA, 2017). The report presents a forecast for international energy markets up to 2050. It states that world energy consumption will grow from 575 quadrillion British thermal units (Btu) in 2015 to 736 quadrillion Btu in 2040, an increase of 28%. How the world will meet this energy demand is depicted in figure 2.1, everything before 2015 is historical data and what comes after 2015 is projected data. It predicts that renewables are the world's fastest-growing energy source, with consumption increasing by an average 2.3% per year between 2015 and 2040.

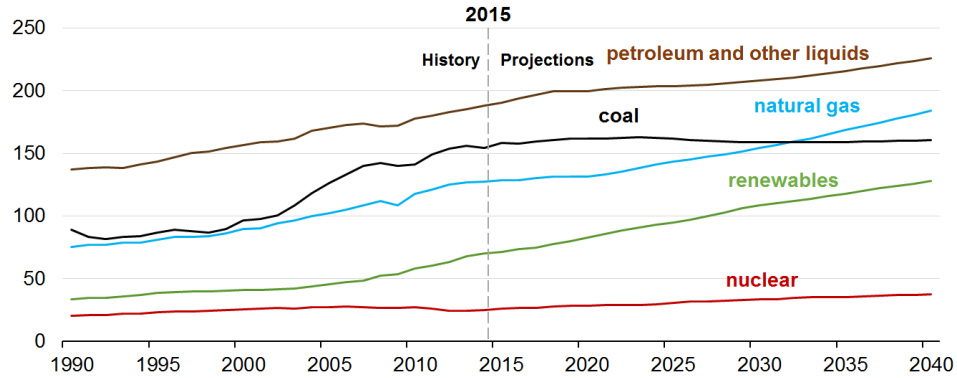

Figure 2.1: Global energy consumption by source in quadrillion Btu between 1990 and 2040 (EIA, 2017)

That the future for renewables is bright, is clear when looking at the global investments in power plants to 2040 in figure 2.2. Renewables capture two-thirds of the investments as they become the least-cost source of new generation for many countries.

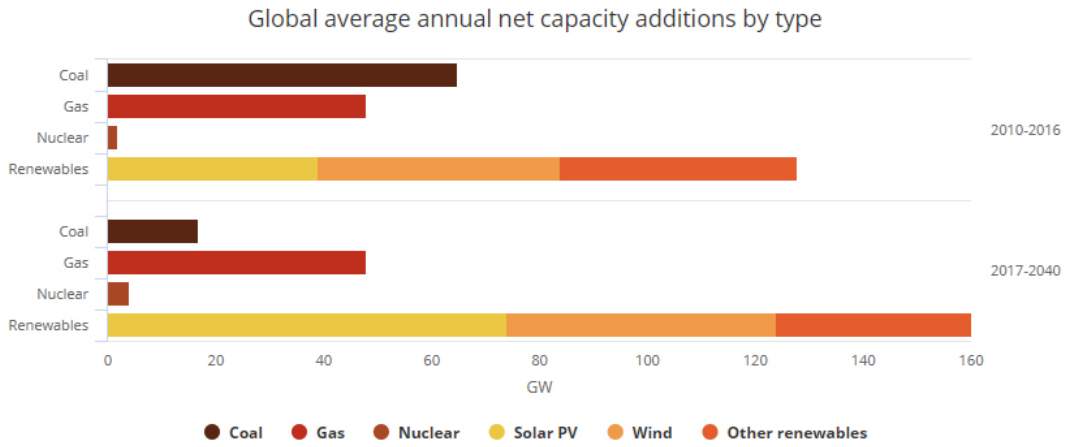

Figure 2.2: Global average annual net capacity additions by type (IEA, 2017)

Figure 2.3 illustrates that renewables are the fastest-growing source of energy for electricity generation, with average increases of 2.8%/year from 2015 to 2040. Non-hydropower renewable resources are the fastest-growing energy sources for new generation capacity. Non-hydropower renewables accounted for 7% of total world generation in 2015; their share in 2040 is 15%, with more than half of the growth coming from wind power.

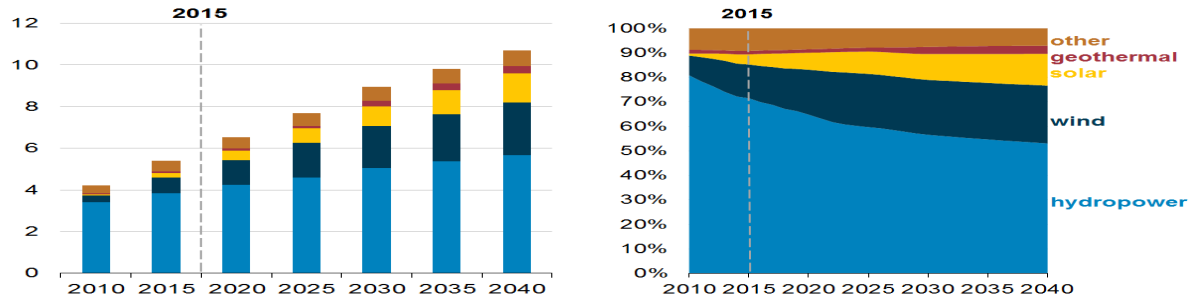

(a) trillion kilowatt hours

(b) percent share of renewable energy

Figure 2.3: World net electricity generation from renewable power (EIA, 2017)

2.1.1. Prospects Offshore Wind Power

At the end of 2016 the global installed wind capacity equaled 486.8 GW, representing cumulative market growth of more than 12 percent relative to the previous year. Overall the global wind power industry installed 54.6 GW in 2016. China remains the largest overall market for wind power since 2009, with Europe in the second spot and North America in third. Due to limitation of the available space onshore and the noise nuisance caused by wind farms operating close to residential areas, the steadily growing wind energy market has expanded towards offshore environments. Offshore wind turbines tend to generate more electricity as the wind offshore is less turbulent and flows at higher speeds than the wind onshore (Bilgili et al., 2011). The total worldwide offshore wind power capacity was 14,384 MW at the end of 2016. Although Asia, and China in particular, is the world leader in wind capacity, Europe precedes Asia in the amount of offshore wind farms. Therefore, the focus in this thesis will be on Europe.

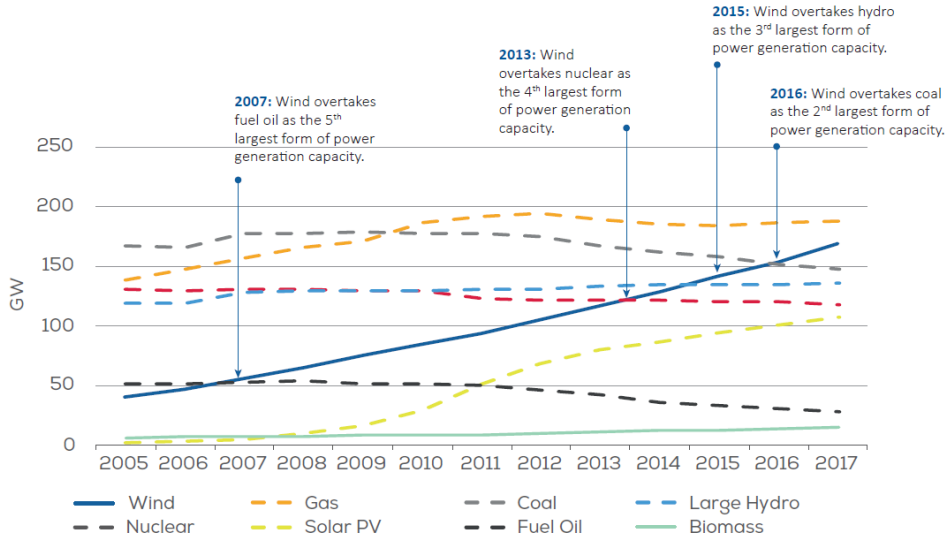

Figure 2.4: Cumulative power capacity in the European Union 2005-2017 (WindEurope, 2018a)

Figure 2.4 provides an overview of the growing contribution of wind energy to the total power capacity of Europe. With milestones in 2007, 2013, 2015 and most recently in 2016 where it overtook coal as the second largest form of power generating capacity, with a total installed of 153,7 GW. Renewable energy accounted for 85% of all new EU power installations in 2017, of which wind power accounted for 55% of the total power capacity installations. With almost 336 TWh generated in 2017, wind power covered 11.6% of the EU's electricity demand. As mentioned above Europe is leading the way in offshore wind farms, with wind energy accounting for 18 % of Europe's total installed power generation capacity in 2017, of which a total of 16.8 GW wind power capacity was installed offshore. Figure 2.5 illustrates the annual and cumulative offshore wind installations from 2000 to 2017 in Europe.

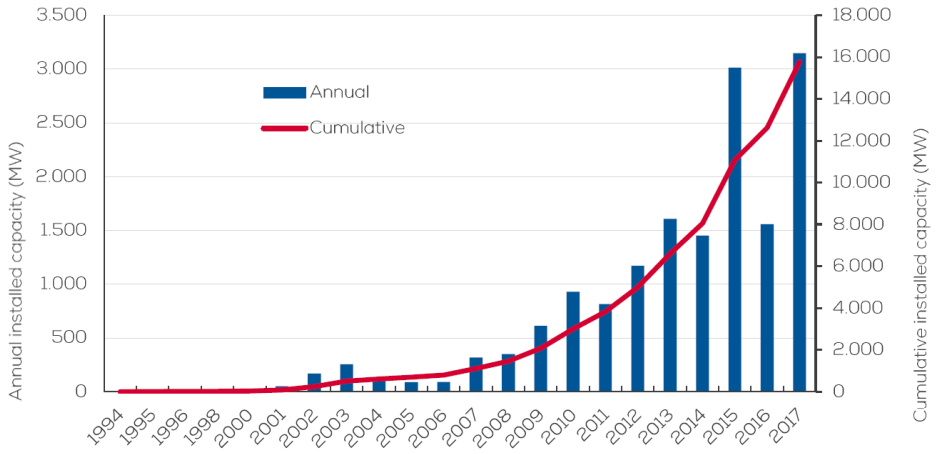

Figure 2.5: Cumulative and annual offshore wind installations 2000-2017 (WindEurope, 2018b)

While the offshore industry had set the target price of EUR 100/MWh by 2020, it was actually reached much faster. Starting in July 2016 with the Dutch tender for the 700 MW Borssele 1&2 at EUR 72.7/MWh, followed by Denmark's nearshore tender which came in at EUR 64/MWh, succeeded by the Kriegers Flak project at EUR 49.9/MWh and ending with Borssele 3&4 for another 700 MW at EUR 54.5/MWh in December of 2016. This price drop has defined the new standard in northern European offshore wind markets at well below EUR 100/MWh. It can be concluded that the industry has exceeded its 2020 targets and four years ahead

of time. A remarkable situation has arisen where offshore is competitive with onshore wind, which has resulted in large investments in offshore not only in Europe, but in Asia and North America as well. For the prospects of offshore wind in Europe, it is expected that Europe will install about 73 GW of new wind power in the period out to 2021 (GWEC, 2017).

2.1.2. Foundations for Offshore Wind Generators

To date, several foundation concepts exit in order to support an offshore wind power generator. The choice for the most appropriate concept is not straightforward. It depends on a large number of parameters such as the water depth, the soil conditions, the expected sea wave heights, the presence of currents at the location, the number of generators to be installed and the size of the power generator.

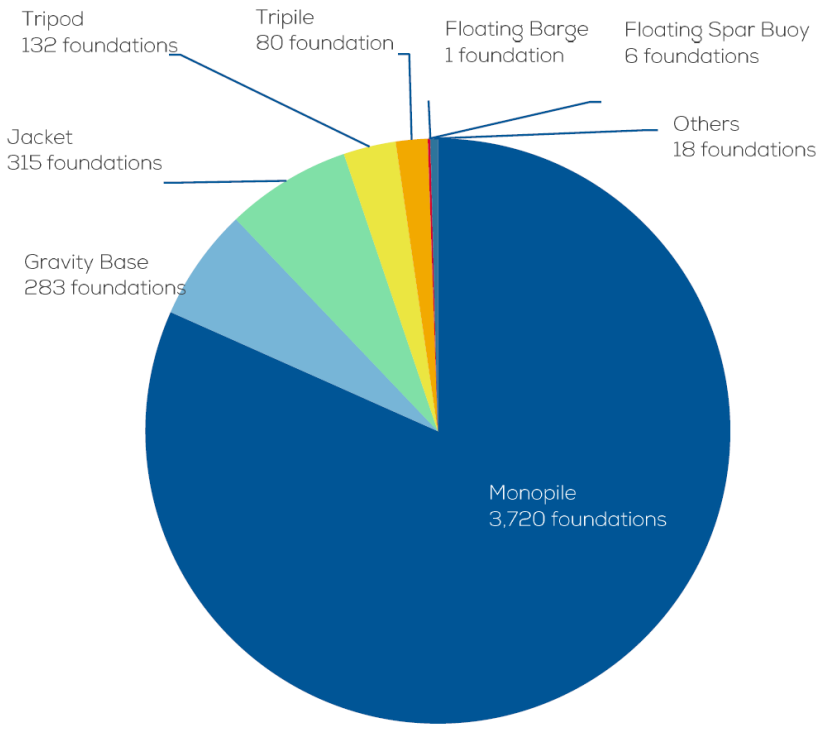

Figure 2.6: Share of substructure types for grid-connected wind turbines (units) (WindEurope, 2018b)

The various foundation types available are the monopile, tripods, tripiles, steel jackets, suction caissons, gravity based foundations and floating foundations. Despite the various foundation types available, the monopile is the most widely used and economically profitable choice for wind turbines installed in water depths up to approximately 40 meters. Figure 2.6 depicts the cumulative installed share between the various foundation concepts in 2017. Monopiles represented 81.7% of all installed substructures in Europe. Tripods (2.9%) and tripiles (1.8%) saw no additional installations although the share in jackets (6.9%) rose due to construction at Beatrice 2. Two new types of foundation were introduced: floating spar buoys and floating barges (WindEurope, 2018b).

To gain an insight in the water depth and distance to shore of wind farms, figure 2.7 is depicted below. It shows the amount of wind farms that are online, under construction, consented and with an application submitted. It becomes clear that almost all of them are within monopile applicable limits, with the main water depth limitation around 40 meters. Therefore it is reasonable to conclude that the monopile foundation will remain the governing foundation type for the near future and this will be the foundation type that will be considered in this thesis.

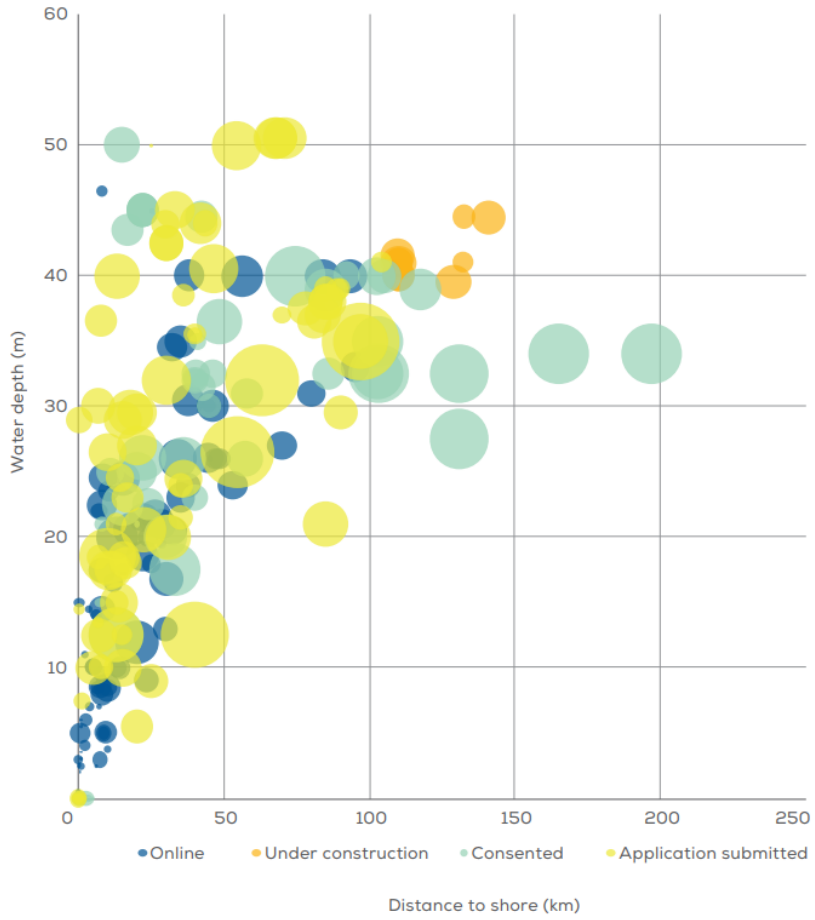

Figure 2.7: Average water depth, distance to shore and size of offshore wind farms under construction during 2016 (WindEurope, 2018b)

2.1.3. Installation process of the monopile foundation

A monopile foundation consists of several circular steel tubes that are welded together to form a single piece. The largest monopile foundations used to date reach a total length of 80 meters, a diameter of 8 meters and a wall thickness of 150 millimeters, an example of such a foundation file is depicted in figure 2.8. For the monopile to be stably installed, the pile is driven into the seabed up to half its total length. This requires tremendous amounts of input energy and special installation equipment. The most widely used installation method is by applying blows to the head of the pile using an impact hammer. This causes the pile to gradually penetrate and lower into the sediment. This process can take several hours and requires hundreds to thousands of strikes to fully install a single pile. These blows, as mentioned before in chapter 1, produce high sound levels that propagate into the underwater sea environment and can be detected tens of kilometers from the construction site. The high noise levels generated by marine piling have drawn the attention of regulatory bodies and environmental organizations in several nations. An overview of the precautions and limitations that have to be met, can be found in section 2.3.1.

Figure 2.8: One of the largest monopile in the world to be installed at Veja Mate (Erneuerbare Energien, 2016)

The sheer size of the monopile (such as depicted in figure 2.8) and the use of an impact hammer will almost certainly cause for the noise level restrictions to be exceeded. Therefore, alternative installation methods should be considered. Alternative methods include the use of a vibratory hammer, a vibro-drill, a special method of piling, namely Blue Piling or even screwing of the foundation pile.

An example of an impact hammer can be seen in figure 2.9. In the figure, the impact hammer (white and red in the picture) is placed at the top of the pile and the pile is kept in place by a special gripper (orange colored equipment in the photo).

One of the alternative methods for piling is Blue Piling technology (Fistuca, 2016). Instead of using the hydraulic impact to generate the force like the impact hammers do, it uses a water column that is lifted by feeding gas and left to fall on the anvil, by igniting the gas, to produce the impact force. The operation principle is illustrated in figure 2.10. The pile is colored yellow and the rest depicts a cross section of the hammer. The first image shows the system at rest and gas is fed into the combustion chamber. In the second image the gas is combusted and this creates the first blow, while water is forced out of the combustion chamber. Then the combustion continues while the water column continues moving upwards. The water column keeps rising until it reaches its highest point. Then the water column falls down and delivers a second blow. In the final image the exhaust gases are released through the exhaust valve. An advantage of this method is that due to the large period of time in which the main force, consisting of the falling of the water column, is transferred to the pile, much lower tensile stresses

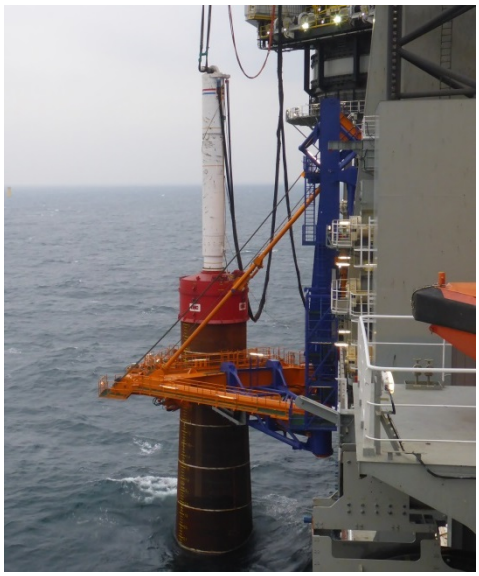

Figure 2.9: Example of an impact hammer (Allnamics, 2017)

occur in the pile material. To clarify, the duration of the force application of an impact hammer equals about 0.01s, compared to the 0.2s of the Blue Piling technology. The low tensile stress results into less fatigue and less vibrations, which in turn cause less noise production. Fistuca, the provider of this technology, claims that noise levels can be reduced by 20 dB (Sound Exposure Level, this will be further explained in section 2.2.4).

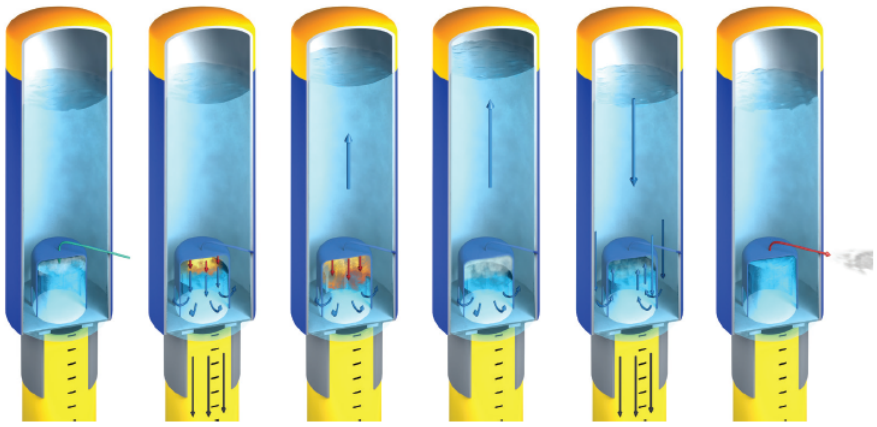

Figure 2.10: Operation cycle of a Blue piling hammer (Fistuca, 2016)

Another alternative for monopile installation is by using a vibratory hammer. This installation technique is based on a different principle than the impact hammer techniques described above. Instead of overcoming the soil resistance with each blow, the vibratory hammer eliminates the resistance of the soil by applying vibrations to the top of the pile. These vibrations cause the pile to vibrate and this in turn causes the soil to loosen, making it possible for the pile to penetrate the soil. An example of such a vibratory hammer is shown in figure 2.11. The vibrating mechanism of the hammer consists of rotating eccentric weights, powered by hydraulic motors. The eccentric weights rotate in direction counter to one another to cancel out the horizontal vibrations, causing only the vertical vibrations to transmit into the pile. As shown in figure 2.11 the vibratory hammer is clamped to the top of the pile. This makes the handling of the pile more efficient, resulting in time and cost reduction (Saleem, 2011). This installation technique, although continuous, produces lower sound peak levels and its effects on fauna are largely unexplored. However, as there is no possibility to perform a static pile capacity test at the final end of installation, because no resistance threshold is overcome, there is uncertainty and speculation in the industry about whether the bearing capacity (the capacity of the soil to support the loads, especially the lateral loads in case of a offshore wind generator) of the pile is met.

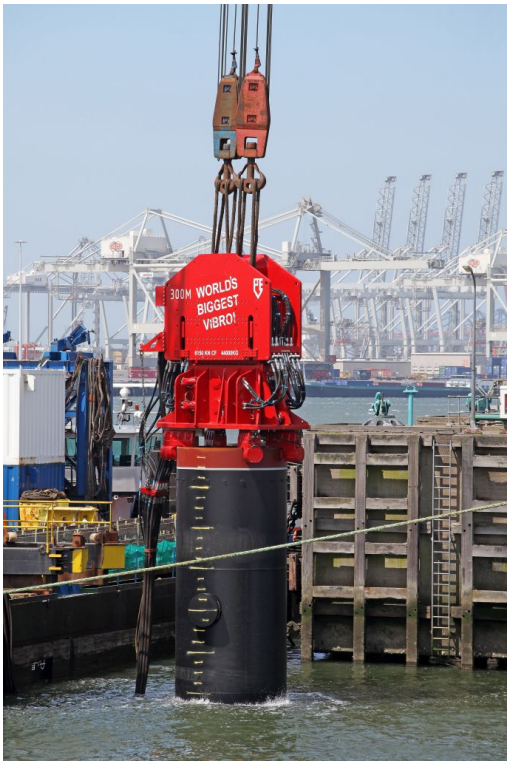

Figure 2.11: Example of a vibratory hammer (ICE, 2018)

Recently a student graduating at the TU Delft researched an innovative new technology for installing monopiles, besides starting a company to continue developing this new technique and it even won the Philips Innovation Award 2017. The technology is based on the same principle technique of the vibratory hammers with the main difference that the vibrating mechanism is not applied at the top of the pile but at the base of the pile, at its tip. Additionally, water is ejected from the bottom of the pile directed upward along the outside to lubricate and liquefy the soil, in order to reduce the soil resistance. For an illustration of the working principle, see figure 2.12 below. The various eccentric vibrating tips are depicted and are installed at the top along the rim of the pile. Unfortunately it will not be possible to retrieve the installation mechanism after installation. However, GBMWorks claims that the total installation costs will be less than the traditional installation methods. The installation technique won't require the piles to be as thick, as the monopile will not endure the fatigue caused by the high impact forces during installation and there will be no need for expensive mitigation methods to reduce the emitted underwater noise. GBMWorks has completed testing in the summer of 2017, when it installed a small pile with one drill head. The results were promising and the company will continue to develop the technology with the aim of bringing it to market and installing their first monopile in 2020.

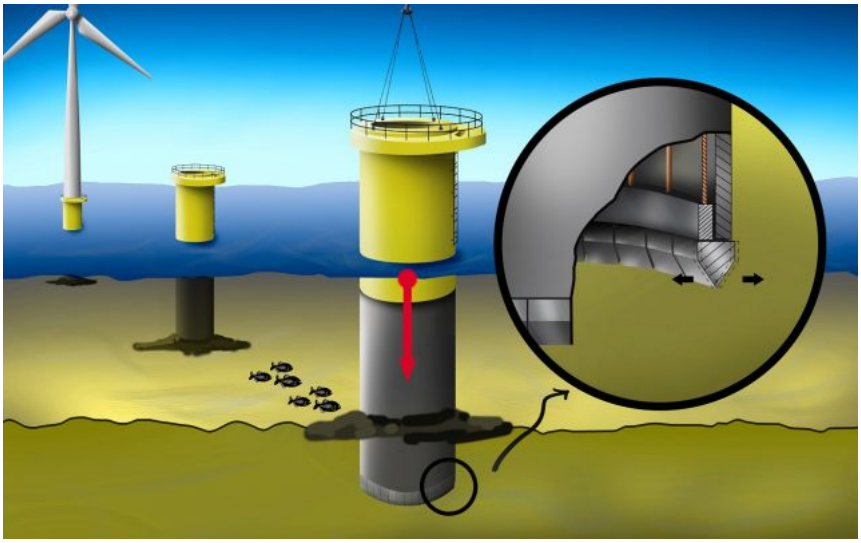

Figure 2.12: Vibro-dill technology (GMBWorks, 2018)

The final installation method to be discussed is the screwing of foundation piles. Screw (or helical) piles are foundations which are screwed into the ground. They are widely used onshore for supporting motorway signs and gantries. In order to install screw piles torque devices are used to effectively screw the anchors into the ground. The Engineering and Physical Sciences Research Council (2018) has started a project that aims to make screw piles a more attractive foundation option for offshore wind farms. To meet offshore demands, screw piles will require geometry enhancement but it is envisaged that these will initially be modest. This will lead to the deployment of several smaller piles or pile groups rather than moving straight to very large single screw piles that may prove difficult to install, using several smaller geometry foundations could reduce the risks during offshore installation and actually be more economic due to lower fabrication costs and demands on installation plant.

At the moment impact hammers are still the preferred installation method, because of their successful track record and that the alternative installation techniques still need more research and testing before becoming a feasible alternative installation technique. Therefore, in this graduation thesis the focus will use the impact hammer as installation technique.

2.2. Ocean Acoustics

Acoustics was originally the study of small pressure waves in air which can be detected by the human ear: sound. The scope of acoustics has been extended to higher and lower frequencies: ultrasound and infrasound. Structural vibrations are now often included in acoustics (Rienstra and Hirschberg, 2017). An impressive list of physicist and mathematicians like Galileo, Newton and Rayleigh have made major contributions to the theory of acoustics in gases, liquids and solids. Newton is normally credited with the first theoretical attempt to describe sound propagation in fluids. Ocean acoustics encompasses the science of sound in the sea as well as the masking of sound by interfering acoustic phenomena. Its origin dates back centuries with Leonardo da Vinci who noted that sound travels to great distances in the sea. It is still believed that sound is the only way to propagate signals to great distances in the sea (Jensen et al., 2011).

2.2.1. Shallow water

The acoustics of shallow water have been thoroughly investigated both theoretically and experimentally. Yet, the accumulation of theory and measurements has failed to produce the quantitative understanding required for accurate prediction of long-range propagation in shallow water, the reason being the complexity of the problem (Jensen et al., 2011).

The ocean is an acoustic waveguide limited above by the sea surface and below by the seabed. For shallow water, the principal characteristic of propagation is that the sound-speed profile is downward refracting or nearly constant over depth, meaning that long range propagation takes place exclusively via bottom-interacting paths. Hence the important ray paths are either refracted bottom-reflected or surface-reflected bottom-reflected. A ray picture of propagation in a 100 meter deep shallow water duct is shown figure 2.13. The sound-speed profile is typical of the Mediterranean in the summer. There is a warm surface layer causing downward refraction and hence repeated bottom interaction for all ray paths. Since the seabed is a lossy boundary, propagation in shallow water is dominated by bottom reflection loss at low and intermediate frequencies (<1 kHz) and scattering losses at high frequencies.

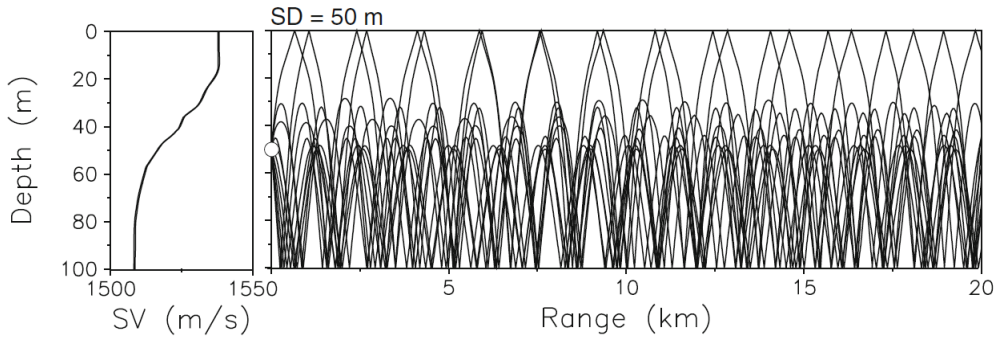

Figure 2.13: Shallow-water propagation for a source at mid-depth (50m), sound velocity profile on the left and ray paths propagation on the right (Jensen et al., 2011)

Figure 2.14 (on the next page) gives an example of transmission-loss variability in shallow water (Fizell, 1987). It displays a collection of experimental data from different shallow- water areas (from 100 to 200 meters deep) all over the world. The data refer to downward-refracting summer conditions in the frequency band 0.5-1.5 kHz. Two features are of immediate interest, one is the spread of the data amounting to around 50 dB at 100 km and caused primary by the varying bottom-loss conditions in different areas of the world. The second feature is the fact that transmission is generally better than free-field propagation ($20logr$, this means that the propagation is not reflected by anything and can spread freely) at short and intermediate ranges but worse at longer ranges. This peculiarity is due to the trapping of energy in the shallow-water duct, which improves transmission at shorter ranges, but, at the same time, causes increased boundary interaction, which degrades transmission at longer ranges.

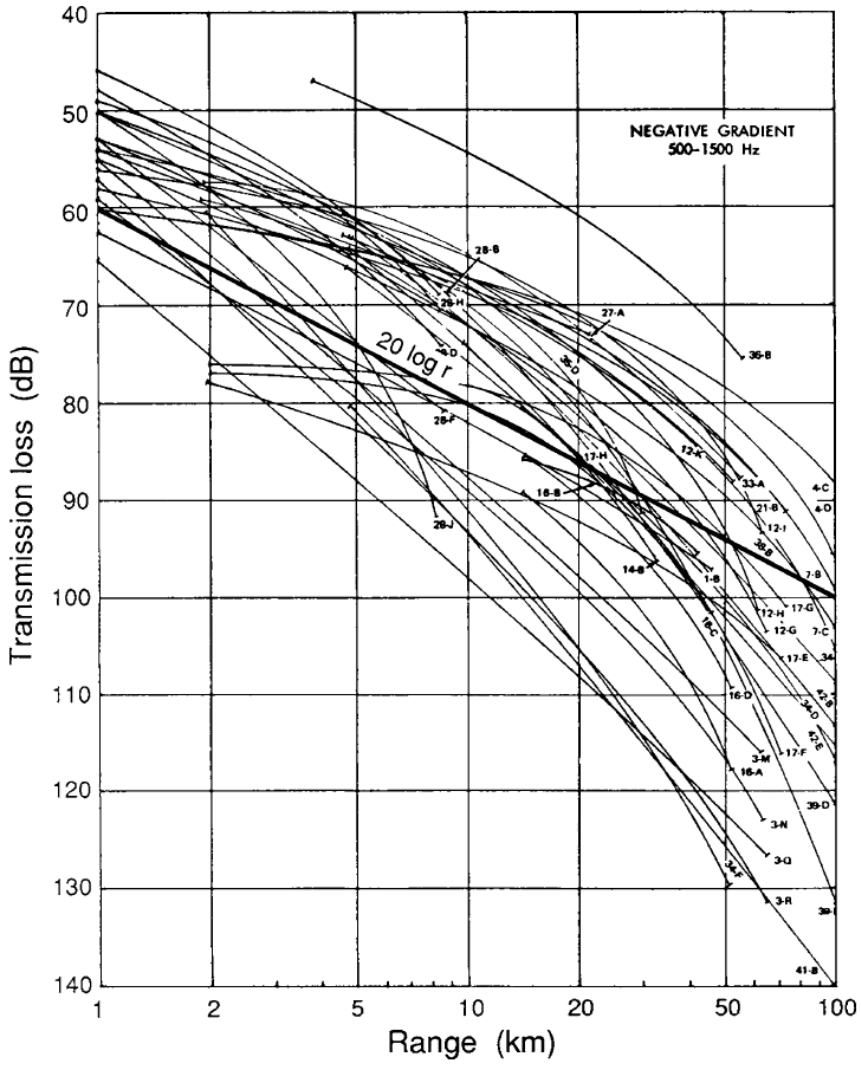

Figure 2.14: Transmission-loss variability in shallow water (Fizell, 1987)

A common feature of all acoustic ducts is the existence of a low-frequency cutoff. This is a critical frequency below which the shallow-water channel ceases to act as a waveguide, causing energy radiated by the source to propagate directly into the soil. This cutoff phenomenon can be calculated with the following formula,

$$f_o = \frac{c_w}{4D\sqrt{1-(c_w/c_b)^2}} \tag{2.1}$$

This expression is exact only for a homogeneous water column with depth D and sound speed c_w overlying a homogeneous bottom with sound speed c_b. Note that for a rigid bottom ($c_b \to \infty$) the cutoff occurs when $D = \lambda/4$, where λ is the acoustic wavelength. For physical realistic bottom speeds, the cutoff frequency is somewhat higher that for a rigid bottom. As an example, let us take $D = 100m$, $c_w = 1500m/s$, and $c_b = 1600m/s$ (sand-silt), which yields $f_0 \simeq 11Hz$ versus 3.75 Hz for a rigid bottom.

Summarizing, the bottom interaction is in general unimportant for large ranges, high frequencies and deep water. However in the case of shallow water, short-range or low frequency a correct treatment of the bottom as a viscoelastic medium is crucial. All of these three aspects apply to the case of predicting the noise levels produced during offshore piling, making the correct modeling of the soil of huge importance.

2.2.2. Wave types

When sound interacts with the seafloor, the structure of the ocean bottom becomes important. Ocean bottom sediments are often modeled as fluids which means that they support only one type of sound wave; a compressional wave. This is often a good approximation since the stiffness of the sediment is usually considerably less than that of a solid. It is well-established that shear rigidity of the ocean bottom affects the propagation of waterborne sound through the coupling of acoustic energy into shear waves. This coupling mechanism is of particular importance in low-frequency shallow-water acoustics, where the excitation of shear waves in the bottom often becomes the dominant loss mechanism for waterborne sound. For such cases the fluid approximation will not suffice and the ocean bottom has to be modeled as a viscoelastic solid described by compressional and shear-wave velocities, the attenuation factors associated with these waves and the material density.

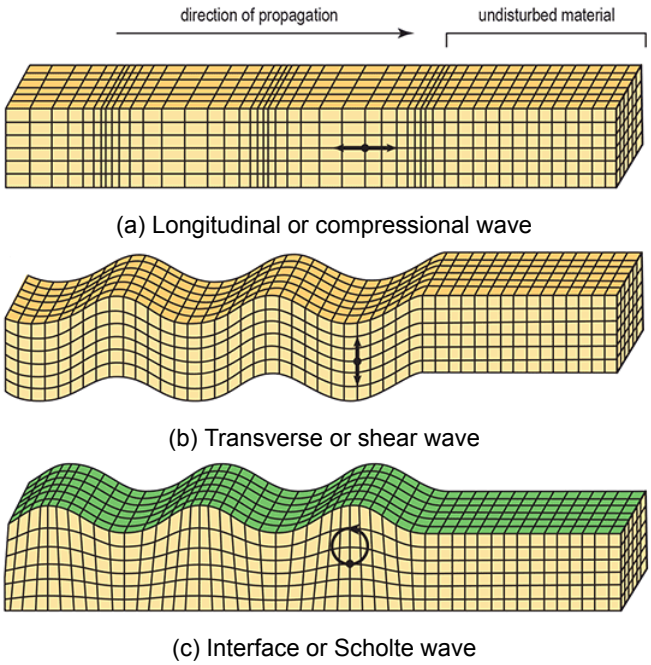

Figure 2.15: Different propagating waves (Peterie et al., 2014)

Figure 2.15 illustrates the different types of waves. The longitudinal or compressional waves (2.15a) propagate parallel to the direction of energy transfer. The longitudinal motion of the particles cause regions of compression and expansion. At the compression regions high pressures occur and low pressures can be found at the expansion regions. The longitudinal waves are able to propagate through gases, fluids and solids as the energy travels through the atomic structure. The transverse or shear waves oscillate perpendicular to the direction of energy transfer. During their propagation, every element of the medium experiences shear stress. To be able to experience shear the medium has to be a solid, as a result shear waves cannot propagate in gases and fluids. The last wave of importance is the interface wave. The interface wave is a guided wave propagating along the interface between two media with different shear speeds. The wave is generally given different names according to the media properties involved. When propagating along a fluid-solid interface it is called a Scholte wave. The wave propagates along the seafloor with exponentially decaying amplitude away from the guiding interface, with the particle motion being elliptical in the depth-range plane.

2.2.3. Sound Attenuation

When sound propagates in the ocean, part of the acoustic energy is continuously absorbed, i.e. the energy is transformed into heat. Furthermore, sound is scattered by different kinds of inhomogeneities, also resulting in a decay of sound intensity with range. These phenomena

are referred to as attenuation. Plane-wave attenuation α, which is the quantity used in the theoretical equations of acoustics, is defined from a decay-law-type differential equation 2.2,

$$\frac{dA}{dx} = -\alpha A \Longrightarrow A = A_0 exp(-\alpha x) \tag{2.2}$$

where A_0 is the *rms* amplitude at $x = 0$. The unit of α is Np/m and x is in meters. For example, a plane wave in free space with sound speed c, angular frequency ω and wave number $k = \omega/c$, that undergoes attenuation has the following form:

$$exp(ikx - \alpha x) = exp[ikx(1 + i\delta] \tag{2.3}$$

where δ is called the *loss tangent.* The plane-wave attenuation α' is often expressed as a loss in decibels per unit distance,

$$Loss = -20log\frac{A}{A_0} \simeq 8.686\alpha x \Longrightarrow \alpha' \simeq 8.686\alpha \tag{2.4}$$

where α' is in dB/m (if x is in meters). Implicit in this treatment is that attenuation is linear with frequency (which is not always the case but can be appropriately addressed - see the discussion below on attenuation is seawater). The attenuation can also be expressed as a function of frequency denoted here as $\alpha^{(f)}$ in units $dB/(mkHz)$. Equation 2.4 becomes,

$$\alpha^{(f)} \simeq 8686\frac{\alpha}{f} \tag{2.5}$$

Alternatively, attenuation can be expressed as a function of wavelength denoted as $\alpha^{(\lambda)}$ in units $dB/wavelength$. For this quantity, the ratio of the intensities in dB between points one wavelength λ apart is required,

$$\alpha^{(\lambda)} = -10log\frac{I(x+\lambda)}{I(x)} = -20log\frac{e^{-\alpha(x+\lambda)}}{e^{\alpha x}} = \alpha\lambda 20loge \tag{2.6}$$

which implies,

$$\alpha^{(\lambda)} \simeq 8.686\alpha\lambda \simeq 54.58\lambda \tag{2.7}$$

The frequency dependence of attenuation can be roughly divided into four regimes of different physical origin as displayed in figure 2.16. The lowest frequency regime, region I, is still not completely understood but it is conjectured that it is related to low-frequency propagation-duct cutoff, or in other words leakage out of the deep sound channel. Unfortunately this region is exactly the region where the main underwater noise is generated by offshore piling. The main mechanisms associated with regions II and III are chemical relaxations of boric acid $B(OH)_3$ and magnesium sulphate $MgSO_4$, respectively. Region IV is dominated by the shear and bulk viscosity associated with salt water (AA'). For reference, also the viscous loss associated with fresh water is shown as curve BB' in figure 2.16.

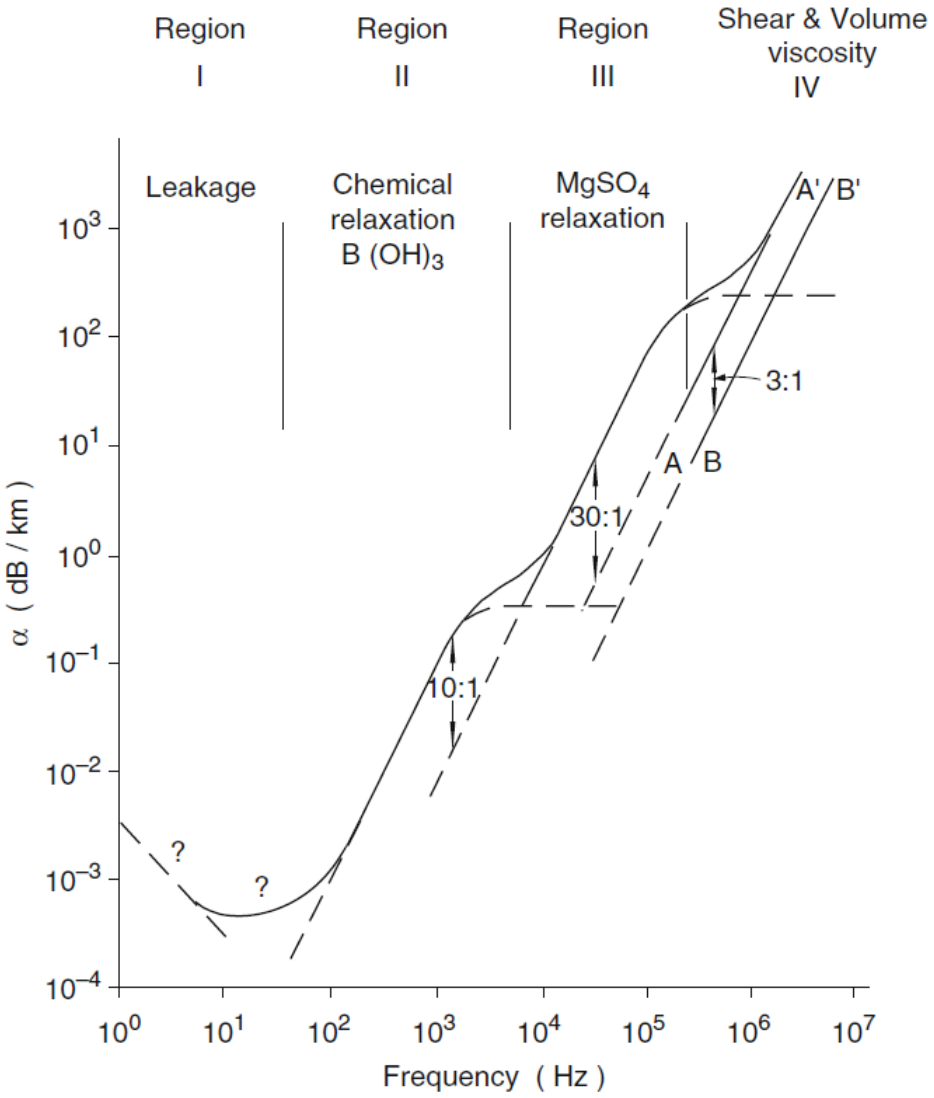

Figure 2.16: Regions of the different dominant processes of attenuation of sound in seawater (Fizell, 1987)

A simplified expression for the frequency dependence (f in kHz) of the attenuation is (Fizell, 1987),

$$\alpha' \simeq 3.3 \times 10^{-3} + \frac{0.11 f^2}{1+f^2} + \frac{44 f^2}{4100+f^2} + 3.0 \times 10^{-4} f^2 \qquad [dB/km] \tag{2.8}$$

with the four terms sequentially associated with regions I-IV of figure 2.16. In summary, from equation 2.8 the attenuation of low-frequency sound in seawater is very small. For instance at 100 Hz a tenfold reduction in sound intensity (-10 dB) occurs over a distance of around $2200km$. Even tough attenuation increases with frequency, no other kind of radiation can compete with sound waves for long-range propagation in the ocean. For example electromagnetic waves, including those radiated by powerful lasers, are absorbed almost completely within distances of a few hundred meters.

2.2.4. Sound notation

Sound levels and other acoustic parameters vary over a wide range, therefore the values relating to sound are measured in a logarithmic unit, namely decibels (dB). A decibel is a ratio of intensities. For example, two intensities I_1 and I_2 have a ratio in decibels of $10log(I_1/I_2)dB$. Ratios can only be calculated in relation to a reference pressure. This reference pressure is

usually different for water and air. The presently accepted benchmark for water, chosen by the US Navy in 1970, reference intensity is the intensity of a plane wave having a rms pressure equal to 10^{-6} pascals (Pa) or 1 μPa. Sound caused by pile driving are non-continuous sounds that are characterized by short bursts of acoustic energy of finite duration. The definitions most commonly used for such non-continuous sounds are Sound Pressure Level (SPL), Single Pulse Sound Exposure Level (SEL), Peak Sound Pressure Level (L_{peak}) and Peak-to-Peak Sound Pressure Level ($L_{peak-to-peak}$) (Robinson et al., 2014). The definitions are listed below.

Sound Pressure Level

This is used for both continuous as non-continuous sound. Acoustic pressure readings vary above and below a mean value with time. To allow for this variation, the Sound Pressure Level is averaged over a specified period of time.

$$SPL = 20log_{10}\left(\frac{p_{rms}}{10^{-6}}\right) \qquad [dB\ re\ \mu Pa] \tag{2.9}$$

Sound Exposure Level

This is a logarithmic measure of the sound exposure of a sound relative to a reference value over a finite time period.

$$SEL = 10log_{10}\left(\frac{1}{t_0}\int_{t_1}^{t_2}\frac{p^2}{10^{-12}}\right) \qquad [dB\ re\ \mu Pa^2 s] \tag{2.10}$$

This eventually results in the energy content of a pulse. The time duration of the pulse is commonly defined as the time occupied by the central portion of the pulse, where 90% of the pulse energy reside. This makes it easy to state the start and end of a pulse.

Peak Sound Pressure Level

The peak sound pressure level is the maximum sound pressure during a stated time interval. A peak sound pressure arises from a positive or negative sound pressure.

$$L_{peak} = 20log_{10}\left(\frac{p_{peak}}{10^{-6}}\right) \qquad [dB\ re\ \mu Pa] \tag{2.11}$$

Peak-to-Peak Sound Pressure Level

The sum of the peak compressional pressure and the peak expansion pressure during a stated time interval is calculated by the following equation:

$$L_{peak-to-peak} = 20log_{10}\left(\frac{p_{peak-to-peak}}{10^{-6}}\right) \qquad [dB\ re\ \mu Pa] \tag{2.12}$$

The use of peak levels of pulsed sound waves is somewhat controversial because decibels were originally used for quantities that may be related to the time-averaged power. However, the usage has now become common practice.

2.3. Underwater Noise

The difference between sound and noise is that noise is unwanted or unpleasant sound. The classification of sound as noise is therefore highly subjective. People are able to indicate whether sound is experienced as noise, however to specify what is experienced as noise by marine life is very difficult.

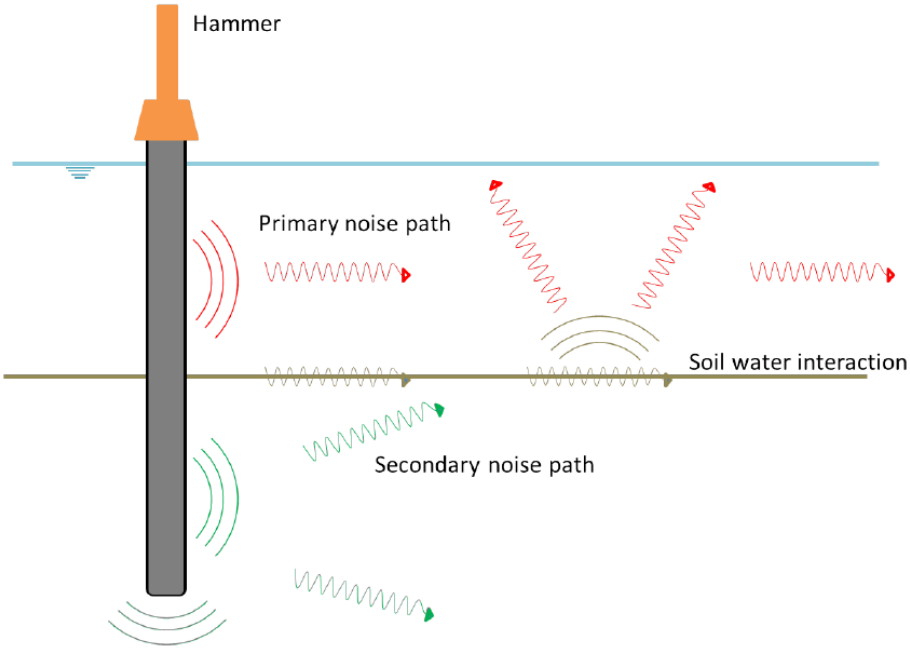

Figure 2.17: Ray paths, propagating in the underwater environment during offshore piling (Van Rhijn, 2017)

To gain insight in the sound radiated due to offshore piling, figure 2.17 displays the different ray paths that are emitted. The first significant noise path is the one radiating from the pile surface, that is caused by the compressing and expanding waves that travel down the pile causing it to vibrate. The submerged parts of the pile efficiently radiate sound into the water, resulting in a high contribution of the noise level. The second noise path is caused by the elastic waves traveling down the pile and interacting with the soil, introducing lateral waves in the seabed. These travel as compressional and shear waves through the soil, as mentioned in section 2.2.2. Soil has a higher damping factor than water, causing the high frequencies to be damped in the soil. Thus, the secondary noise path consists of mainly low frequency waves. Lastly, the interface waves, Scholte waves as discussed previously, represent the final noise path. These waves travel along the interface of the seabed and the water and leak vibrations into the water layer. As monopiles are increasing in size, their natural frequencies shift towards the lower frequencies, resulting in the fact that the secondary noise path and the leakage caused by the Scholte wave become of greater importance and their contribution to the noise levels will increase.

2.3.1. International regulations

The high noise levels generated by marine piling have naturally drawn the attention of regulatory bodies and environmental organizations in several nations. Regulations on underwater noise mitigation differ greatly between the countries bordering the North Sea and the Baltic Sea. The countries in question, Germany, the United Kingdom, the Netherlands, Belgium, Denmark, France, Sweden, Poland and Norway. Standard regulations include the use of Acoustic Deterrent Devices (ADD) and a soft start, which consist of a first blow with a lower amount of energy being used to repel marine life in the vicinity of the construction site.

The Netherlands

The Netherlands imposes sound level restrictions that vary between 164 to 175 $dB\ re\ 1\ \mu Pa^2$, depending on the season and the amount of piles to be installed. The seasonal variance is mainly due to the breeding season of the harbor porpoise, as it is considered to be the most sensitive species.

Germany

The Federal Maritime and Hydrographic Agency (BSH) has assigned the regulations in Germany. These state that the involved parties must do everything within their power to generate as less noise as possible. The noise thresholds are set to a maximum SEL of 160 $dB\ re\ 1\ \mu Pa^2$ and a peak level at 190 $dB\ re\ 1\ \mu Pas$ at 750 meters from the piling location. The noise levels must be measured within the lower one-third of the water column and the parties must use one or more noise mitigation systems to decrease the sound levels when necessary. Additionally, continuous porpoise detectors (C-PODs) are used to detect their presence

The United Kingdom

In the United Kingdom the focus is on the detection of marine life. A separate environmental assessment is required per project and the attendance of trained marine mammal observers (MMO) is required, that use visual inspections and passive acoustic detection devices. When a mammal is detected in the proximity of the construction site the installation ceases. Seasonal restrictions based on fish breeding seasons also apply.

Belgium, Denmark, France, Norway, Sweden and Poland

Belgium and Denmark impose noise threshold levels, like Germany. In France, no piling of offshore wind farms is allowed and furthermore, Norway, Sweden and Poland do not dictate any limitations or regulations. The general belief is that countries will tend to impose noise threshold in the future following the example of Germany who set the strictest limitations.

3

Elastic Medium Model

In this chapter the Elastic Medium Model, created by Tsouvalas and Metrikine (2014), will be introduced. The propagation of mechanical disturbances in layered acousto-elastic media is addressed using the normal mode method. This approach is common when taking into account wave propagation in acoustics. Another method is by using the wavenumber integration approach which is not dependent on the pole contributions being dominant. However, the modal methods are generally preferred because of their robustness and computational efficiency (Jensen et al., 2011). The normal mode method involves solving a depth-dependent equation that has a set of modes of vibration of the shell structure. The frequencies of these vibrations produce the horizontal wave numbers which are finally associated with the modal propagation. The complete acoustic field is then constructed by summing up the various contributions of each of the modes weighted in accordance to the source depth.

The Elastic Medium Model describes the soil as a three-dimensional elastic continuum that is terminated at a convenient depth with a rigid boundary. The total system including pile, fluid and elastic medium is shown in figure 3.1.

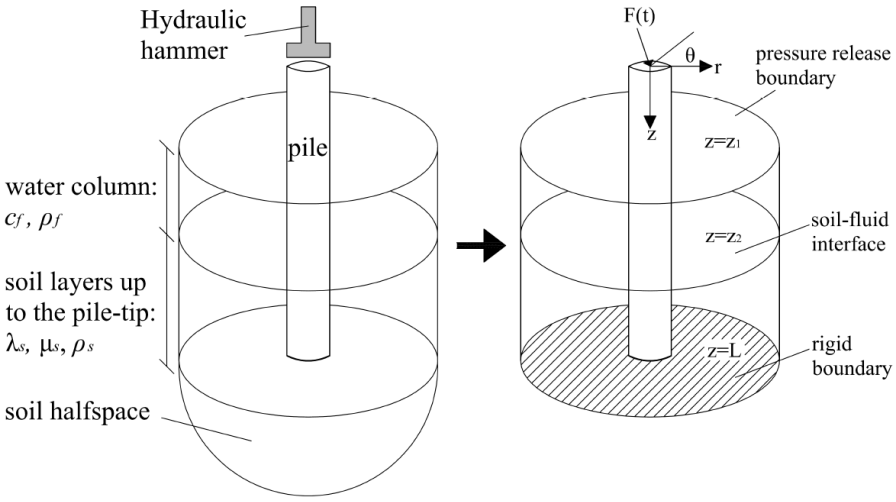

Figure 3.1: Geometry of the model (Tsouvalas, 2015)

3.1. Model interface

The interface of the Elastic Medium Model exists of an excel file, depicted in figure 3.2. The excel file is divided in eight partitions, that all describe a main component of the model. Each partition will be discussed separately.

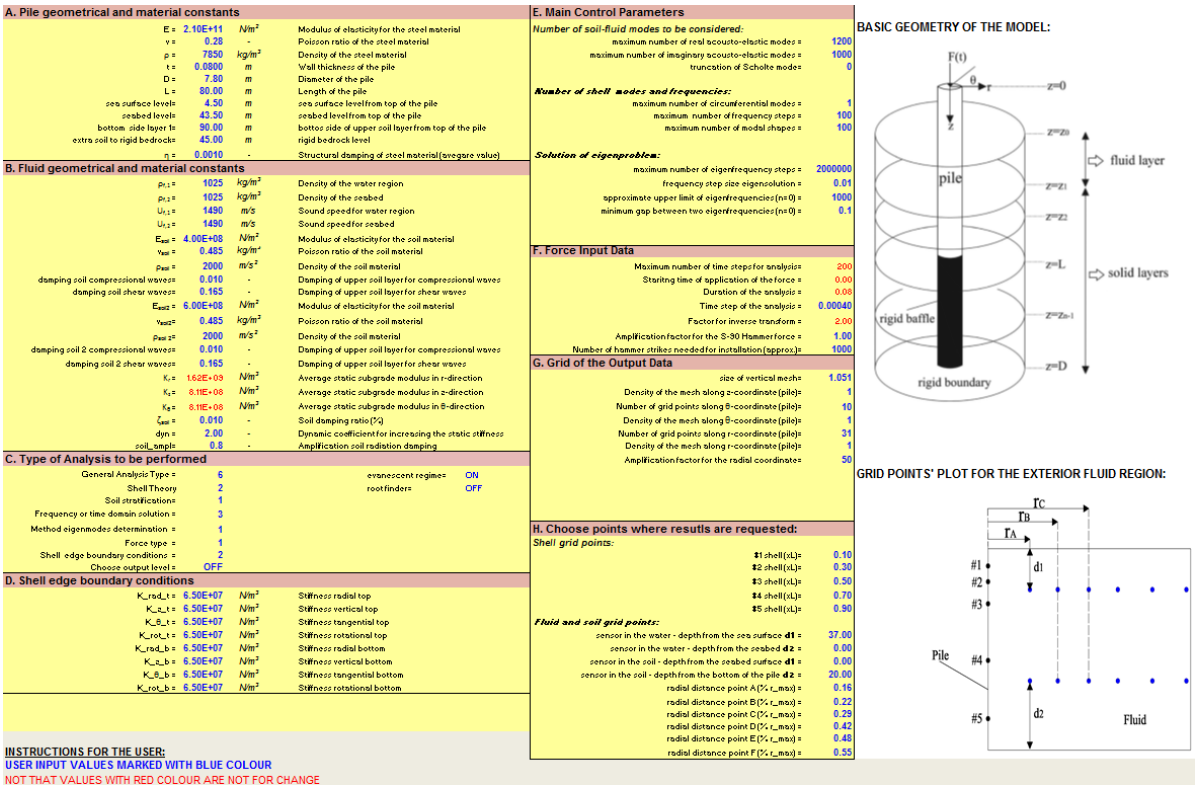

Figure 3.2: Interface of the Elastic Medium Model

A. Pile

The first partition describes the main characteristics of the pile. The pile geometry along with how the pile is positioned with regards to the different fluid and soil layers is inserted. The extra soil is added below the tip of the pile up to a rigid boundary to incorporate the propagation of waves in all directions.

B. Fluid & Soil

This partition accounts for the fluid and soil properties. The fluid properties are reasonably straightforward as the characteristics of sea water are well-known. The soil properties need more attention. The modulus of elasticity, Poisson ratio, density, compressional wave and shear wave damping have to be inserted. The first three can be obtained from basic soil data, while the later two need some work. The modulus of elasticity, the Poisson ratio and the density determine the compressional and shear wave speed, with these quantities, the attenuation factors are derived as described in Buckingham (2005).

C. Analysis

In this partition, the analysis is specified. The model can run seven different sections of the total model. The options are stated below,

1. Eigenproblem of the shell
2. Eigenproblem of the soil-fluid region
3. Force response of the coupled system

4. Eigenproblem of the soil-fluid region + forced response of the coupled system
5. Forced response of the in-vacuo shell
6. Eigenproblem of the shell + eigenproblem of the soil-fluid region + forced response of the coupled system
7. Calculation of the plots and results at the output coordinates

This has the advantage that, when changing some parameters, not the entire model has to run again. When for instance, one would like to change the number of force and/or frequency steps, function 3 can be selected. Changing the coordinates of the output points only requires to run the model with function 7 selected. To run the entire model by default function 6 has to be selected. Furthermore, the model offers the possibility to select multiple different hammer types and force diagrams in this partition.

D. Main Control

The most important properties in this section are the amount of modal shapes and frequency steps. Choosing to little steps will result in an incomplete analysis but choosing it too high would result in a very long computations. Accordingly, it is important to choose the maximum number of frequency steps in correspondence with the associated modes. By taking the maximum mode, which corresponds with twice the maximum number of frequency steps, this problem is covered.

E. Force

The amount of frequency steps selected in previous partition determines the time the model is able to analyze. This is due to the application of the Discrete Fourier Transform. As a result, a fixed frequency-time relation is introduced (for more on this phenomenon see chapter 5).

F. Grid

This section defines the grid size of the analysis. The density in the vertical, radial and angular direction has to be inserted. The mesh determines the accuracy of the model, for each analysis a trade-off between accuracy and computational time has to be made.

G. Output points

In the last partition the coordinates of the output points are defined. These are the points for which the specific output data will be calculated and exported. There are five points that are located on the edge of the pile and twelve points are located in both the fluid layer as the soil layer. This is clearly depicted in the right bottom part of figure 3.2. The radial distance for the points located in the fluid and soil layers can be calculated with equation 3.1.

$$r = R_{hell} + \beta(\alpha \cdot r_{max} - 1) \tag{3.1}$$

3.2. Layered media

In this section an elaboration on the characteristics of the shallow water environment and the solution method of the Elastic Medium Model will be described. The case of offshore installation of a monopile is quite a special one. The science of ocean acoustics, as mentioned before, is well documented and has been around for centuries, however shallow water acoustics still have quite some challenges and when introducing a mechanical disturbance, like the installation of a monopile by hammering, the circumstances become rather complex. This makes the modeling of underwater sound propagation in such cases somewhat unique with respect to the available literature of underwater acoustics.

The propagation of mechanical disturbances in layered acousto-elastic media is addressed using modal methods. Modal methods are often applied in the solution of problems related to wave propagation in acoustic or acousto-elastic waveguides ((Jensen et al., 2011)). They are preferred over wavenumber integration techniques mainly because of their robustness

and computational efficiency. Waveguides are characterized by two closely spaced surfaces in one of the principal directions, see figure 3.3. Here a simple discrete model of the ocean environment is shown. It consists of a layered waveguide with plane, parallel interfaces and with each layer assumed to be homogeneous. Although simplified, such a model is reasonable for modeling propagation in many ocean-acoustic scenarios. Further, the fact that solutions can be obtained in terms of basic physical components makes the horizontally stratified ocean model attractive in terms of physical understanding of the underlying propagation mechanism.

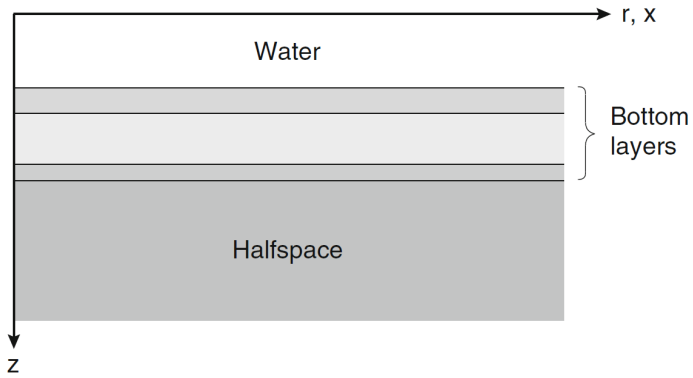

Figure 3.3: Example of a waveguide

The energy, once released in such systems, is guided through multiple reflections at the upper and lower boundaries parallel of the two surfaces. A solution to the system of equations, describing propagation of mechanical disturbances in waveguides, requires the simultaneous satisfaction of a system of equations of motion together with a number of boundary and interface conditions. It is well-known that a non-trivial solution exists for discrete values of the wavenumber k, which being a function of the excitation frequency ω, describes the propagation or decay parallel to the boundaries of the waveguide. These values of k can be found by solving a classical eigenvalue problem. Whereas the solution of such eigenvalue problems is rather straightforward for acoustic waveguides (Jensen et al., 2011), this is not the case for elastic or porous layered media. When one considers wave propagation in layered media, there is the challenge that infinitely many roots exist and additionally that these roots are closely spaced in the complex plane. To date, the focus has been almost solely placed on the real-valued roots which correspond to propagating modes in the waveguide. As a result, investigations into the completeness of the modal sum and into the contributions of the evanescent spectrum for the source-waveguide interaction remain scarce. Such an analysis was done by Tsouvalas (2015), to ensure the accuracy of the Elastic Medium Model.

3.3. Evanescent spectrum

The evanescent spectrum, which consists of purely imaginary and/or complex-valued modes, decays rapidly for increasing distance from the source. However, its contribution is rather significant in the vicinity of a load and is very essential for the source-waveguide interaction, should this be considered. Which is the case when considering the installation of a foundation pile for an offshore wind pile. Furthermore, the inclusion of the leaky modes in the solution is most important for cases with few propagating modes, e.g. in low-frequency, shallow-water acoustics Jensen et al. (2011), which is a situation that applies as well, when large diameters ($D > 5m$) piles are considered low frequencies become more important. More in depth information on this topic can be found in the PhD dissertation of Tsouvalas (2015).

3.4. Visco-elastic modeling of the seabed

It is well-established that shear rigidity of the ocean bottom affects the propagation of waterborne sound through the coupling of acoustic energy into shear waves. This coupling

mechanism is of particular importance in low-frequency shallow-water acoustics, where the excitation of shear waves in the bottom often becomes dominant loss mechanism for water-borne sound. Under these circumstances, a realistic physical model of the ocean bottom is that of a viscoelastic solid described by compressional and shear-wave velocities, the attenuation factors associated with these waves and the material density. This makes the bottom able to facilitate the three different wave types mentioned in section 2.2.2, compressional, shear and interface waves. A seismic interface wave is a guided wave propagation along the interface between two media with different shear speeds. The wave is generally given the name Scholte wave when propagating along a fluid-soil interface. To further illustrate the importance of modelling the ocean bottom as a visco-elastic medium, the conclusions of a study, performed by Tsouvalas (2015), where the soil was modeled as an acoustic fluid and as an acousto-elastic medium, are cited below.

It was shown that, although the equivalent fluid model could provide reliable predictions at frequencies higher than $100 - 200Hz$, the deviations between the two models at the low frequency bandwidths are significant. The fluid model has the tendency to underestimate the noise levels especially close to the seabed. This is mainly attributed to the presence of the Scholte wave which is altogether neglected when the seabed is modeled as an acoustic fluid. Additionally, the influence of the soil elasticity and soil layering were investigated. It was shown that the shear rigidity of the soil plays a significant role for the correct estimation of the noise levels close to the seabed surface due to the energy transferred into the interface waves. The higher the shear rigidity of the seabed, the larger the penetration depth of the Scholte wave into the fluid region, and, consequently, the higher the noise levels close to the soil-water interface.

4

Case study

In this chapter the input parameters, used as input for the Elastic Medium Model, which was described in chapter 3, will be discussed. The Veja Mate project offers a great opportunity to investigate the noise propagation when utilizing a large impact hammer on very big foundation piles. Additionally it offers the possibility to validate the Elastic Medium Model, regarding the sound levels it predicts, with the measured sound levels at the installation site. The data from the Veja Mate project for the soil and further environmental parameters, will serve as a base case for the model calculations.

4.1. Veja Mate project

Offshore Windforce (OWF), a Boskalis company, was contracted to engineer, provide, construct and install 67 foundation piles for the offshore wind farm Veja Mate. The offshore wind farm is located in the southeastern part of the North Sea. It covers an area of approximately 50 km^2. The distance to the nearest coast is almost 95 km, which is at Borkum, Germany. The location and layout of the the wind farm is depicted in figure 4.1. Construction started early April 2016 and finished in September 2016. The monopiles were loaded at the port of Eemshaven from where they were transported and installed at the construction site by the installation vessel Scylla of the company Seajacks. The installation hammer used for this project was the IHC S-4000 which has a maximum impact energy of 4000 kJ.

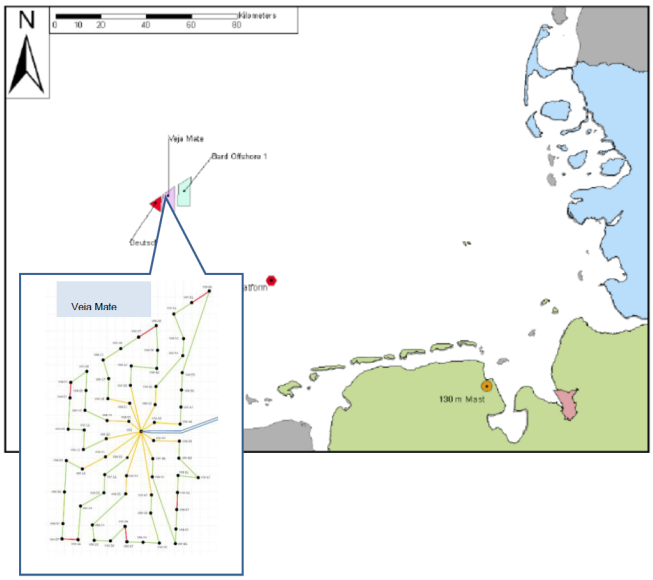

Figure 4.1: Location and layout of the Veja Mate offshore wind farm

The Veja Mate wind farm is located within the German Exclusive Economic Zone, therefore the German noise regulations apply. This made the application of noise mitigation methods to dampen the sound levels necessary, a Hydro Sound Damper and two Double Big Bubble Curtains were used.

4.2. Noise monitoring

The monitoring of the noise levels being emitted during installation of the monopiles, was done by a German company, Institut fur Technische und Angewandte Physik (ITAP). To comply with the noise limitations imposed by the BSH, noise monitoring is required at 750 and 1500 meters from the pile and in the lower one third of the water column. During the installation of each foundation pile, three hydrophones (two at 750 meters and one at 1500 meters) were deployed at approximately 2 meters above the seabed. The hydrophones had a 24 bit resolution, a sampling rate of 44 kHz and were equipped with GPS to track their location. After the installation of three monopile, a report was submitted by ITAP to OWF with the results of the sound measurements. The reports describe the noise mitigation system(s) used, the water depth and soil type at the location, sound exposure and peak levels and various graphs of the sound levels over time and versus blow energy.

Unfortunately, the data of the hydrophones was not available for this research. This data would have given even more insight in the noise levels emitted and pressure fronts reaching the various locations, especially the time traces would have been valuable. Nonetheless, the sound levels will be used as a reference in order to validate the model's predictions. Additionally, the Elastic Medium Model does not incorporate noise mitigation systems yet and because most of the foundation piles of the Veja Mate wind farm were installed with noise mitigation systems, it will be impossible to accurately compare most of the Veja Mate data with the model. However, one foundation pile was installed without any noise mitigation system and will therefore be used as a reference case throughout this graduation thesis.

4.3. Monopile VM58

Monopile VM58 is the only foundation pile that was installed without any noise mitigation system. It was hammered up to a depth of 36.82 meters with a total amount of 4532 blows of the impact hammer. This took place on April 13th 2016. The pile was installed at the eastern side of the wind farm where the soil is densest and a maximum input energy of 2100 kJ was used during installation. The pile has a diameter of 7.8 meters at its base and 6.5 meters at its top, with a total length of 80 meters. Table 4.1 state the characteristics of the pile in more detail.

Table 4.1: Dimensions and properties of monopile VM58

Pile	VM58
Type	Monopile
Length	80.00 m
Diameter over Length	6.5 (0 m <L≤ 10 m)
	6.5 m → 7.8 m (10 m <L≤ 25 m)
	7.8 m (25 m <L≤ 80 m)
Average thickness	80 mm
Mass	1300 metric ton
Water depth	39.00 m
penetration	36.82 m

With the parameters of the pile, it is possible to determine the ring frequency, this is the frequency at which the pile moves radially outward and inward in its entirety. The formula for calculating it is stated in equation 4.1.

$$f_r = \frac{1}{\pi d}\sqrt{\frac{E}{\rho\,(1-v^2)}} \tag{4.1}$$

The reference case has a diameter of $7.8m$ and typical steel characteristics of a modulus of elasticity of $2.10*10^{11}N/m^2$, a density of $7850kg/m^3$ and a Poisson ratio of 0.28[-]. Using these parameters in equation 4.1, the ring frequency equals $220Hz$. It is not expected that, in the frequency response spectra, there will be any energy located at frequencies larger than the ring frequency. Tsouvalas (2015) has shown that the critical range, i.e. the frequency range in which the pile is an efficient radiator of sound, depends largely on the diameter of the pile. In all cases the maximum pressure level is reached at frequencies below the ring frequency and around the ring frequency the majority of the energy is absorbed by the pile itself and almost no energy is irradiated into the fluid domain, additionally the vibration modes of the pile with frequencies below the ring frequency are best matched to the surrounding fluid and therefore able to radiate considerable energy into the fluid domain.

4.4. Impact diagram

The impact hammer introduces an impact force on the top of the pile to penetrate the latter further into the soil. The impact diagram shows how the force varies over time and the diagram serves as input for the acoustic model considered in this study. To be able to make accurate predictions of the sound levels, produced during installation of the reference foundation pile (VM58), it is critical to use an impact diagram that equals the force used during the installation of pile VM58. Unfortunately, the input force was not measured during the project and therefore a drivability program, GRLWEAP (Goble and Rausche, 1976), was used to generate an appropriate force diagram.

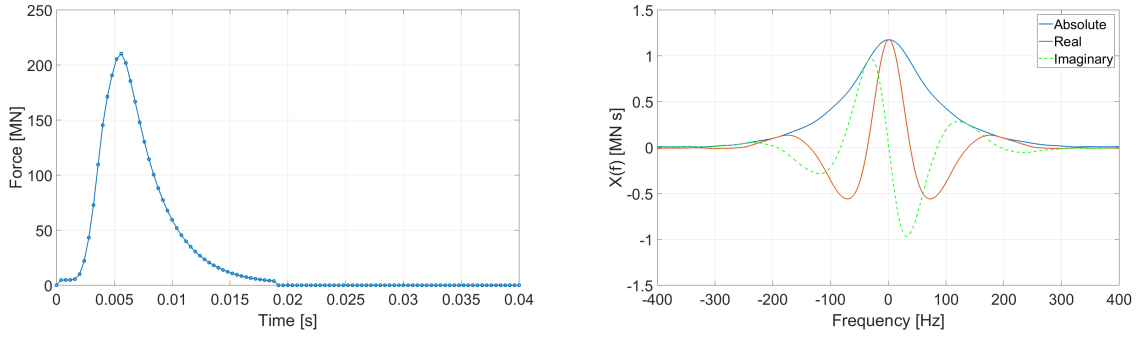

(a) Time domain (b) Frequency domain

Figure 4.2: Impact diagram

The main input in GRLWEAP is hammer type, cushion, pile specifications and soil parameters. For the hammer selection, a large data file which contains almost all available commercial hammers is available. This data contains the information of the fall height of masses, velocity and weight of the mass and of total system. Soil data is inserted as unit shaft and tip resistance per depth, further information will follow in section 4.5. The predictions that were made for the Veja Mate project estimated the maximum required energy at 2100 kJ. However when examining the piling log file for monopile VM58, it becomes clear that the maximum did not exceed 1800 kJ. Using all available information, the result of GRLWEAP produces the required impact diagram. This is depicted in figure 4.2. The impact diagram is shown in the time domain along with its representation in the frequency domain.

4.5. Soil data

The soil data is of large importance for making accurate noise level predictions. This was already made clear in chapter 3. The soil data that is available from the Veja Mate project

exists of a Cone Penetration Test (CPT). The results of the CPT analysis are shown in figure 4.3. For a more insightful overview, table 4.2 states the values accompanying the results of the CPT analysis.

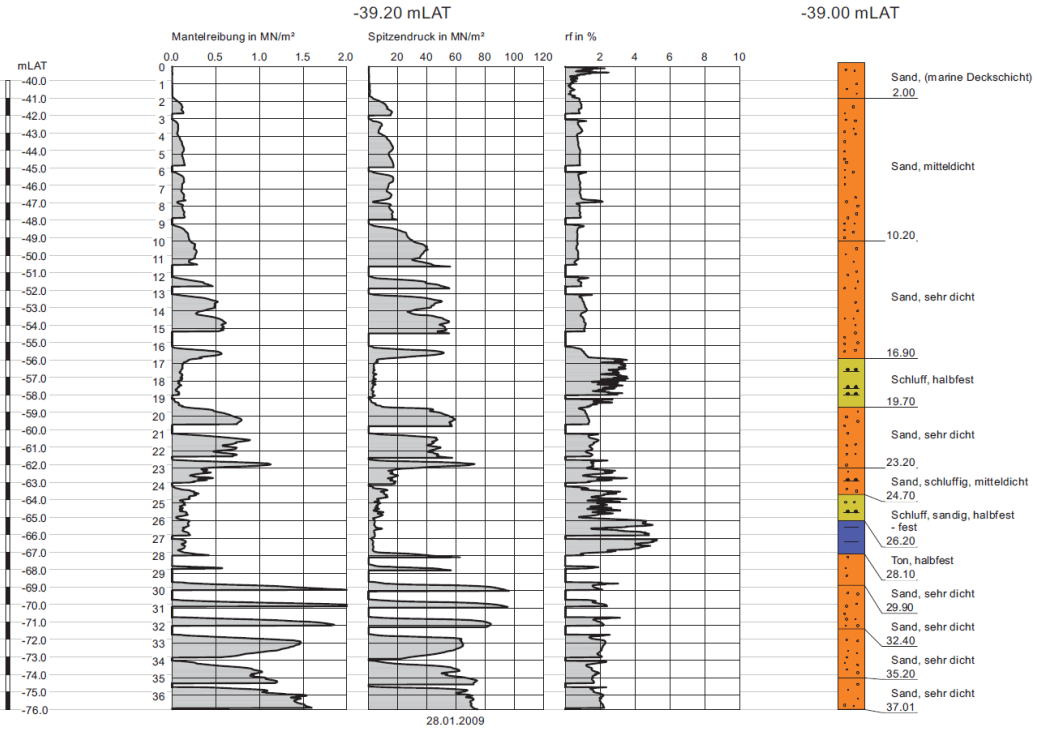

Figure 4.3: Shaft and tip resistance from CPT at VM58

Table 4.2: CPT data at VM58

Layer	Depth	Material	Saturated density	Constant volume friction angle	Average measured cone resistance	Average measured shaft resistance
	m	-	kN/m^3	°	MN/m^2	kN/m^2
S1	2.0	Sand	19	20	8	-
S2	10.2	Sand	19	30	20	-
S3	16.9	Sand	19.5	35	45	-
C1	19.7	Clay	20	-	5	200
S4	23.2	Sand	20.5	37.5	55	-
S5	24.7	Sand	21	30	22.5	-
C2	26.2	Clay	20	-	10	200
C3	28.1	Clay	20	-	5	200
S6	29.9	Sand	21	37.5	70	-
S7	32.4	Sand	20.5	38	100	-
S8	37.0	Sand	21	37.5	80	-

The information from the CPT analysis can be used to determine the properties of the soil. The information needed as input for the viscoelastic bottom of the Elastic Medium Model include the following properties: the compressional wave speed c_p, the shear wave speed c_s,

the compressional wave attenuation α_p, the shear wave attenuation α_s and the density ρ. From the CPT data it is clear that the main soil material is sand. Hegazy and Mayne (2006) derived an empirical correlation between cone tip resistance and shear wave speed, stated in equation 4.2.

$$c_s = (10.1log(\bar{q}_t) - 11.4)^{1.67} \cdot (r_f)^{0.3} \tag{4.2}$$

In equation 4.2, $\bar{q}_c$ equals the average cone tip resistance in kPa and r_f is the friction ratio in percentage, these can both be extracted from figure 4.3. The shear and Scholte wave propagation are mainly vertical polarized and hence most influenced by the upper soil layer. As a consequence, a medium dense sand layer is inserted and used as a reference case for the complete seabed. In section 7 the sensitivity of the soil parameters is discussed during a parametric study. The average cone tip resistance is chosen at 1.5 MPa, together with a friction factor of 1%, results in a shear wave speed of 260 m/s. According to the same work, performed by Hegazy and Mayne (2006), the soil unit weight can be derived from the shear wave speed using the following empirical formula,

$$\gamma = 8.32log(c_s) - 1.61log(z) \tag{4.3}$$

where z equals the depth in the soil. Finally, the density of the soil can be calculated by $\rho = \gamma/g$. This results in the following soil properties, that serve as input for the Elastic Medium Model.

Table 4.3: Fluid and soil properties that serve as input for the Elastic Medium Model

Layer	Depth	E	v	ρ	c_p	c_s	α_p	α_s
	m	MN/m^2	-	kg/m^3	m/s	m/s	dB/λ	dB/λ
Fluid	39	-	-	1035	1490	-	-	-
Medium dense sand	36.5	400	0.485	2000	1520	260	1.2	3.8

4.6. Wave speeds

Now that the soil and fluid properties have been derived, it is possible to evaluate how the pressure waves will propagate in the underwater environment. The soil and fluid properties determine the wave speeds with which pressure fronts will travel and these in turn determine when the fronts will pass the various locations at which predictions will be made. This is useful to validate the predictions and determine the physical meaning of the time trace results.

Table 4.4: Time of arrival of the different waves at various locations

		100m	200m	300m	400m	500m	600m	700m	750m	800m
c_p water	$1490m/s$	$0.067s$	$0.134s$	$0.201s$	$0.269s$	$0.336s$	$0.403s$	$0.470s$	$0.503s$	$0.537s$
c_p soil	$1520m/s$	$0.066s$	$0.132s$	$0.197s$	$0.263s$	$0.339s$	$0.395s$	$0.461s$	$0.493s$	$0.526s$
c_s soil	$260m/s$	$0.385s$	$0.769s$	$1.154s$	$1.539s$	$1.923s$	$2.308s$	$2.692s$	$2.885s$	$3.077s$

The wave speeds in the underwater environment are the compressional wave speed, c_p, in the water and in the soil and the shear wave speed, c_s in the soil. It should be noted that the wave speeds stated, are in fact the phase speeds in an unbounded medium. They determine the smallest time moment that waves start arriving at the various locations, before this time moment there cannot be any excitation of any of the physical quantities. The time moments are determined for various locations with increasing range from the pile. The locations will be 100, 200, 300, 400, 500, 600, 700, 750 (reference point) and 800 meters. The results are stated in table 4.4.

5

Noise prediction at large distances

This chapter will elaborate on the theoretical principles that form the basis of the alterations that will be made in order to extend the range of the model.

5.1. Discrete inverse fourier transform and limitations

The fast fourier transform introduces a periodic effect that limits the time for which it is applicable. Because time- and frequency domain can be quite difficult concepts to comprehend and to clarify the relations and characteristics between the two, a short elaboration is given.

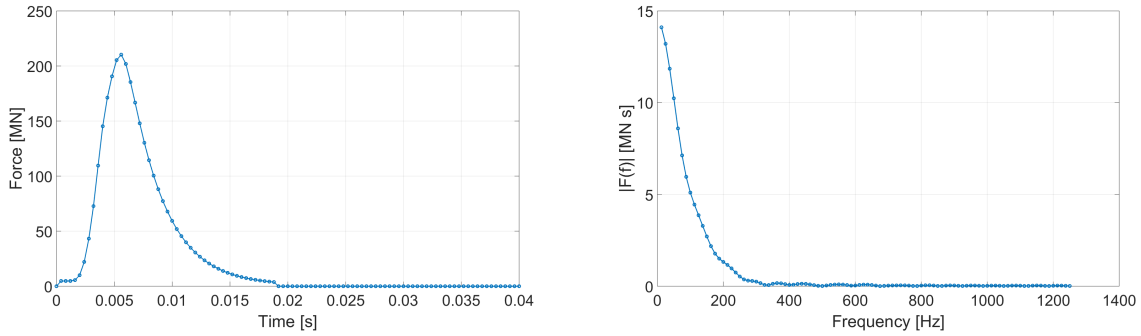

(a) Force diagram (b) Absolute excitation spectrum

Figure 5.1: Force diagram and the corresponding excitation spectrum

The forward fourier transform introduces a frequency spectrum, which is defined by the time step from the discrete signal in the time domain. The frequency spectrum will show a maximum frequency dictated by $f_{max} = 1/2t_{min}$. For example, if the force diagram has a minimum step size of $0.0002s$, the maximum frequency will be $2500Hz$. Additionally the amount of discrete points that are chosen has a large influence on the time frame that can be correctly calculated. The amount of discrete points are divided in equally spaced frequency steps from 0 up to the maximum frequency and define frequency resolution. The time frame is determined by the smallest frequency, similarly as the maximum frequency is dependent on the smallest time step, $t_{max} = 1/f_{min}$. This is illustrated with the force diagram and its spectrum in figure 5.1. The minimum time step is $0.0002s$, the maximum frequency is $2500Hz$ and the discrete steps amount to 100. This in turn determines the minimum frequency step ($25Hz$) and therefore the time window equals $0.04s$. A more straight forward way of determining the time window is by multiplying the time step with double the amount of discrete steps. However the relation between time- and frequency domain become more apparent, following the steps above.

The time window is decisive in the assessment of the sound levels. The pressure response time trace should always start with a value of zero at time moment 0 s and decay to zero again when the pressure wave has passed, as the source emits a finite amount of noise after one blow. One can imagine that if a point in the fluid is far from the pile, it is possible that the pressure wave has not yet reached this point or is arriving just at the end of the time window. This will result in erroneous results where the time trace does not show a decay to zero and energy is transported to the begin of the signal, resulting in a beginning value that is not zero. This can be seen in figure 5.2. here the correct pressure response time trace at 50 and the incorrect one at 500 meters from the pile, where aliasing is present, are depicted.

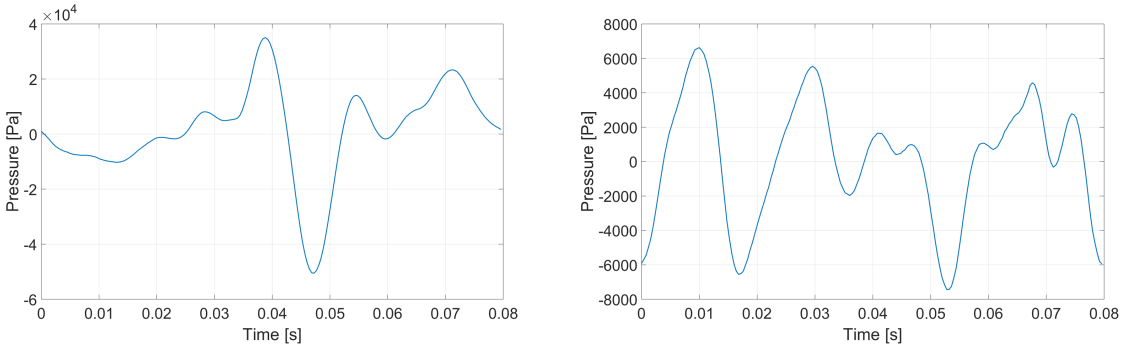

(a) Correct time trace pressure response $r = 50m$, $z = 2m$ above seabed

(b) Aliasing example $r = 500m$, $z = 2m$ above seabed

Figure 5.2: Time trace results, correct and aliasing example
The correct time trace starts and decays to zero, where the aliasing sample clearly does not

To be able to look at points located at large ranges from the pile, the time window has to be significant and this is not possible with the original setup. Currently to achieve such a large time window, the amount of steps has to be drastically increased. This leads to long computational times and the need for high amounts of memory allocation, as this scales exponentially with the amount of steps. Therefore, a new approach is necessary, which minimizes computational effort and the need of memory allocation and can increase the time window. The proposed approach is explained in the following section.

5.2. New method and implementation

To succeed in the goal of this graduation thesis, the time window has to be extended. How this is achieved is discussed below. Instead of the fast discrete fourier and inverse fourier transform a numerical inverse fourier transform will be derived and its main parameters will be examined.

5.2.1. Numerical inverse fourier transform

The first difference of the approach is to use a numerical method to transform the response in the frequency domain to the time domain instead of the inverse fast fourier transform/discrete fourier transform. The derivation is described below step by step.

The inverse Fourier transform defined in this work reads:

$$f(t) = \frac{1}{2\pi}\int_{-\infty}^{\infty} \tilde{F}(\omega) exp(i\omega t) d\omega \tag{5.1}$$

It is possible to multiply expression 5.1 by 2 and focus on the positive half of the frequency spectrum, because the spectrum is symmetrical with respect to $\omega = 0$.

$$f(t) = 2\left(\frac{1}{2\pi}\int_{0}^{\infty} \Re e[\tilde{F}(\omega) exp(i\omega t)] d\omega\right) \tag{5.2}$$

Using Euler's formula and the fact that $\tilde{F}(\omega)$ is a complex number, it is clear that 5.2 becomes:

$$f(t) = \frac{1}{\pi}\int_0^\infty \Re e[\left(\Re e(\tilde{F}(\omega)) + i\Im m(\tilde{F}(\omega))\right)(cos(\omega t) + isin(\omega t))]d\omega \tag{5.3}$$

As the outcome has to result in a real number, parts of the expression introducing an imaginary part are removed and equation 5.3 becomes:

$$f(t) = \frac{1}{\pi}\int_0^\infty (\Re e(\tilde{F}(\omega))cos(\omega t) + i\Im m(\tilde{F}(w))isin(\omega t))d\omega \tag{5.4}$$

The properties of integrals allow the break up of the integral of 5.4.

$$f(t) = \frac{1}{\pi}\int_0^\infty \Re e(\tilde{F}(\omega))cos(\omega t)d\omega - \frac{1}{\pi}\int_0^\infty \Im m(\tilde{F}(w))sin(\omega t)d\omega \tag{5.5}$$

The only problem remaining in the expression is the upper boundary of infinity. This is replaced by a maximum frequency beyond which there is no more energy in the frequency domain. This enables the integral to be written in the following summation:

$$f(t) = \frac{1}{\pi}\sum_0^\Omega \left(\Re e(\tilde{F}(\omega))cos(\omega t) - \Im m(\tilde{F}(\omega))sin(\omega t)\right)\Delta\omega \tag{5.6}$$

5.2.2. Integral limits

The maximum frequency Ω has to be determined. It has to be large enough to include all the frequencies that carry energy and as small as possible to not waste any computational time calculating the responses of frequencies where no energy is present. The maximum frequency can be determined by looking at the spectrum of the force. As the force is what introduces energy into the system, the frequencies with no energy in the force spectrum will have no energy in the response.

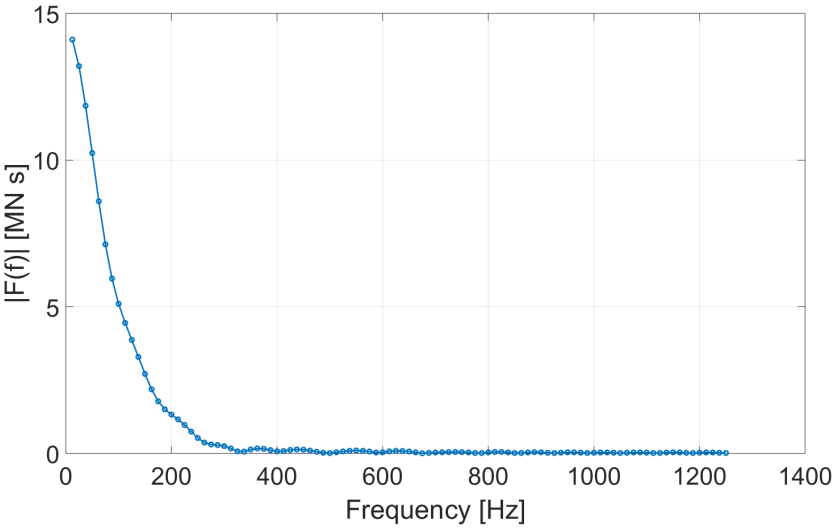

Figure 5.3: Absolute excitation spectrum

From figure 5.3 it becomes clear that beyond $400Hz$ there is no more energy inserted into the system. This will be the maximum frequency Ω in equation 5.6. Comparing the maximum frequency determined earlier, when illustrating the relation between time- and frequency domain, it becomes clear that the maximum frequency is significantly higher $1250Hz > 400Hz$ than the frequencies carrying energy. It would be possible to increase the time step, resulting in a smaller maximum frequency however this would cause the loss of information of the force

diagram. To clarify, the maximum frequency of the model would become $400Hz$, when the time step would equal $0.00125s$. Unfortunately, with a time step of $0.00125s$ information of the force diagram would be lost, as illustrated by figure 5.4.

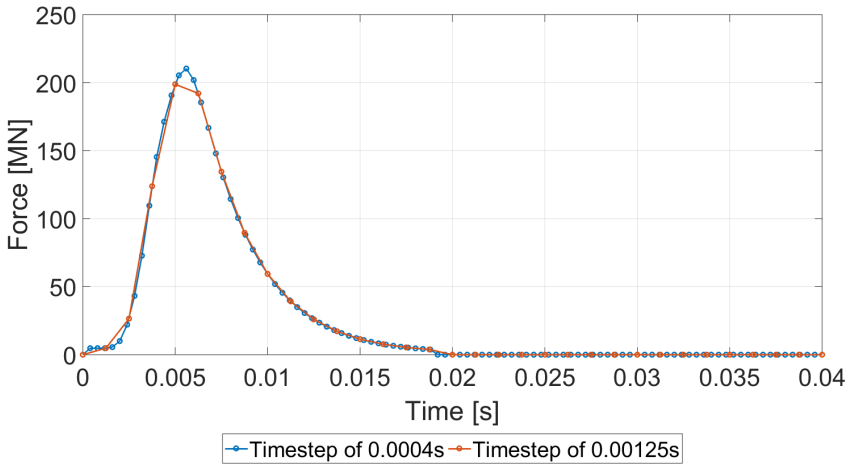

Figure 5.4: Force diagram with missing information

5.2.3. Creating a continuous function in the frequency domain

Equation 5.6 still has one limiting factor which is the $\Delta\omega$. Its size determines the maximum time period for which the outcome is valid, as mentioned above. To increase the time period the frequency step size of the output has to become as small as possible. Resulting in a continuous function for the response in the frequency domain. Once the continuous function is determined, the response in the time domain for any time moment can be calculated.

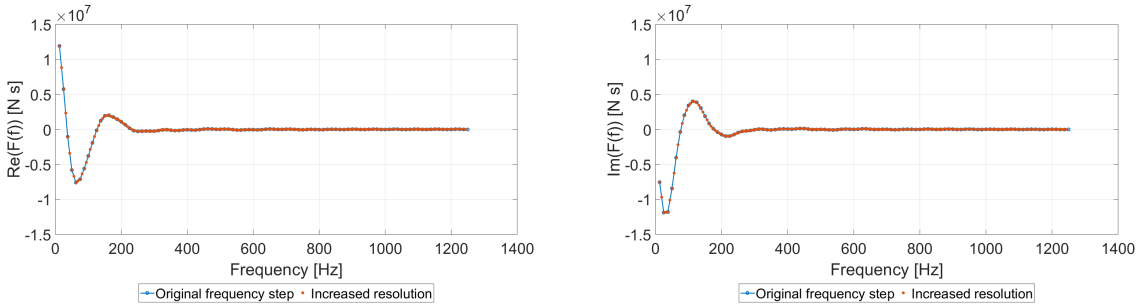

(a) Real part (b) Imaginary part

Figure 5.5: Spectra of the force, original and increased resolution

To illustrate how this approach would work, an example will be discussed. The force diagram will be transformed to the frequency domain, after which the resolution will be increased and using the inverse fourier transform the time trace will be recreated, which should be valid for, in theory, infinite time. In figure 5.5, the force spectrum is shown for a force diagram with a time step of $0.0004s$ and 100 steps. It is illustrated how the resolution is increased by linear interpolation between the points.

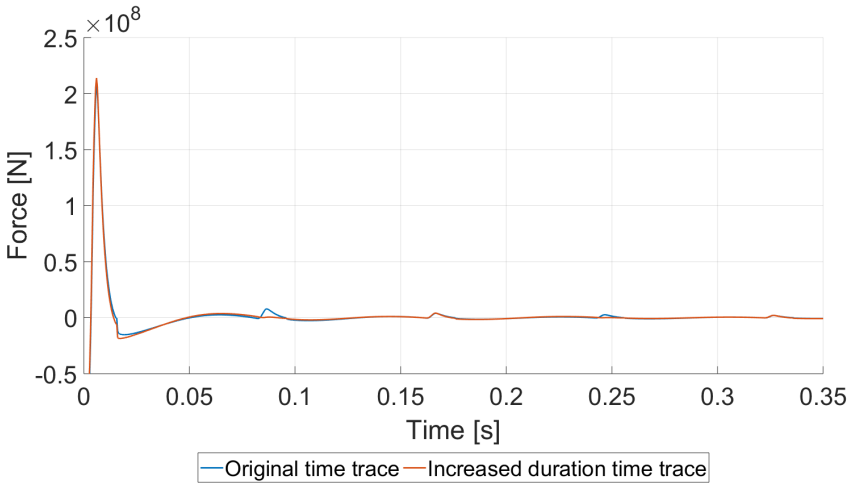

Figure 5.6: Time trace of the force input, increased time window

Now that the resolution of the force spectrum is increased, it can be transformed to the time domain. Figure 5.6 shows the original and the new result in the time domain. To illustrate the effect the calculations were made beyond the point for which the original result is valid. The periodic effect is clearly visible in the zoomed in figure 5.7. The time for which the result is valid has doubled by halving the frequency step as expected. This confirms that increasing the resolution of the spectrum, increases the time window for which it is valid. Strikingly, there seems to be a large error at the beginning of the signal (signal does not start at 0 but at a fairly large negative value), this was not solved and the error became larger with the increased resolution. This could be because the resolution of the frequency domain is still not high enough and maybe the first frequency (fundamental frequency) is incorrectly represented.

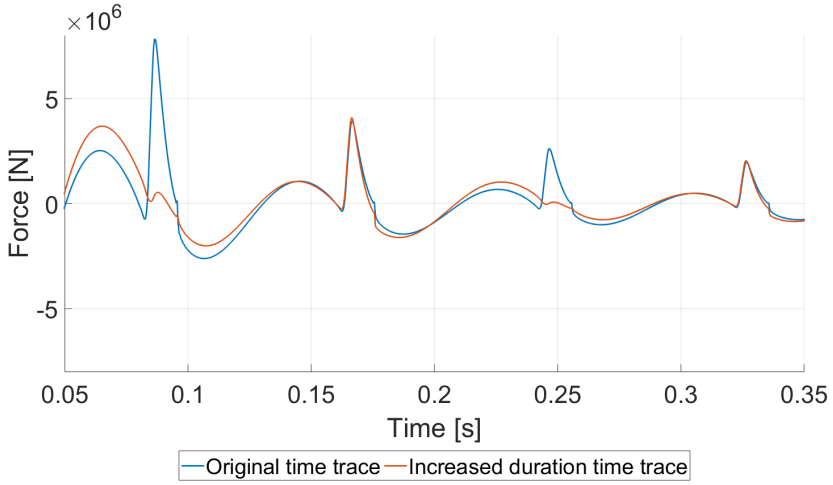

Figure 5.7: Periodic effect

The example shows that the suggested approach is valid and can increase the time window, as expected. It should be noted that the resolution used for the example was not high enough, leading to some inconsistencies like the values near time moment 0 s, where they do not equal zero as they should.

6

Model predictions and validation

In this chapter the results will be discussed. All the results are evaluated at close range and at the reference point of 750 m. To gain insight in the evolution of the pressure waves, points with increasing range in between these main locations will be analyzed as well.

6.1. Resolution increase with interpolation scheme

Using the input parameters from chapter 4 and a limited amount of steps (100), the Elastic Medium Model was run. The pressure spectra that are calculated by the model will be analyzed below. This will be done for several points at different ranges from the pile, from 30 meters up to 750 meters.

6.1.1. Short range

The pressure spectrum at 30 meters from the pile and at 2 meters above the seabed, is depicted below in figure 6.1. One of the first noticeable things is that the amount of frequencies that carry no energy is very large. This is something that was expected and discussed in section 5.2.2, however the maximum frequency is even lower than anticipated. The expectation was that the maximum frequency would lie around 400Hz and concluding from the figure the maximum frequency equals about 250Hz. A short elaboration on this will follow in section 6.2. It is important to note that up to now, no changes to the original model were made and were not needed for the approach suggested.

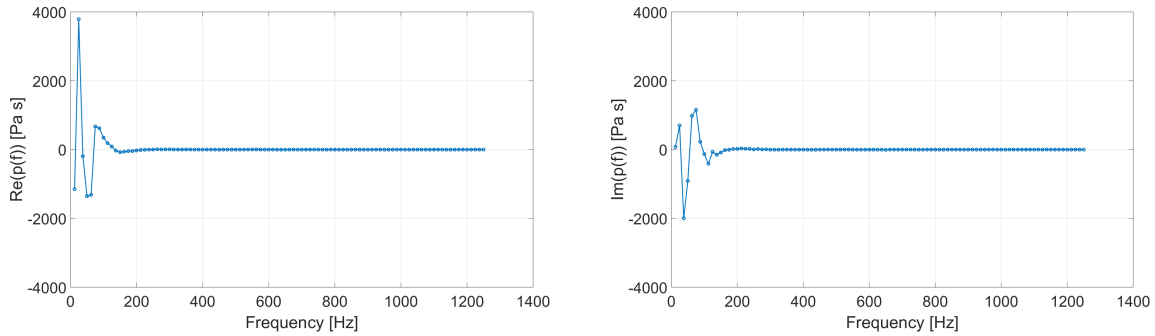

(a) Real part (b) Imaginary part

Figure 6.1: Pressure response spectra at 30 meters from the pile

With the frequency step size of 12.5Hz, the maximum time window it defines, is equal to 0.08s. The result in the time domain is determined by applying the inverse fourier transform and the resulting time trace is displayed in figure 6.2.

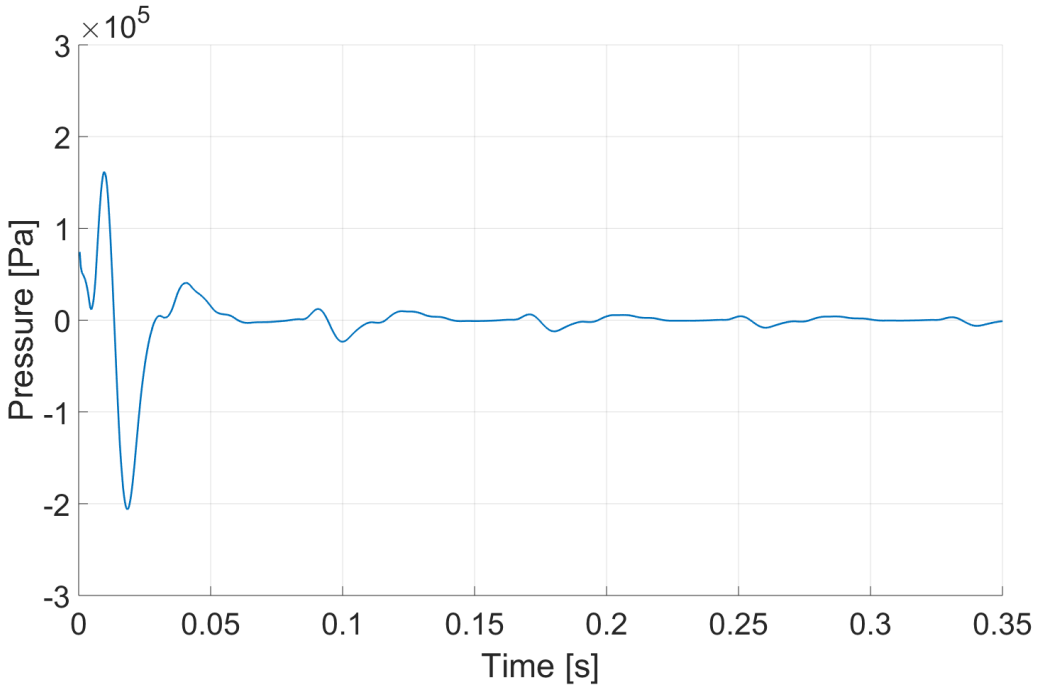

Figure 6.2: Time trace response at 30 meters from the pile

The first notable aspect of the figure is that there seems to be a pressure at the very beginning (at $t = 0$). This is impossible as there has to be a delay from when the force starts acting on the pile to the moment where the first pressure wave arrives at the point 30 meters from the pile. Therefore, the conclusion is that there is information, more specifically frequencies, missing in the pressure response spectrum. Furthermore, it can be concluded that the time trace is valid for the $0.08s$. After which, a repetitive signal manifests. The period of this repetitive signal equals $0.08s$ precisely the duration of the time window the spectrum describes. Every cycle the signal decays, but retains exactly the same shape. This however does not have a physical meaning. To remove this periodic signal, increase the time window and increase the resolution the approach discussed in last chapter will be applied.

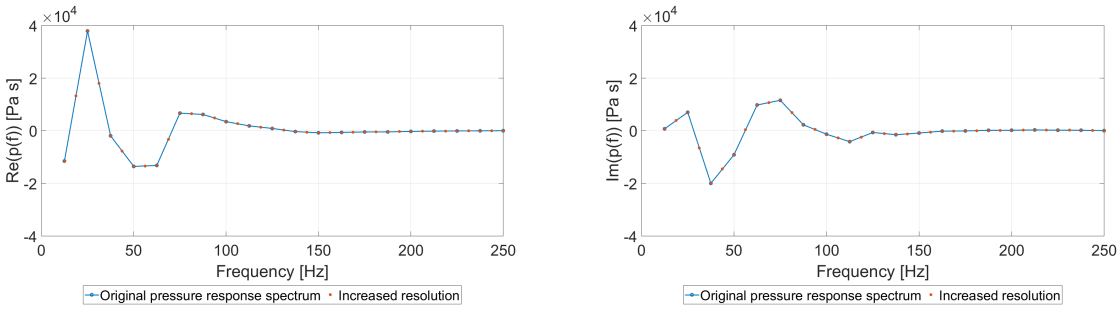

(a) Real part of the pressure response spectrum (b) Imaginary part of the pressure response spectrum

Figure 6.3: Resolution increase by linear interpolation

To add resolution to the output pressure spectrum a linear interpolation scheme is used. This is depicted in figure 6.3. The maximum frequency is lowered to $250Hz$ (further argumentation can be found in section 6.2) and the frequency step size is halved, what would in theory increase the time window to two times it original size (from $0.08s$ to $0.16s$). Applying the

inverse fourier transform to the spectrum with increased resolution results in the following time trace.

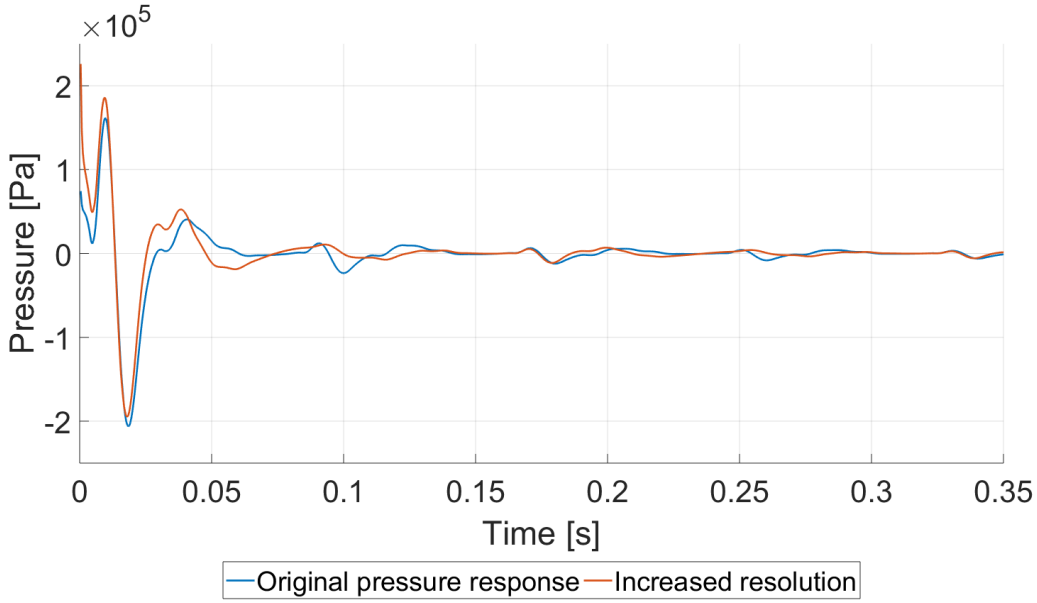

Figure 6.4: Time trace response at 30 meters from the pile with increased resolution in the frequency response spectrum
The periodic effect is clearly visible and like in figure 5.7 the period is doubles when the resolution is increased by halving the frequency step size

From figure 6.4 several things are notable. The periodic signal that was visible between $0.08s$ and $0.16s$ has disappeared. In stead the periodic signal shapes after the $0.16s$ as was expected. However the resolution increase did not lead to the diminishing of the starting error. The approach seems successful at extending the time window but unable to correct the starting error. To increase the time window even further the resolution of the spectrum was increased with a frequency step size of 2 and $1Hz$. The spectra are depicted in the figure 6.5 and figure 6.6.

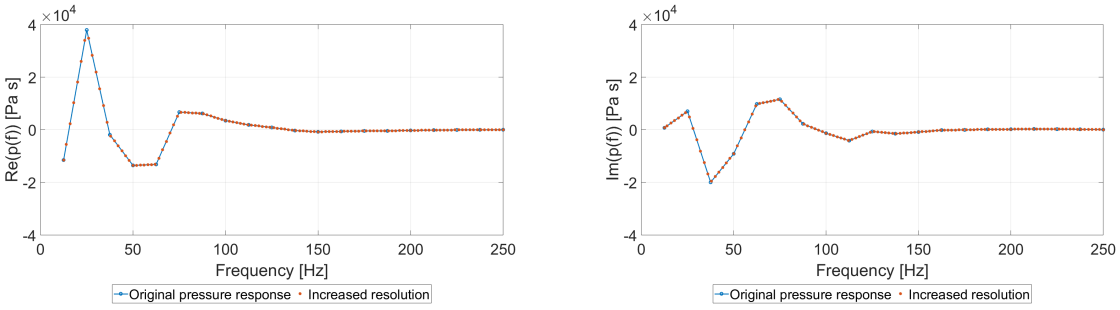

(a) Real part (b) Imaginary part

Figure 6.5: Resolution increase by linear interpolation
Frequency step of $2Hz$

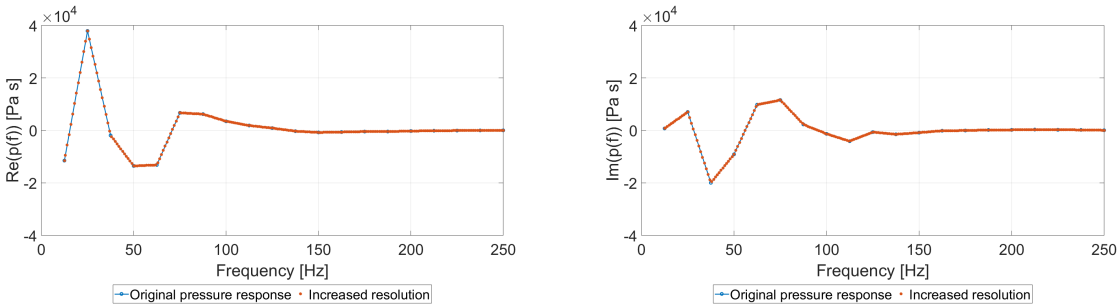

(a) Real part (b) Imaginary part

Figure 6.6: Resolution increase by linear interpolation
Frequency step of $1Hz$

To see if the time extension continues to work and if the addition of more frequencies can resolve the issue with the starting pressure, from both the spectra the time trace is determined using the inverse fourier transform. The result can be found in figure 6.7. The time window in both cases is increased as expected. The spectrum with the frequency step of $2Hz$ results in a time trace that is valid up to $0.5s$ and the spectrum with the $1Hz$ frequency step defines a time window of $1s$.

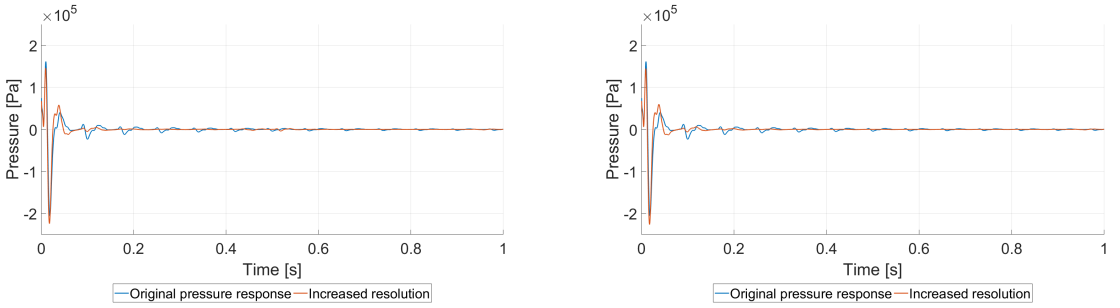

(a) Defined by a frequency step of $2Hz$ (b) Defined by a frequency step of $1Hz$

Figure 6.7: Time trace response at 30 meters from the pile with increased resolution in the frequency response spectrum
Time window is extended as anticipated, however the error at the beginning of the signal remains in both cases

Unfortunately, the error at the beginning of the time trace was not solved by adding resolution to the response spectrum. It is possible that this is due to the share of energy located below the lowest frequency or in between the frequencies that were calculated by the model. The only possible way to add resolution below the lowest frequency calculated by the model ($12.5Hz$), would be by assuming that at $0Hz$ the pressure response is equal to 0 Pas. However there is no value addition if resolution is added in this manner. See figure 6.8 for the outcome of such an interpolation with a frequency step of $1Hz$ in the frequency domain with its related time trace.

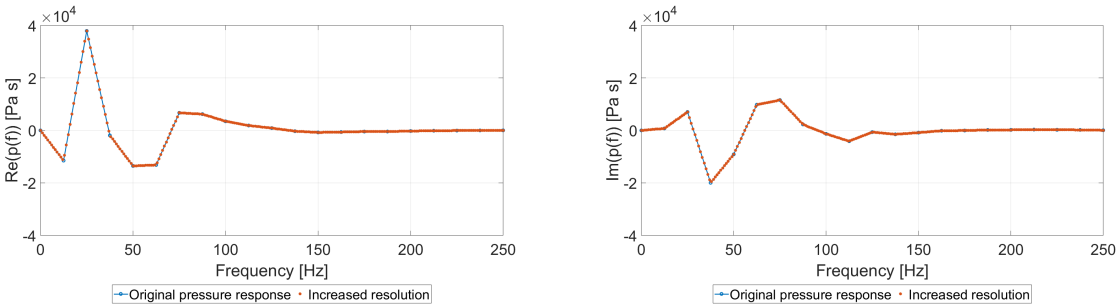

(a) Real part (b) Imaginary part

Figure 6.8: Interpolation below the lowest calculated frequency

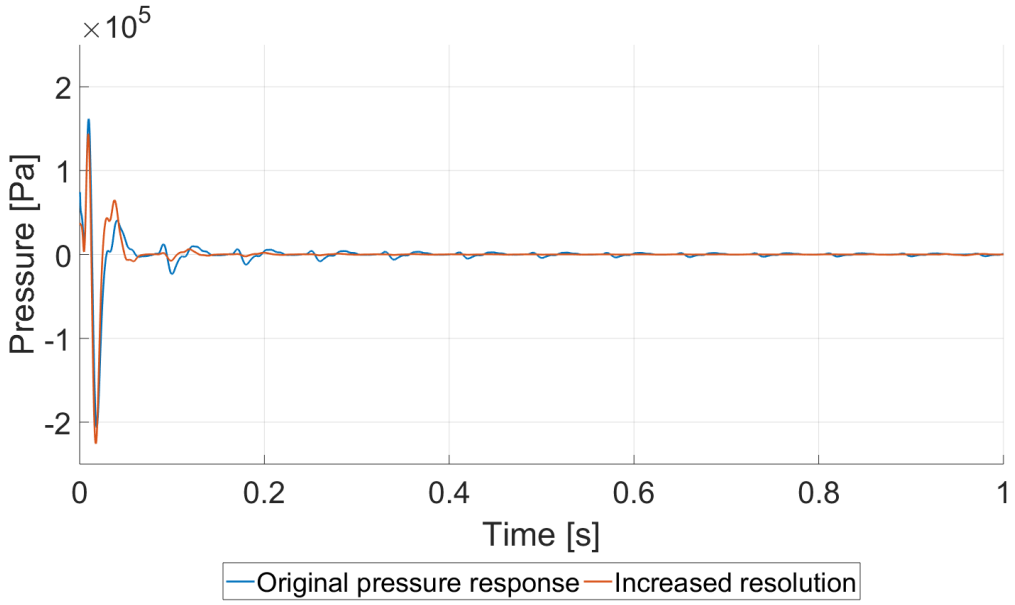

Figure 6.9: Comparison of the time traces
The error at the beginning of the signal does remain but is reduced, implying that there is energy located beneath the minimum frequency originally calculated.

After analyzing the outcome for a point close to the pile (30 meters), it seems that the interpolation method for adding resolution in the frequency domain is partly successful. It was concluded that by adding energy located at frequencies between calculated frequencies by linear interpolation, the time window can be extended. The periodicity scales with the frequency step. To clarify, when the frequency step is equal to $2Hz$ the periodic signal develops after $0.5s$ and then has a period of $0.5s$. When a similar comparison is done with a frequency step of $1Hz$, the period of the repeating signal is $1s$. Additionally, it is apparent that there is an error at the beginning of the pressure time trace. This could be the result of energy located at frequencies smaller than the lowest frequency or in between the frequencies that were calculated by the model and that this energy is insufficiently represented by the interpolation scheme. This suspicion is confirmed when analyzing the time trace where resolution was added below the minimum frequency originally calculated. This caused the error at the beginning to become smaller, but not totally disappearing.

6.1.2. Reference point at 750m

The approach used above for the short range location will be applied to the reference point at 750 meters from the pile and located 2 meters above the seabed. The frequency response spectrum for the pressure is displayed in figure 6.10.

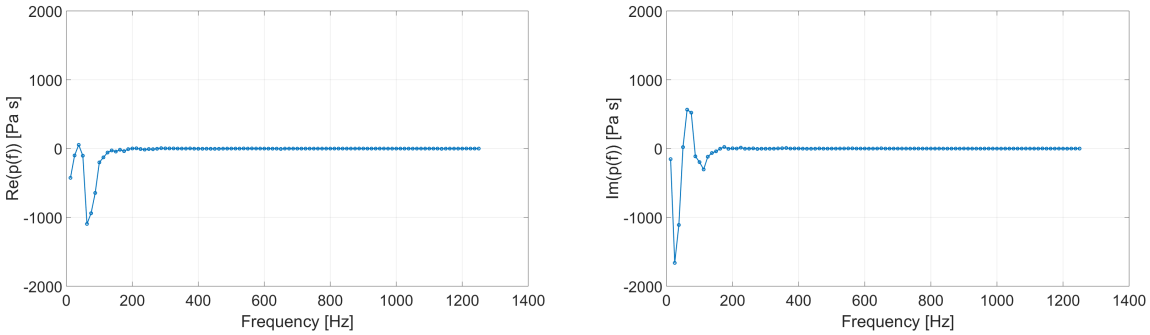

(a) Real part (b) Imaginary part

Figure 6.10: Pressure spectra at 750 meters from the pile

Again it stands out that a lot of frequencies carry no energy as established before. This is due to the current setup of the model and it becomes clear that a lot of computational power is wasted by calculating the results for frequencies that are not being excited. In section 7.6 there is an elaborate discussion on the computational time of the model and how to use it efficiently. The corresponding pressure response in the time domain is derived and depicted in figure 6.11.

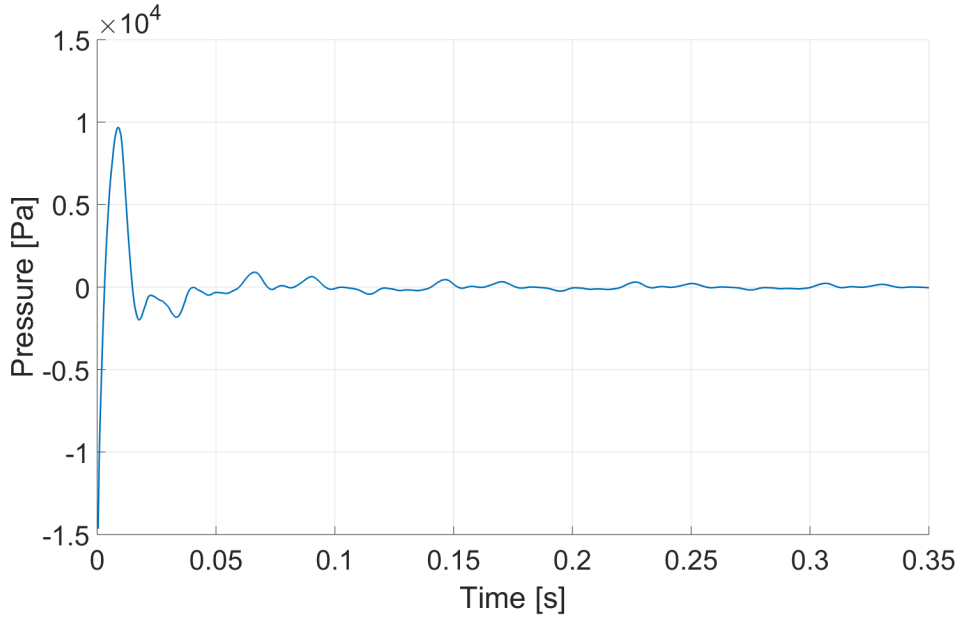

Figure 6.11: Original pressure response for a point located 750 meters from the pile
It is quite apparent that this time trace is incorrect. There cannot be a pressure wave arriving at such an early moment in time

It quickly becomes clear that this time trace is incorrect. It is impossible for any wave traveling through any media present in the system, that it will arrive at such an early moment in time. In section 4.6, the wave speeds present in the system and the time of arrival at the location of 750 meters were determined, for the primary wave this would equal around $0.5s$. This is outside of the time window that the frequency response spectrum can define ($0.08s$). For this time window at this location there should not be any response, as no waves could

have arrived. However the model did calculate that frequencies carry energy and therefore, a response is present, although this wave does not have any physical meaning. Additionally, the periodic effect detected earlier, is less obvious for this location, but a closer look shows the exact same characteristics of the repeating signal after the maximum time moment has passed. Namely, a decaying signal with the same period as the duration of the time window and consisting of the same shape each period. To describe the response in the time domain, a higher resolution of the frequency response spectrum is necessary. To be able to accurately describe the first arriving wave the spectrum would need a frequency step size of $2Hz$. Nevertheless, this would mean the wave would arrive at the end of the time window ($0.5s$) and to be sure a frequency step of $1Hz$ will be created. The result of the linear interpolation up to a frequency step of $1Hz$ is displayed in figure 6.12.

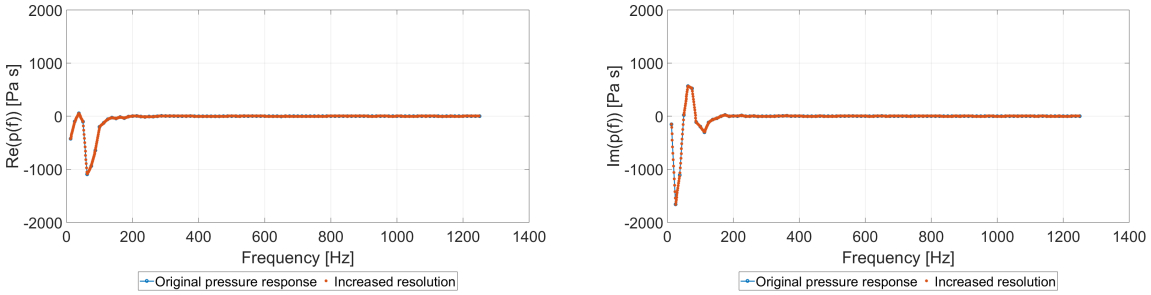

(a) Real part (b) Imaginary part

Figure 6.12: Response spectra with a frequency step of 1Hz

With the resolution of the response spectrum increased up to a frequency step of $1Hz$, it should be valid for a time window of $1s$. This should be enough to accurately describe the arrival of the first pressure wave around $0.5s$. By applying the inverse fourier transform the time trace is equal to figure 6.13.

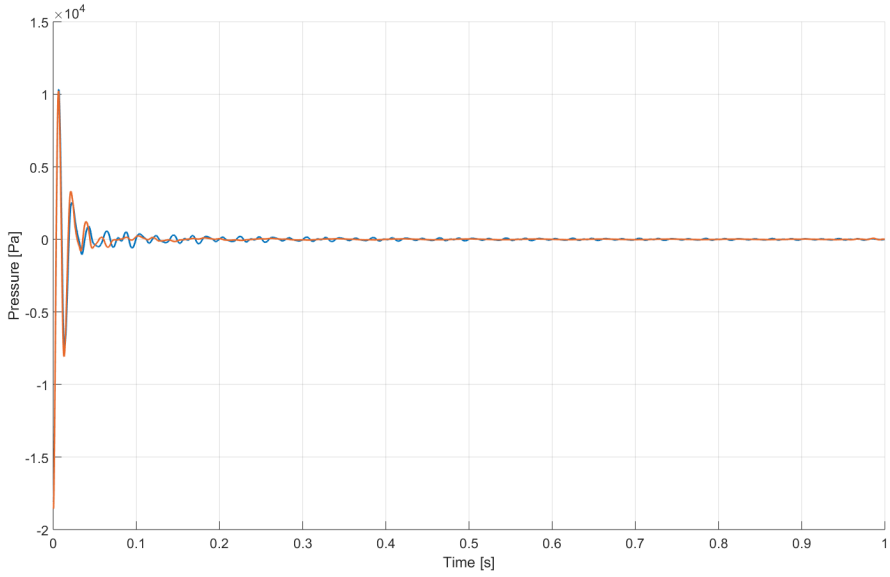

Figure 6.13: Time trace comparison for original and increased response spectra
The increased resolution of the response spectra are unable to extend the time window of the pressure time trace at the reference point of 750 m

In contrary to what was expected, the spectrum with the increased resolution is not able to accurately describe the time trace. It is almost exactly the same as the time trace described by the spectrum with lower resolution. The periodic effect up to $1s$ is removed, however the signal has no physical meaning. For this point no additional resolution increase was done below the lowest calculated frequency as this frequency is very close to the cutoff frequency ($12.5Hz \approx 10Hz$), that was calculated with equation 2.1. Below this frequency no energy will be present in the system at such a distance from the pile. This is due to the properties of the underwater environment acting as a waveguide, as mentioned in section 2.2.1.

6.1.3. Conclusion

The first conclusion that can be made is one regarding the computational effort of the model. It becomes quite clear that the model with the current setup calculates a lot of frequencies that carry no energy. Additionally, as excepted the lower frequencies are the ones carrying the energy but with the large frequency step size only a small amount of these frequencies are calculated. The result for short range points showed that the suggested approach was able to extend the time window, however no value was added as the pressure waves had all passed and the only thing that was achieved was the addition of 0 values once the waves have passed. It has to be mentioned that the approach was unable to add resolution to overcome the incorrect pressure values at the beginning of the time trace. This could be because some low frequencies are incorrectly represented by the linear interpolation scheme. For points located at larger ranges from the pile the suggested approach does not work. The resolution increase does not change the time trace. The only conclusion to be made here is that more resolution is needed at the low frequencies and the energy located at these frequencies cannot be calculated by linear interpolation of the data determined by the model. Furthermore, the expectation of the maximum frequency lying around $400Hz$ (5.2.2) was incorrect and it actually equaled more or less $250Hz$.

It becomes clear that the suggested approach has its limitations and that higher resolution is needed, that cannot be created by linear interpolation. Together with the fact that the model is calculating responses at frequencies that carry no energy and wastes computational effort, leads to the conclusion that an alternative approach is needed to achieve accurate results for points located a medium to long ranges from the pile. The alternative approach will be discussed in section 6.2.

6.2. Alternative approach

In order to resolve the issues that arose from the interpolation method, an alternative approach is suggested. In section 6.1 it became clear that a higher resolution is needed to accurately predict the time traces for medium to long range locations from the pile and that a large amount of frequencies were being calculated that carried no energy. Up to now there were no alterations made to the Elastic Medium Model, however to be able to use the model more efficiently some alterations will have to be made.

The characteristics of the fast fourier transform, mentioned in chapter 5, are the cause of the high amount of frequencies carrying no energy. To refocus the computational power of the model towards the lower frequencies, the input for the model will be based on the force spectrum instead of the force diagram. This will make it possible to determine which frequencies the model will calculate. In order to do this, the resolution of the force spectrum has to be increased. This is straight forward as the frequency spectrum of the force spectrum is known. In figure 6.14 the real and the imaginary part of the force in the frequency domain are displayed with the increased resolution. This is achieved by interpolation. The frequency step is decreased from $12.5Hz$ to $0.25Hz$. This would allow for a response spectrum that is valid for a time window of $4s$, which is enough to describe the waves arriving at the reference point, $750m$.

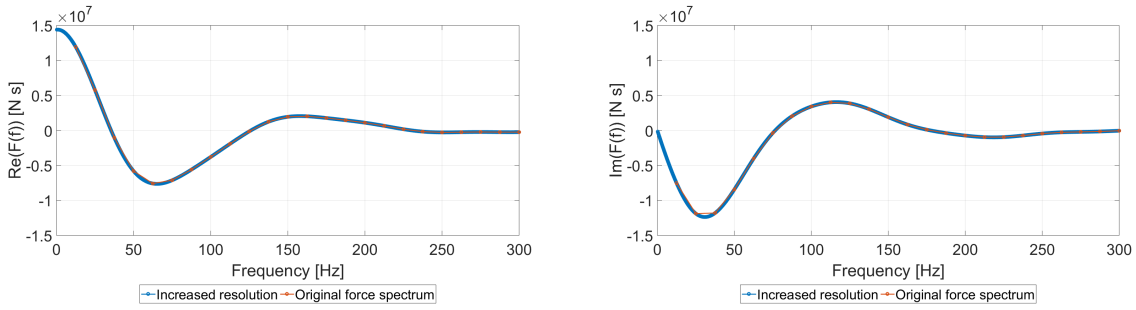

(a) Real part (b) Imaginary part

Figure 6.14: Force spectra

These force spectra will be used as input of the model. The maximum frequency has been brought down to a maximum of $250Hz$. This is based on the results of section 6.1. To interpret why there is no energy beyond this maximum frequency, the various resonance frequencies present in the system are reexamined. In chapter 4 the ring frequency was calculated with equation 4.1,equalling $220Hz$. It was stated that namely frequencies below the ring frequencies are able to radiate considerable energy into the fluid domain and that around the ring frequency all the energy is absorbed by the pile itself and almost no energy is irradiated into the fluid domain. Looking at the frequency response spectrum of figures 6.1 and 6.10, it confirms that around and above the ring frequency little energy is present. Next to the lowering of the maximum frequency, the resolution of the force spectrum has been increased significantly. However the amount of frequencies adds up to 1000 in total and it is not possible to run the model with such a high amount of steps. This is due to the fact memory has to be allocated for each frequency and for the calculations the increase of memory necessary does not scale linearly but exponentially with the amount of frequencies to be calculated. Therefore, the choice was made to run the model in bins, the size of each bin being 100 frequencies. In total the Elastic Medium Model will be run 10 times and the output files will be added to create a full data set with all the frequencies selected above.

6.3. Results

In this section the results from the increased force spectrum will be discussed. The time traces resulting from the response spectra will be analyzed and the sound pressure levels that are produced by the pressure waves at various ranges from the pile are evaluated.

6.3.1. Response spectra

The results from the simulations are assembled to form a complete response spectrum. The response spectra for the same points as in section 6.1, are displayed in figure 6.15 and figure 6.16. The results are confirming the conclusions that were made in section 6.1.3.

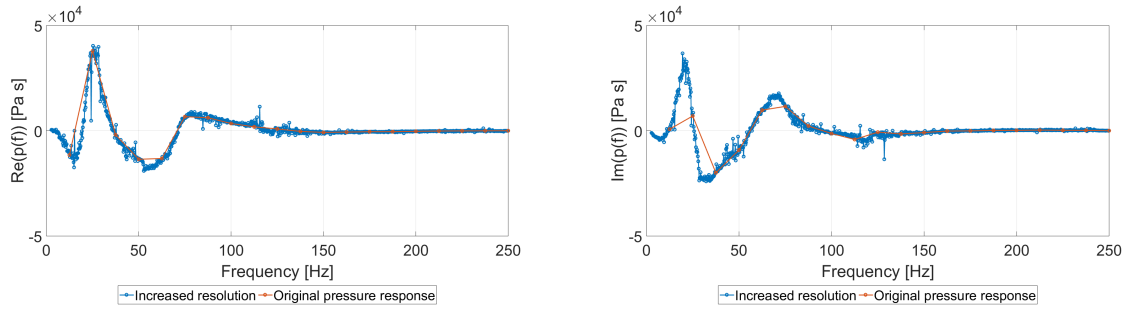

(a) Real part (b) Imaginary part

Figure 6.15: Pressure response spectra at 30 meters from the pile and 2 meters above the seabed

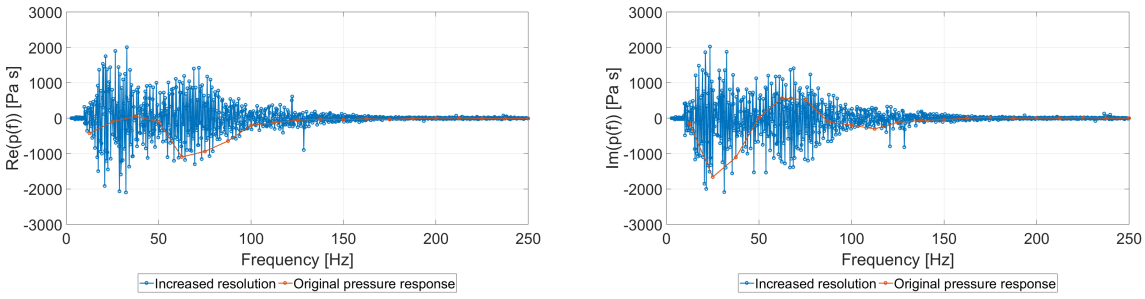

(a) Real part (b) Imaginary part

Figure 6.16: Pressure response spectra at 750 meters from the pile and 2 meters above the seabed

Strikingly, the response spectra for the location 30 meters from the pile compare relatively well. Although some frequencies are missed in the original response spectrum (depicted in figure 6.16a by the orange data), the original spectrum is highly accurate. When looking at the response spectrum for the 750 meters location this is totally not the case. A large amount of frequencies carrying energies are not described by the original spectrum. It was expected that frequencies were missed but that the data would be so scattered, was not anticipated, however evaluating the equation for the pressure response spectrum, the range dependent factor resulting in the scattering is clearly present (this will be further discussed in section 7.7). The trend of the response spectrum at the location close to the pile is not present at the location far from the pile. In order to determine how the response spectra develop in regards to range, the response spectra of locations 200, 300, 400, 500, 600 and 700 meters from the pile are analyzed as well. The response spectra are displayed in figure 6.17.

From figure 6.17 on this page (that displays the real part of the pressure response spectrum) and figure 6.18 on the next (that displays the imaginary part of the pressure response spectrum), it becomes clear that with increasing range the frequency response spectrum becomes more scattered and seams to introduce an oscillatory effect around the x axis. Additionally, the original response spectra, with the large frequency step, compare worse to the response spectra with higher resolution when increasing the range. This leads to the conclusion that with increasing range the resolution needed to accurately describe the response spectra increases as well. This makes sense because looking at a location far away from the pile the time between the first and the last pressure wave increases due to the difference in wave speeds. Additionally, the first cutoff frequency is confirmed as there is no energy located below $10Hz$ (the cutoff frequency as calculated with equation 2.1).

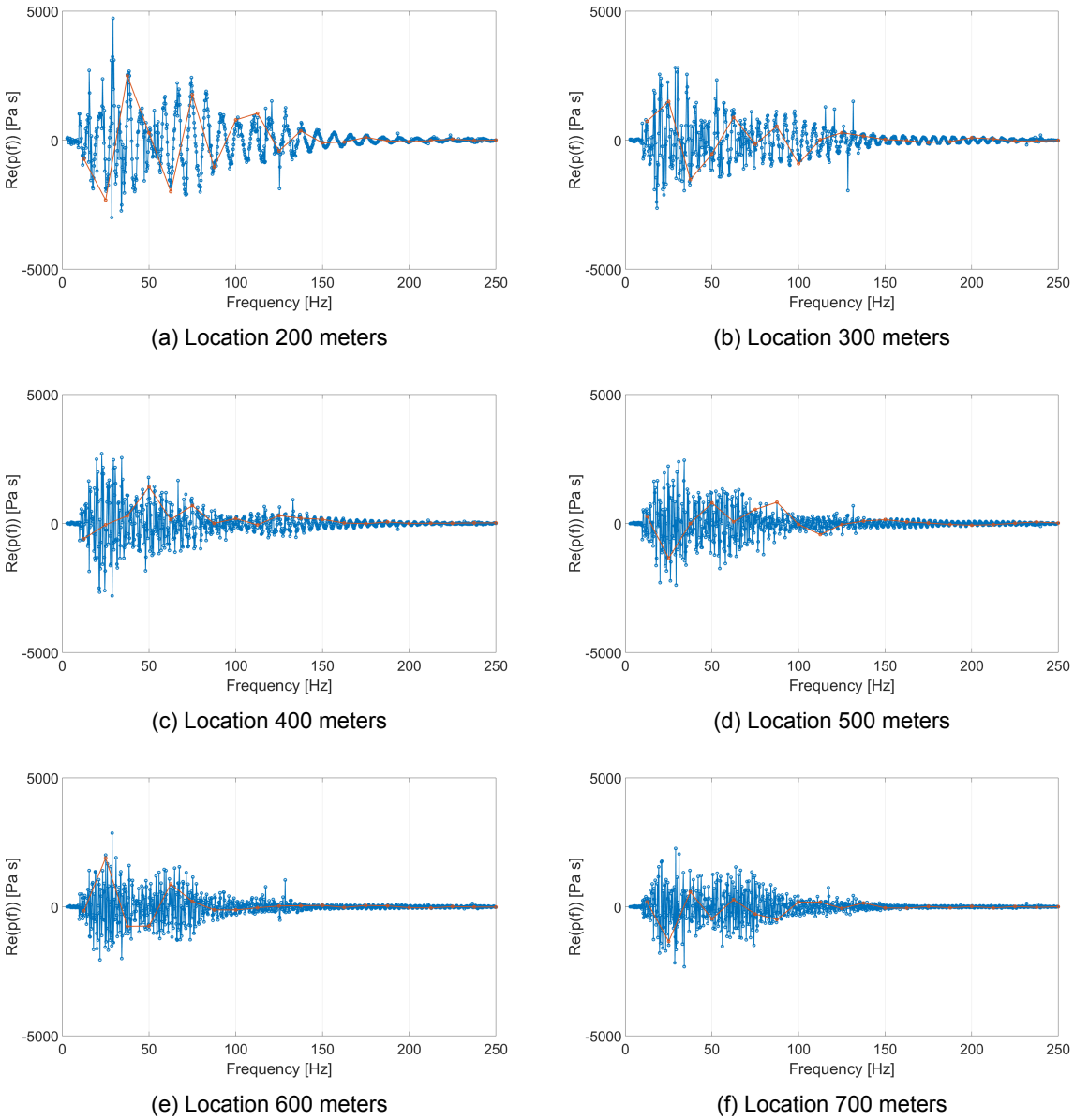

(a) Location 200 meters

(b) Location 300 meters

(c) Location 400 meters

(d) Location 500 meters

(e) Location 600 meters

(f) Location 700 meters

Figure 6.17: Real part of pressure response spectra at various ranges from the pile
With increasing range the response spectra become more scattered

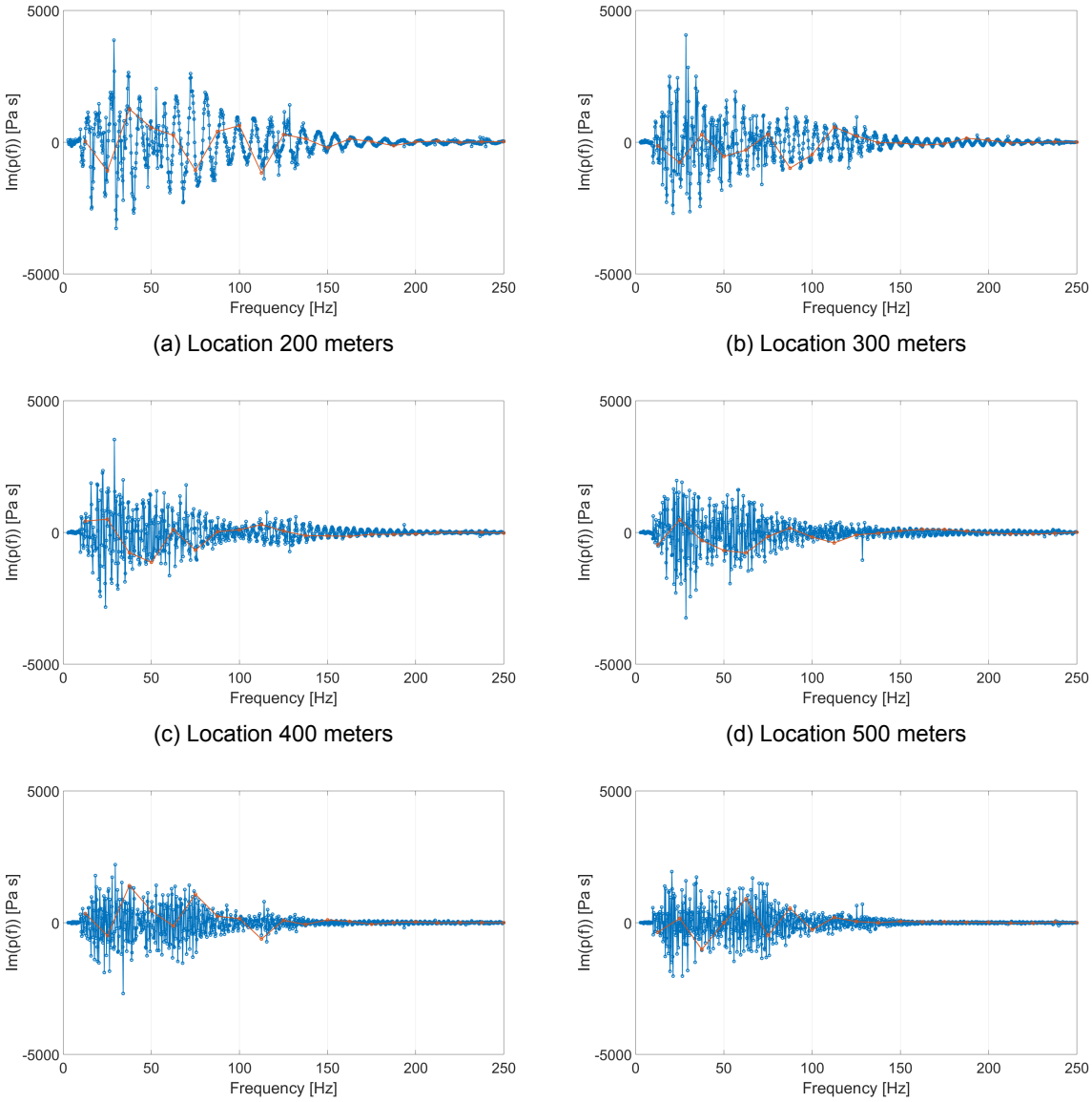

(a) Location 200 meters

(b) Location 300 meters

(c) Location 400 meters

(d) Location 500 meters

(e) Location 600 meters

(f) Location 700 meters

Figure 6.18: Imaginary part of pressure response spectra at various ranges from the pile
With increasing range the response spectra become more scattered

6.3.2. Time traces

To see how the frequency response spectra of section 6.3.1 describe the time traces for various ranges from the pile, they are transposed to the time domain with the inverse fourier transform. The results are analyzed in this section. First the short range and reference point, at 750 meters, will be examined, after which the same points, as in section 6.3.1 with increasing range, will be discussed.

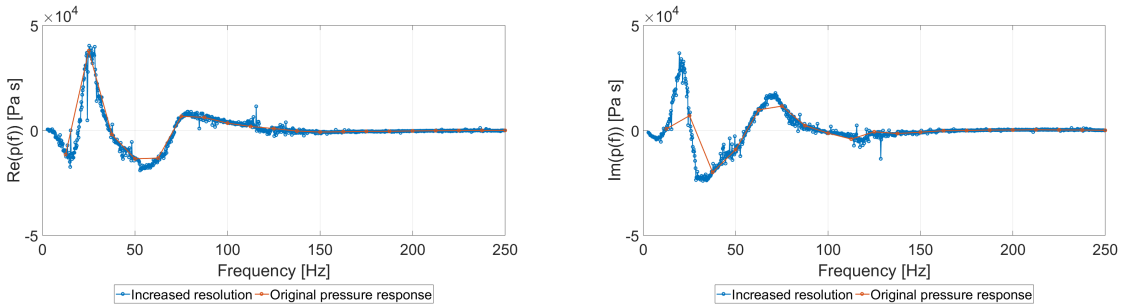

(a) Real part (b) Imaginary part

Figure 6.19: Frequency response spectra at 30 meters

First the short range location close to the pile (30 meters) will be examined. The frequency response spectra and the time traces they define are depicted in figure 6.19. The orange data is with the coarse frequency step ($12.5Hz$) and the blue data corresponds to the fine frequency step ($0.25Hz$).

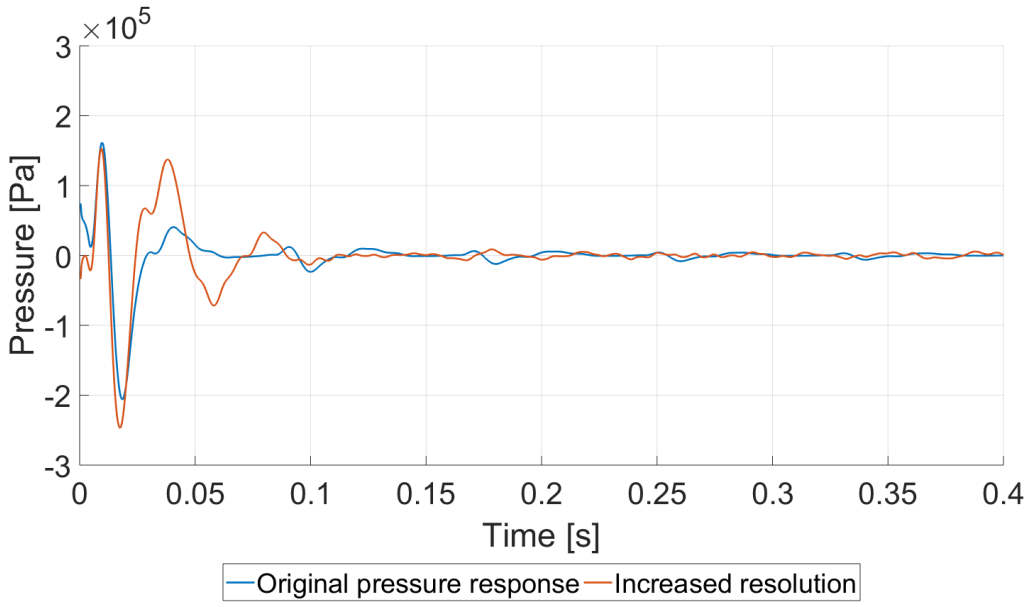

Figure 6.20: Pressure time traces of the original pressure response and of the pressure response determined by the spectra with high resolution. The time trace with the increased resolution gets rid of the error at the start $r = 30m, z = 2m$ above seabed

The first thing that is noticed is the fact that the time trace is only depicted up to $0.4s$. This is due to the fact that the pressure at this location reduces to 0 very quickly. Showing more time moments would only make the comparison less clear. It should be noted that the response

spectrum with the high resolution does accurately describe a time window up to $4s$. There is no repeating signal within this time window. Comparing the two time traces, it shows that the response spectrum with the coarse frequency step is in fact unable to describe the beginning of the signal and is missing the correct description of the second pressure wave, which is smaller than it should be. The time trace described by the high resolution spectrum accurately describes the pressure waves at this location and the error at the beginning of the signal is gone. This leads to the conclusion that the time trace is valid up to the $4s$ as expected.

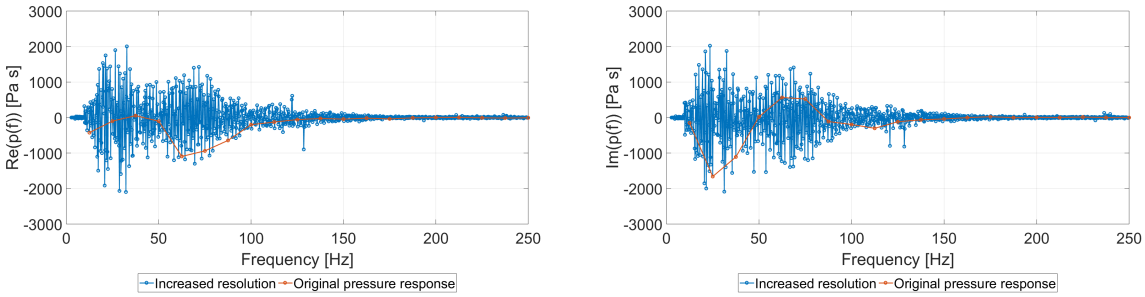

(a) Real part (b) Imaginary part

Figure 6.21: Frequency response spectra at 750 meters

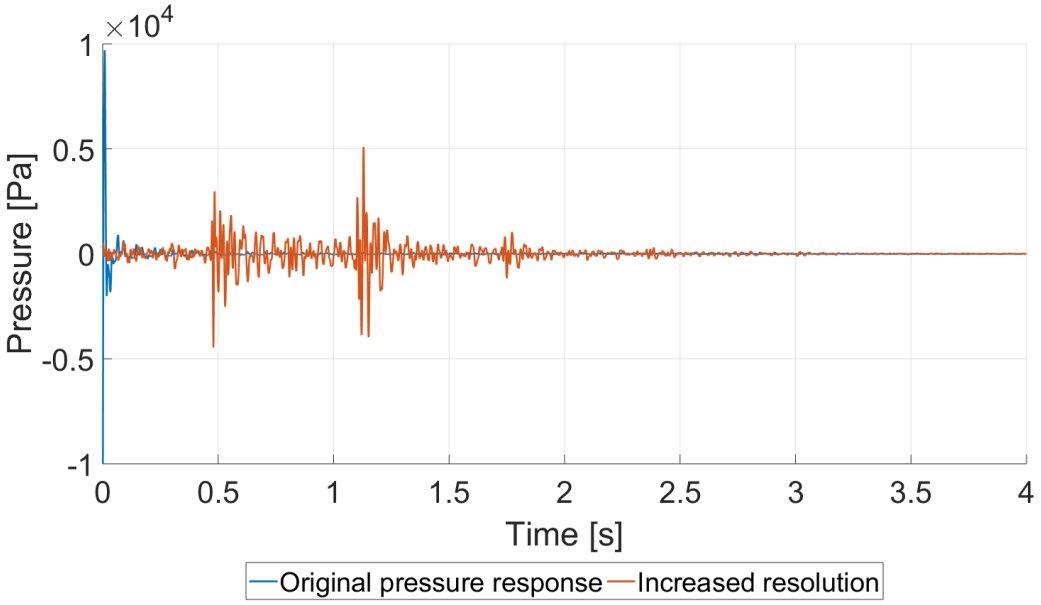

Figure 6.22: Pressure time traces of the original pressure response and of the pressure response determined by the spectra with high resolution. The time trace with the increased resolution shows an entirely different time trace and the first pressure wave arrives at a moment in time that is to be expected
$r = 750m, z = 2m$ above seabed

Next is the reference point at 750 meters from the pile. The result is displayed in figure 6.21, with the orange data equaling the coarse frequency step and the blue data as the high resolution spectrum. It is clear that the time trace with the coarse frequency spectrum is incorrect as concluded in section 8.1. The time trace defined by the response spectrum with high resolution does get rid of the errors of the earlier result. The first pressure wave arrives

at a moment in time that is to be expected (for more info see section 4.6). For a better analysis of this time trace, it is displayed by itself in figure 6.23.

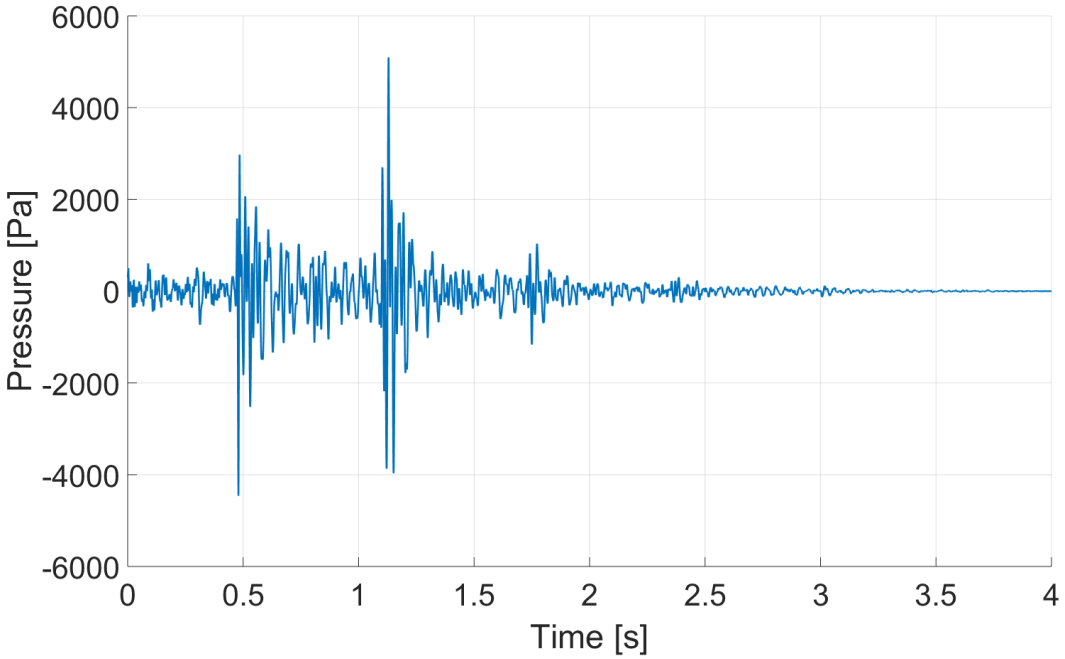

Figure 6.23: Pressure time trace determined by pressure response spectra with high resolution $r = 750m, z = 2m$ above seabed

To determine if the time trace signal calculated is accurate, the various visible wave fronts have to be explained. The first wave front arrives at $0.5s$ and corresponds to the compressional wave traveling through the water. The second wave front has not been predicted beforehand (section 4.6) and the Scholte wave front should arrive just before $3s$. In order to validate these statements, the evolution of these waves will be tracked by looking at points increasing in range from the pile up to the reference point of 750 meters. This is displayed in figure 6.24 on the next page. What can be concluded is that there is a primary pressure front that propagates, between the 300 and the 400 meter locations, a second and even a third pressure front become visible.

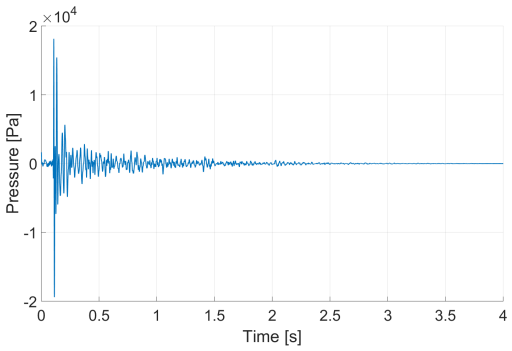

(a) Location 200 meters

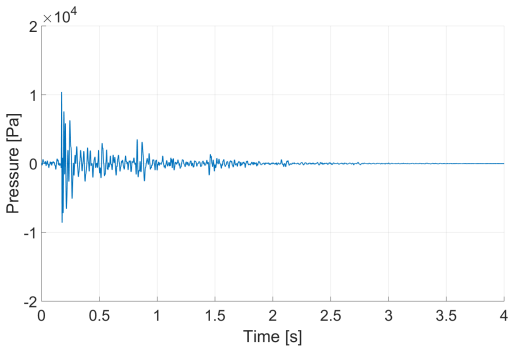

(b) Location 300 meters

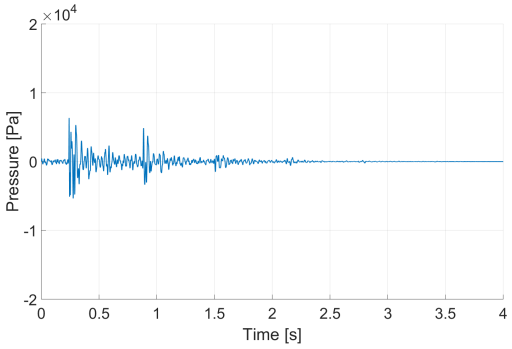

(c) Location 400 meters

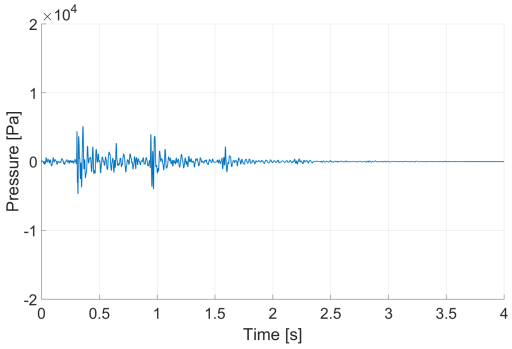

(d) Location 500 meters

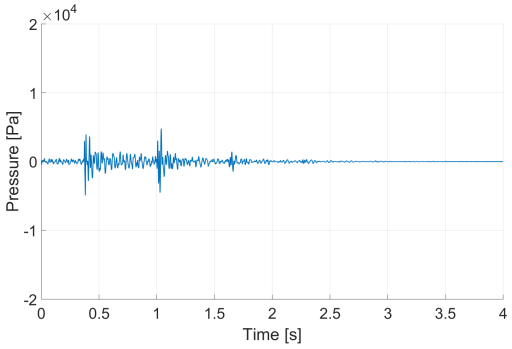

(e) Location 600 meters

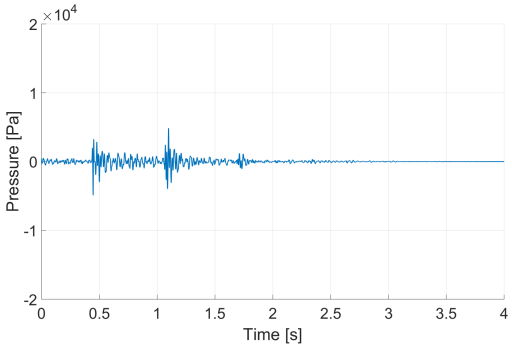

(f) Location 700 meters

Figure 6.24: Pressure time traces at various ranges from the pile
there is a primary pressure front that propagates, between the 300 and the 400 meter locations, a second and even a third pressure front become visible

Overlaying the pressure time traces allows for insight in how the pressure waves propagate. Figure 6.25 shows that the primary pressure wave decays with increasing range and that when the secondary pressure wave manifests from 300 meters and beyond this actually becomes the pulse with the highest pressure. Additionally a third pressure wave seems to arise at 500 meters, however it does not seem to be able to develop as the second pressure wave. The presence and magnitude of the secondary and even a small third wavefront were unexpected. These wave fronts seem to re-radiate into the water region via the soil region. However because of their magnitude it seems unlikely these are truly a physical phenomenon, further insight will have to be gained to explain these wave fronts further. This will be done in the parametric study (in chapter 7).

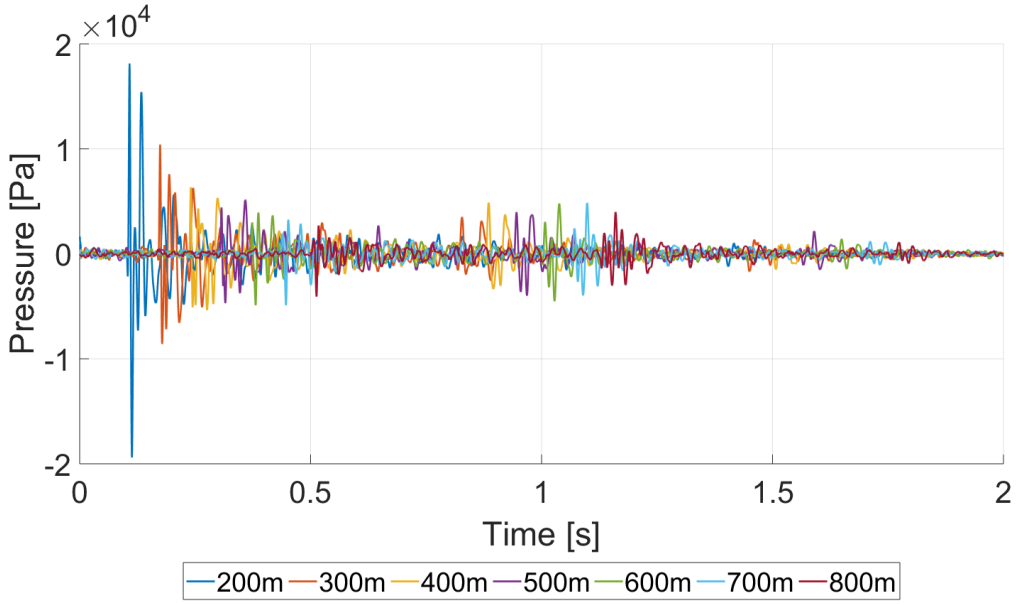

Figure 6.25: Overlaying pressure time traces from 200 up to 800 meters in steps of 100 meters
The primary pressure wave decays with increasing range. The presence and magnitude of the secondary and even a small third wavefront were unexpected

The time moments at which the Scholte wave should arrive were calculated in section 4.6. However it is impossible to identify the Scholte wave in the time traces of figure 6.24, therefore the location in the water column will be lowered to the point at the soil-water interface. This will be done in the following section.

6.3.3. Scholte wave

To be able to identify and analyze the contribution of the Scholte wave, the results at the soil-water interface have to be evaluated. The results are calculated for the same distances from the pile as before, 200, 300, 400, 500, 600 and 700 meters. The results are displayed in figure 6.26 and it should be noted that these are time traces of the vertical displacement of the soil.

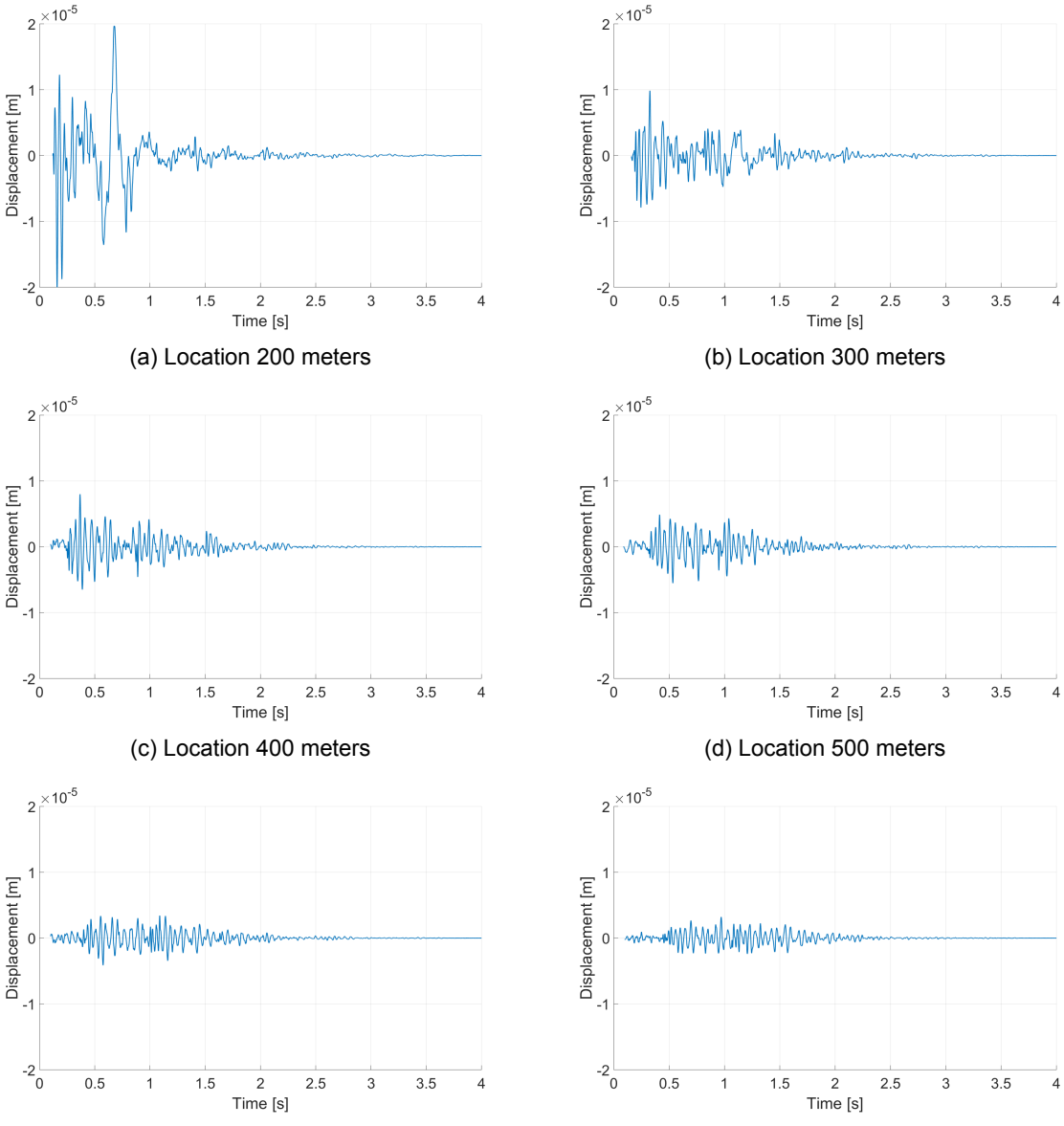

(a) Location 200 meters

(b) Location 300 meters

(c) Location 400 meters

(d) Location 500 meters

(e) Location 600 meters

(f) Location 700 meters

Figure 6.26: Vertical displacement time traces of the soil at various ranges from the pile at the soil-water interface For the locations between 200 and 400, the Scholte wave can be detected (the large vertical displacement with the longer period)

At first sight it is hard to identify the Scholte wave in the time traces above, therefore a closer look is needed. To start, figure 6.27 depicts the time trace of the 200 meters location. Here the Scholte wave would arrive around $0.76s$ as calculated in section 4.6. What is visible in the time trace is that indeed, a strong vertical motion is present around this moment in time. This is highlighted in figure 6.27 in orange. This can be the Scholte wave passing this location. To be able to track the evolution of this Scholte wave the succeeding points will be evaluated.

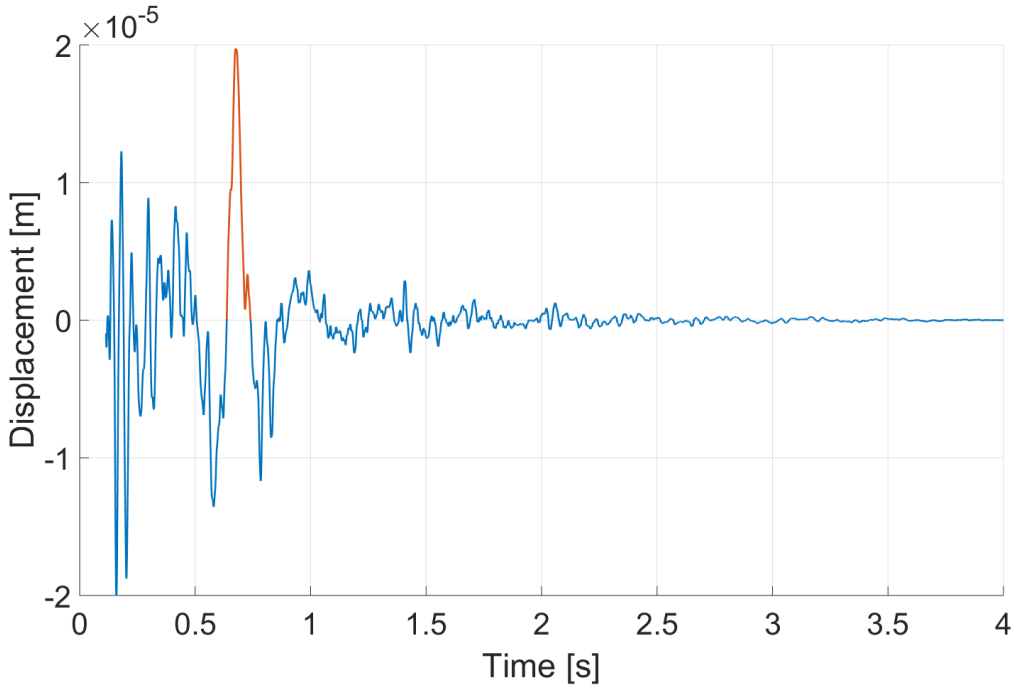

Figure 6.27: Vertical displacement of the soil at the soil-water interface at 200 meters from the pile
Highlighted in the figure is the Scholte wave

In figure 6.28 the vertical displacement at the location of 300 meters from the pile is depicted. At this location the Scholte wave would arrive around 1.15s (section 4.6). Again the highlighted part shows a steady vertical motion around this moment in time. It should be noted that it has decayed considerably.

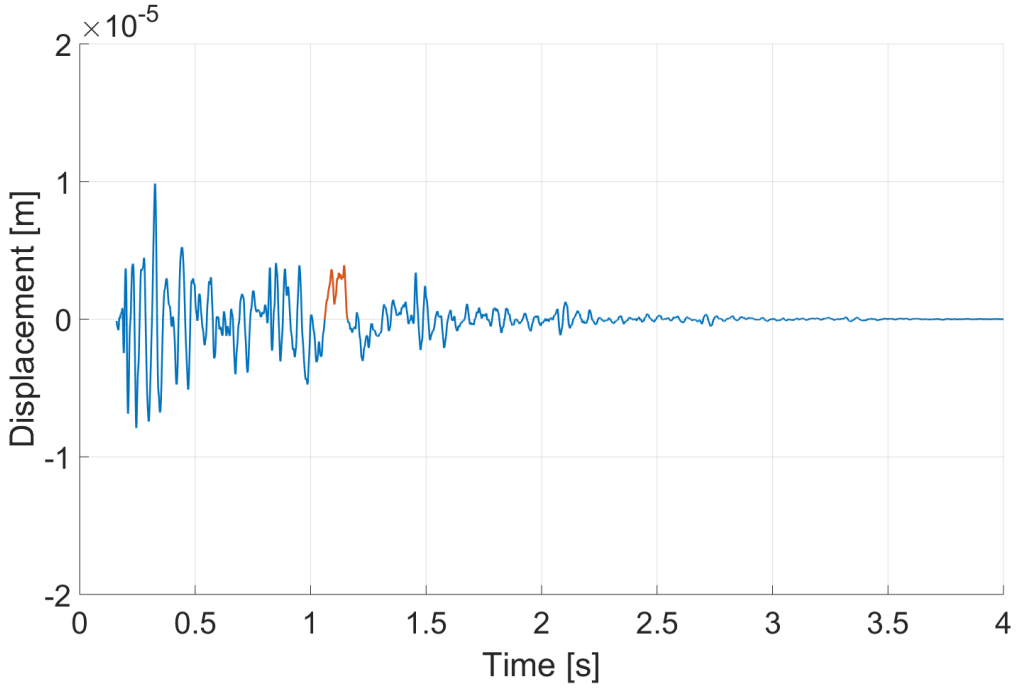

Figure 6.28: Vertical displacement of the soil at the soil-water interface at 300 meters from the pile
Highlighted in the figure is the Scholte wave

Finally, the locations 400 and 500 meters from the pile are analyzed in figure 6.29. At these locations the Scholte wave would arrive around 1.53s and 1.92s respectfully. At 400 meters from the pile a part is highlighted around the time the Scholte wave should arrive. However at this moment it is unclear if the vertical displacement depicted in the time trace is caused by the Scholte wave. It has decreased significantly and at the 500 meters location it has become impossible to identify any vertical motion caused a Scholte wave.

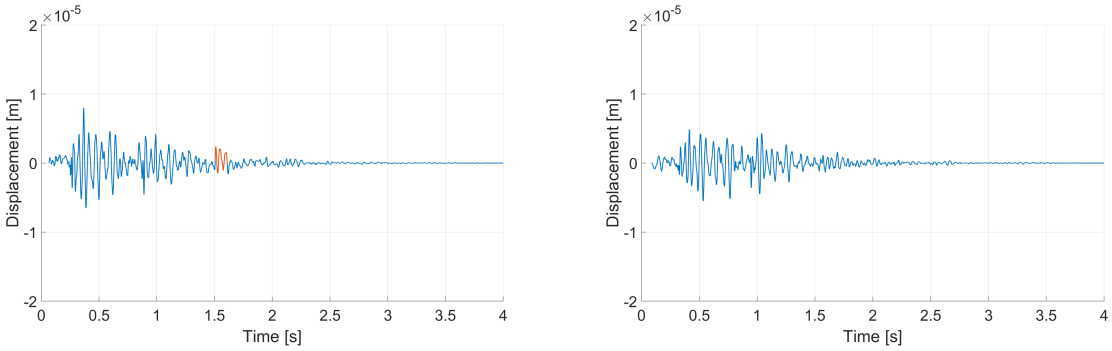

(a) Location 400 meters (b) Location 500 meters

Figure 6.29: Vertical displacement of the soil at the soil-water interface at 400 and 500 meters from the pile
Highlighted in the figure 6.29a is the Scholte wave, in figure 6.29b it is impossible to identify the Scholte wave

When evaluating if the Scholte wave is present up to the location of 750 meters and trying to determine the Scholte waves' contribution in the pressure response time trace, it can be concluded that the Scholte wave is not easily identified. It is hardly possible to pinpoint any contribution in the pressure response time trace and even in the vertical displacement time trace at the soil-water interface it seems that the Scholte wave is only present up to a range of 400 meters. This leads to the conclusion that the Scholte wave does not contribute significantly to the pressure response at a range of 750 meters from the pile, as it has been attenuated.

6.3.4. Sound levels

From the sound pressure time traces the sound levels can be calculated. This will be done for all locations to gain insight in the evolution of the sound levels with range. Additionally they will be compared to the sound levels that were measured during the installation of the wind farm Veja Mate and the extrapolation method for sound level prediction, that was applied to the model output before any changes were made, will be evaluated. The sound exposure levels are calculated with equation 6.1 derived from formula 2.10 and the peak level is defined by equation 2.2.4 from chapter 2.

$$SEL = 10log_{10}\left(\sum \frac{f(t)^2}{10^{-12}}dt\right) \tag{6.1}$$

Table 6.1: Sound exposure levels

Distance [m]	30	100	200	300	400	500	600	700	750	800
SEL [dB re 1 $\mu Pa^2 s$]	208.1	194.3	187.0	184.3	182.8	181.4	180.2	179.6	179.3	178.3
L_{peak} [dB re 1 μPa]	227.8	215.0	205.8	200.3	196.0	194.2	193.8	193.8	194.1	192.2

Table 6.1 states the Sound Exposure (SEL) and the peak level (L_{peak}) predicted by the model for points with increasing range from the pile. The SEL and L_{peak} decrease as they should, with quite a rapid decrease at locations close to the pile and with a smaller decrease when

looking a locations of 400 meters and above. It seems that the L_{peak} decreases at a smaller rate than the SEL, which continues to decrease at a constant, higher rate from 400 meters and on. This is illustrated by figure 6.30.

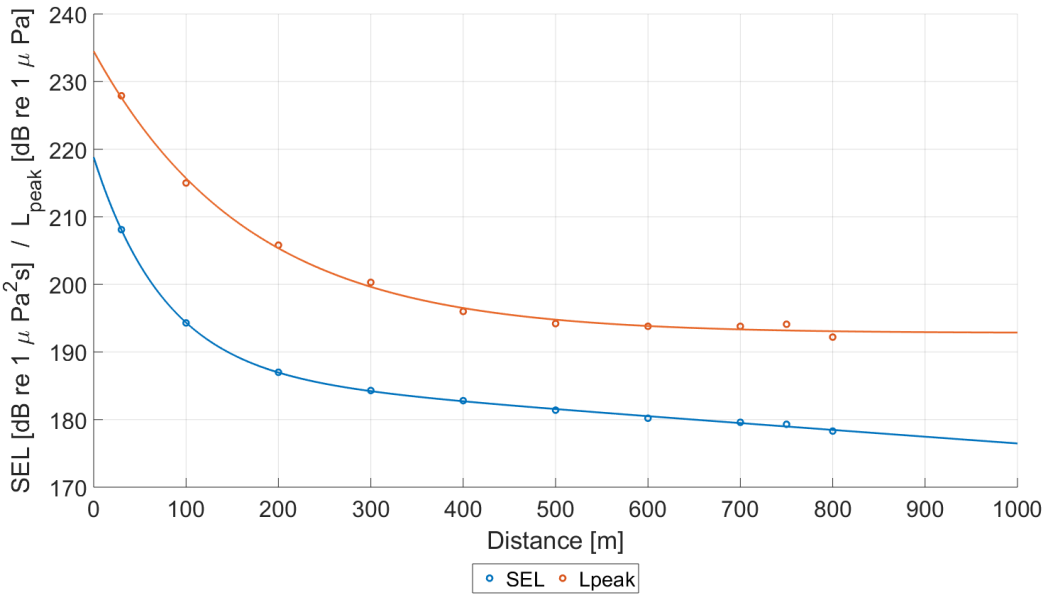

Figure 6.30: Sound exposure levels with increasing distance
The logarithmic trend with which the sound levels develop with increasing range is clearly visible

That the exposure level decays exponentially is no surprise. This logarithmic decay is actually the way the model results from close to the pile (up to 100 meters) were extrapolated to make predictions at farther locations before this graduation thesis. To be able to validate the calculated sound levels, they will be compared to the measured sound levels of the Veja Mate project base case of chapter 4. The measurements were done at 2 meters above the seabed and at 750 meters from the pile.

Table 6.2: Comparison of sound exposure levels, measured vs modeled

	Measured	Model prediction	$\Delta SEL/\Delta L_{peak}$
SEL	178	179.3	+1.3
L_{peak}	199	194.1	-5.1

Table 6.2 compares the sound levels predicted by the model and measured during the installation of the Veja Mate foundation pile. The results lead to the conclusion that the SEL compares well to the measured sound level. However, the peak level is underestimated. Although this seems like quite a large difference, it should be noted that the model predictions are based on only one simulation. The model can be calibrated to better represent the case study. Furthermore, to gain insight in the importance and sensitivity of the model a parametric study will be performed in section 7.

In section 6.3.3 it was concluded that the Scholte wave does not propagate up to the range of 750 meters and that it therefore will not have an influence on the sound levels at this location. This leads to the conclusion that the sound pressure level will be a result of the compressional waves traveling through the water. It is important to realize that the secondary

noise path, re-radiating into the fluid layer from the seabed, has a large contribution to the sound levels. However, up to now it is unclear if this secondary wave front is actually a physical phenomenon or a result of the model setup. This will be further investigated in chapter 7. To gain insight in the sound levels without the secondary wave front, they will be calculated with the time traces up to 1 second and is illustrated in figure 6.31. This will allow for a comparison to be made between the measured levels and the predicted values, of which it is clear they are defined by physical phenomena. The SEL and peak levels are calculated at the range of the reference point, 750 meters. The result are stated in table 6.3.

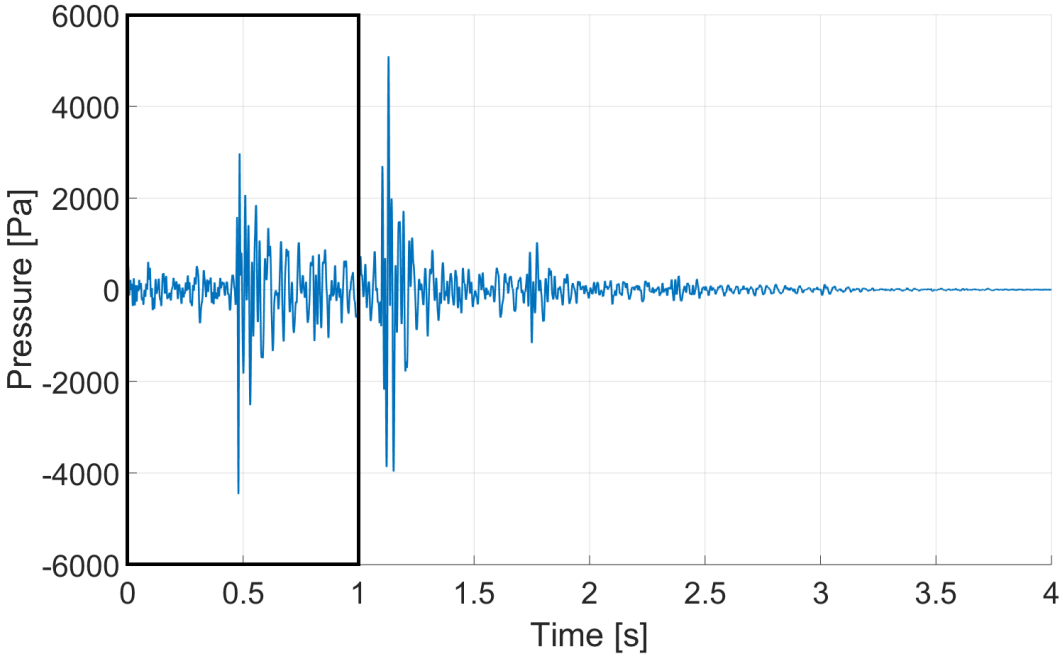

Figure 6.31: Time trace of the pressure at 750 meters and 2 meters above the seabed
The box indicates the time window within which the time trace is correct. The primary pressure wave arrives and outside the box a secondary pressure wave arrive and even a small tertiary front can be detected. However up to now it is unclear of its meaning and therefore the sound levels will be calculated with the smaller time window

Table 6.3: Sound levels calculated with the smaller time window, compared with the measured data

	Measured	Time window of 1 seconds	$\Delta SEL/\Delta L_{peak}$
SEL	178	175.5	-2.5
L_{peak}	199	192.9	-6.1

From table 6.3 it can be concluded that by capturing the primary wave train, the sound levels are somewhat underestimated. The peak level is determined by the primary pressure wave and will not increase when extending the time window. However, the sound exposure level could increase somewhat when the time trace is elongated. It is hard to do so as the physical meaning of the secondary wave front is still unclear. The conclusion that the Scholte wave does not have influence on the sound levels seems justified as there is no pressure wave visible around the time it would arrive, nevertheless the influence of the soil remains the large unknown and further study into its sensitivity will be done in the parametric study of the following chapter.

6.4. Conclusion

To begin, the frequency response spectra show that the increased resolution is of great importance to accurately describe the pressure time traces. The frequency response spectra for points close to the pile need less resolution than points located at farther locations. The coarse step size used in section 6.1 does not suffice. Even for the point located close to the pile ($30m$), the time trace shows an error. The shape does seem to be accurately described but it looks like it is somehow stretched and the second peak is lower than it should be. The high resolution spectra drastically improve the time traces for all points.

When overlaying the time traces of the pressure for points increasing in range a interesting phenomenon was identified. The primary pressure wave decays with increasing range but a secondary pressure waves increases and even becomes the main pressure wave, showing higher pressures than the primary pressure wave for the same location. This secondary pressure wave is the result of waves traveling through the soil and being re-radiated into the fluid layer. Additionally, a third pressure wave becomes visible from 500 meters and onwards, however this does not manage to develop like the secondary one. Up to now it is unclear if this secondary wave front is actually a physical phenomenon or a result of the model setup. For instance it could be a result of pressure waves traveling through the soil and reflecting from the rigid boundary at the bottom of the soil layer and then re-radiating back into the water region. Its magnitude is reason to remain skeptical of its physical meaning and therefore further investigation will be done in chapter 7.

It was hard to identify the Scholte wave from the pressure time trace and therefore the vertical displacement of the soil at the water-soil interface was studied. For a location of 200 meters from the pile the Scholte wave is definitely present and easy to identify. Increasing in range and looking at 300 meters from the pile, it becomes less obvious if and where the Scholte wave is present. It no longer stands out and has the same magnitude as the rest of the vibrations. When looking at the time traces for points even further from the pile the Scholte wave seems to loose its contribution to the overall vibrations and looking at 500 meters from the pile it has become impossible to identify the Scholte wave. This leads to the conclusion that the Scholte is attenuated for locations of 500 meters or more. It should be noted that this is based on a single case study where the soil attenuation factors are still one of the large unknowns. Additionally, the soil elasticity will have a significant effect on the speed with which the Scholte wave travels and therefore the range it can reach. Chapter 7 will investigate the attenuation factor's influence further.

The sound levels predicted by the model and measured at the Veja Mate wind park when installing the foundation pile, were compared and it was determined which pressure waves contribute most to the sound levels. The sound levels decay with increasing range and this decay can be estimated with a logarithmic function. Comparing the model predictions with the measurements led to the conclusion that the model is capable of performing a reasonable estimation of the sound levels that will be produced. The sound exposure level (SEL) was slightly over estimated by 2 dB re 1 $\mu Pa^2 s$ and the peak level was underestimated by approximately 5 dB 1 re μPa. Although this seems like quite a large difference, it should be noted that this is based on only one calculation and this peak level is reached by the secondary pressure wave re-radiating into the fluid layer. A calibration of the soil could lead to better estimates regarding the peak level. A further analysis of the time trace at the 750 meters location resulted in the conclusion that by capturing the primary wave train, the sound levels are actually underestimated. The peak level is determined by the primary pressure wave and will not increase when extending the time window. However, the sound exposure level could increase somewhat when the time trace is elongated. It is hard to do so as the physical meaning of the secondary wave front is still unclear. The conclusion that the Scholte wave does not have influence on the sound levels seems justified as there is no pressure wave visible around the time it would arrive, nevertheless the influence of the soil remains the large unknown and further study into its sensitivity will be done in the following chapter.

7

Parametric study

To see how sensitive the Elastic Medium Model is, a parametric study was performed. The results will be discussed in this section. In the graduation thesis of Van Rhijn (2017), a similar parametric study was performed. The conclusions from that study showed that the soil attenuation factors and the setup of the model with two soil layers had little to no effect on the sound pressure levels. However the sensitivity study of the soil elasticity led to the conclusion that it is of high importance. The influence was large at frequencies below $200Hz$ and at locations close to the soil-water interface. This is confirmed by the parametric study done by Tsouvalas (2015), who did a similar analysis. Because it was not yet possible to accurately predict the pressure response spectrum for large distances from the pile, the sensitivity study of the attenuation factors will be reproduced and evaluated for the reference point at 750 meters. Additionally the influence of the penetration depth of the pile in the soil and the bottom rigid boundary will be analyzed to improve insight in the time traces gained in section 6.3.2. Furthermore, simple scaling of the input force will be performed to investigate if the sound levels, measured at Veja Mate, can be achieved by increasing the input force and the computational time will be considered. The chapter will finish with a discussion.

7.1. Penetration depth

The influence of the penetration depth is an interesting property to examine as the sound levels produced when the pile's penetration depth is small will definitely not be same as the sound levels when the pile is nearly fully installed and has reached its final depth. This is because the soil has a large contribution in propagating the pressure waves, particularly propagating the energy at low frequencies, and with a small penetration depth little energy will be introduced to the underwater environment. A second reason for investigating the penetration depths' effects is to explain the various pressure fronts present in the pressure time traces of section 6.3.2. More specifically, the secondary front detected was related to re-radiating pressure waves, leaking from the soil into the water layer and even a third pressure wave was identified which still has to be explained. These waves originate from the section of the pile that is penetrated in the soil, therefore the penetration depth should have a clear effect on these wave fronts.

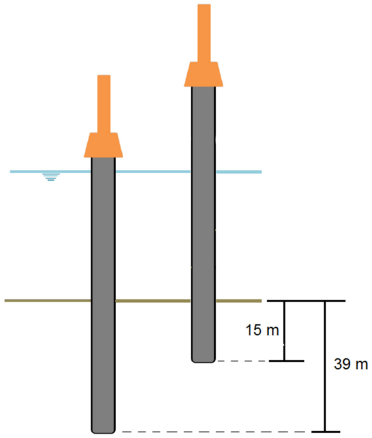

Figure 7.1: Case study with various penetration depth, 15 and 39 meters

To analyze the effect of the pile penetration, the depth, to which the pile has penetrated the soil, is reduced to 15 meters in contrary to the original 39 meters. Although the input energy of the impact hammer often varies at different stages of installation of the pile (the further the penetration, the higher input energy is required), the input energy is assumed to be the same for both cases investigated here. This is justified by Van Rhijn (2017), who investigated the effect of the soil resistance on the impact diagram. The setup of the two conditions is illustrated in figure 7.1. The results of both case studies is depicted in figure 7.2. It displays the pressure time trace at a location 700 meters from the pile and 2 meters above the seabed.

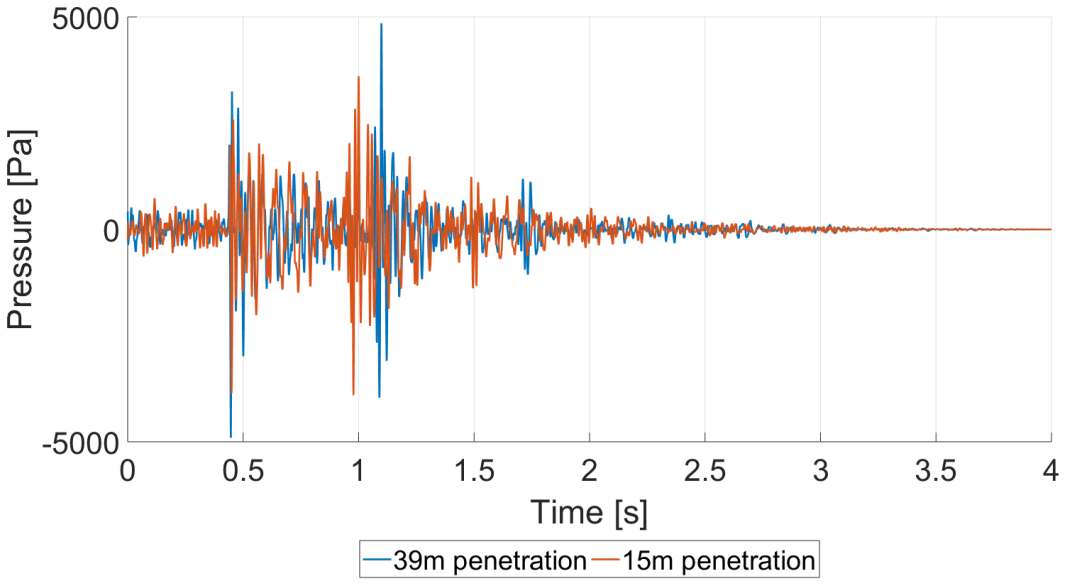

Figure 7.2: Pressure time trace for different penetration depths of the pile
The arrival of the primary pressure wave remains the same, but the secondary and tertiary wave fronts shift in time due to the lower penetration depth
r = 700m, z = 2m above seabed

Analyzing the results in figure 7.2, the first pressure front coincides for both time traces. This is logical as this is the pressure front traveling through the water layer and little to no

change of this pressure front was to be expected. The secondary and tertiary wave fronts do show a difference. This confirms the suspicions that the pile penetration depth would have an influence on these wave fronts. The results show that when the penetration depth is smaller, the secondary and tertiary wave fronts manifest quicker. This is consistent as the distance these waves have to travel has become smaller. To further check this phenomenon the pressure time traces of various ranges are evaluated to see if the secondary and tertiary wave fronts appear at a shorter range. This is depicted in figure 7.3. The secondary wave front manifested itself at a range of 300 meters and the tertiary wave front was first detected at a range of 500 meters with the penetration depth of 39 meters (section 6.3.2).

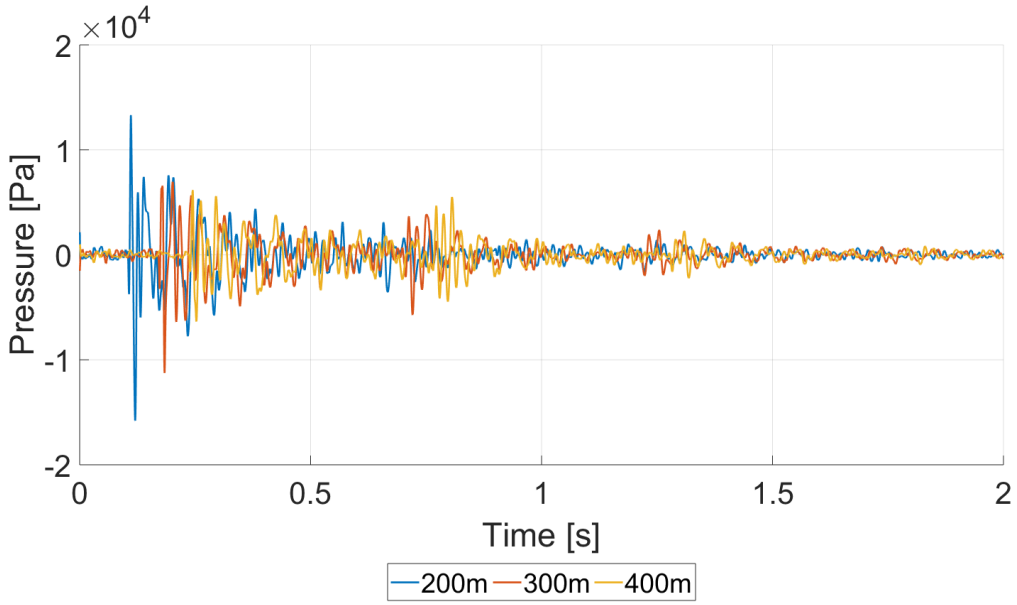

Figure 7.3: Pressure time traces for various ranges from the pile with a penetration depth of 15 meters z = 2m above seabed

From analyzing the result in figure 7.3 it becomes apparent that the secondary wave front can be detected at 200 meters, appose to the 300 meters before, and the tertiary wave front, that was only detected at 500 meters in the first case study, now can be detected at a range of 300 meters. This confirms the statements above that the secondary and tertiary wave fronts are related to the pile penetration depth, with an increasing depth resulting in later and farther re-radiation of the pressure waves traveling through the soil.

7.2. Rigid boundary impact

The influence of the rigid boundary is an important effect to examine, to be able to truly weigh the importance of the secondary and tertiary wave fronts identified earlier. For instance, the these waves are clearly dependent on the penetration depth and to see if these waves travel through the soil and into the water layer with or without reflecting at the rigid boundary, would change their importance quite significantly.

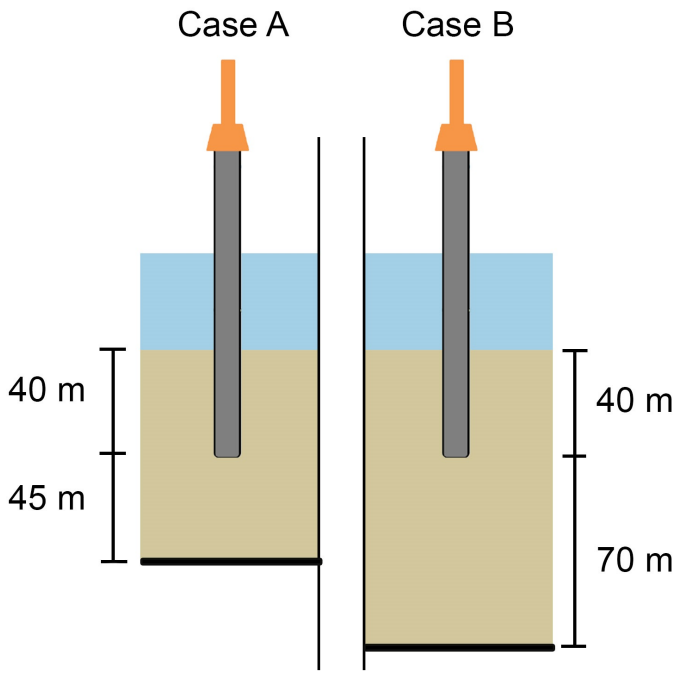

Figure 7.4: Setup of the parametric study to investigate the effect of the rigid boundary

To investigate what the influence of the rigid boundary is, it is lowered, this is depicted if figure 7.4. The time trace will be compared to the original at a location of 700 meters from the pile and 2 meters above the seabed as before. The result is displayed in figure 7.5.

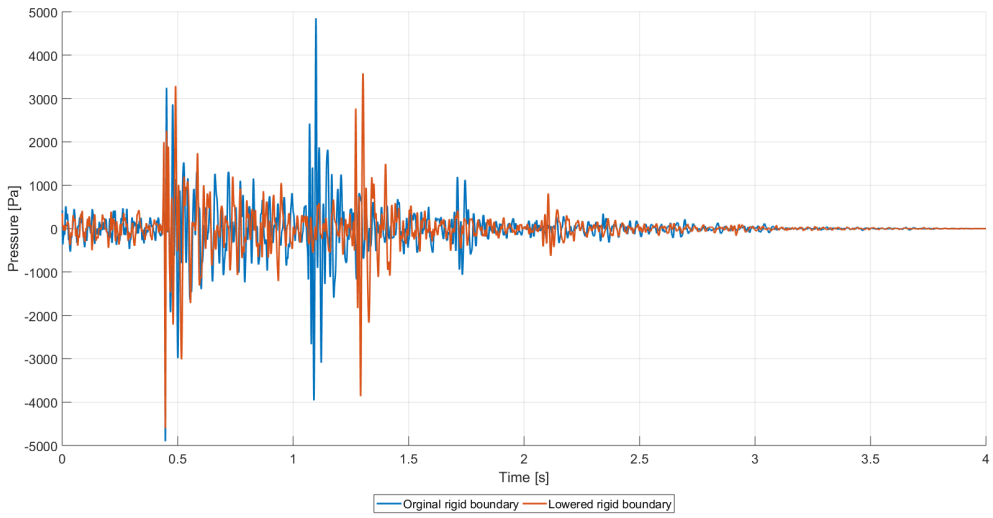

Figure 7.5: Pressure time trace for different depths of the rigid boundary
Clearly the second and third wavefronts are influenced by the lowering of the boundary
It can be concluded that these wavefronts are reflected from the rigid boundary
r = 700, z = 2m above seabed

Figure 7.5 clearly shows the relation between the rigid boundary and the secondary and tertiary wavefronts. By lowering the boundary, these wavefronts are delayed and therefore, it can be concluded that these wavefronts are actually reflected of the rigid boundary. It

is remarkable that these waves are so significant, as it wasn't expected that waves traveling through the soil, other than the Scholte wave, would have such a contribution to the pressure in the water layer. This could be due to the fact that the soil is modeled as fluidized layer with a soil elasticity that isn't very high. Additionally, it remains the question how physical these reflected waves are, because in practice there is no rigid boundary in the seabed. However, different soil layers are present and if the layers differ significantly in density, it could be possible that waves would reflect of the interface between those layers. Furthermore, when evaluating the sound levels without the secondary and tertiary wavefronts, the sound levels are underestimated, just like the fluid models underestimate the noise levels. By neglecting the secondary and tertiary wavefronts and remembering that the Scholte wave had little to no impact on the sound levels (6.3.4), one would effectively be evaluating the time trace of a fluid model.

7.3. Soil attenuation factor

As mentioned numerous times before, the soil properties are of large importance to accurately capture the wave propagation through the seabed. Mainly, the Scholte wave propagation which introduces energy that re-radiates into the water region and can contribute to the sound levels in that way. Unfortunately, the soil properties are also the hardest to model correctly as they can vary significantly in radial and vertical direction. Therefore, the attenuation factor, especially for the shear waves, is still one of the largest unknowns in this complicated case study. To analyze the sensitivity of this parameter and see if the Scholte wave is able to propagate up to the large distance of the reference point (at $750m$), the attenuation factor for the shear wave is lowered. Table 7.1 states the original and altered case study soil characteristics.

Table 7.1: Parameters for the two cases studied examining the effect of the attenuation factor for the shear waves

	E	ν	ρ	c_p	c_s	α_p	α_s
	MN/m^2	-	kg/m^3	m/s	m/s	dB/λ	dB/λ
Case A	400	0.485	2000	1520	260	1.2	3.8
Case B	400	0.485	2000	1520	260	1.2	1.1

The results from the two cases is plotted in the figure 7.6 and figure 7.7 on the next page. Figure 7.6 depicts the pressure time trace at 200 meters and 750 meters from the pile and 2 meters above the seabed. It becomes clear that the time traces are barely influenced by the lowering of the attenuation factor for the shear waves.

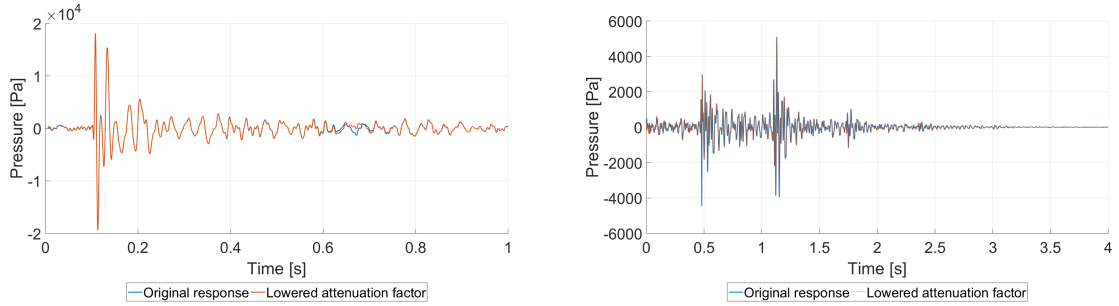

(a) $r = 200m, z = 2m$ above seabed

(b) $r = 750m, z = 2m$ above seabed

Figure 7.6: The effect of the stronger Scholte wave is small at $200m$ and non existing at $750m$

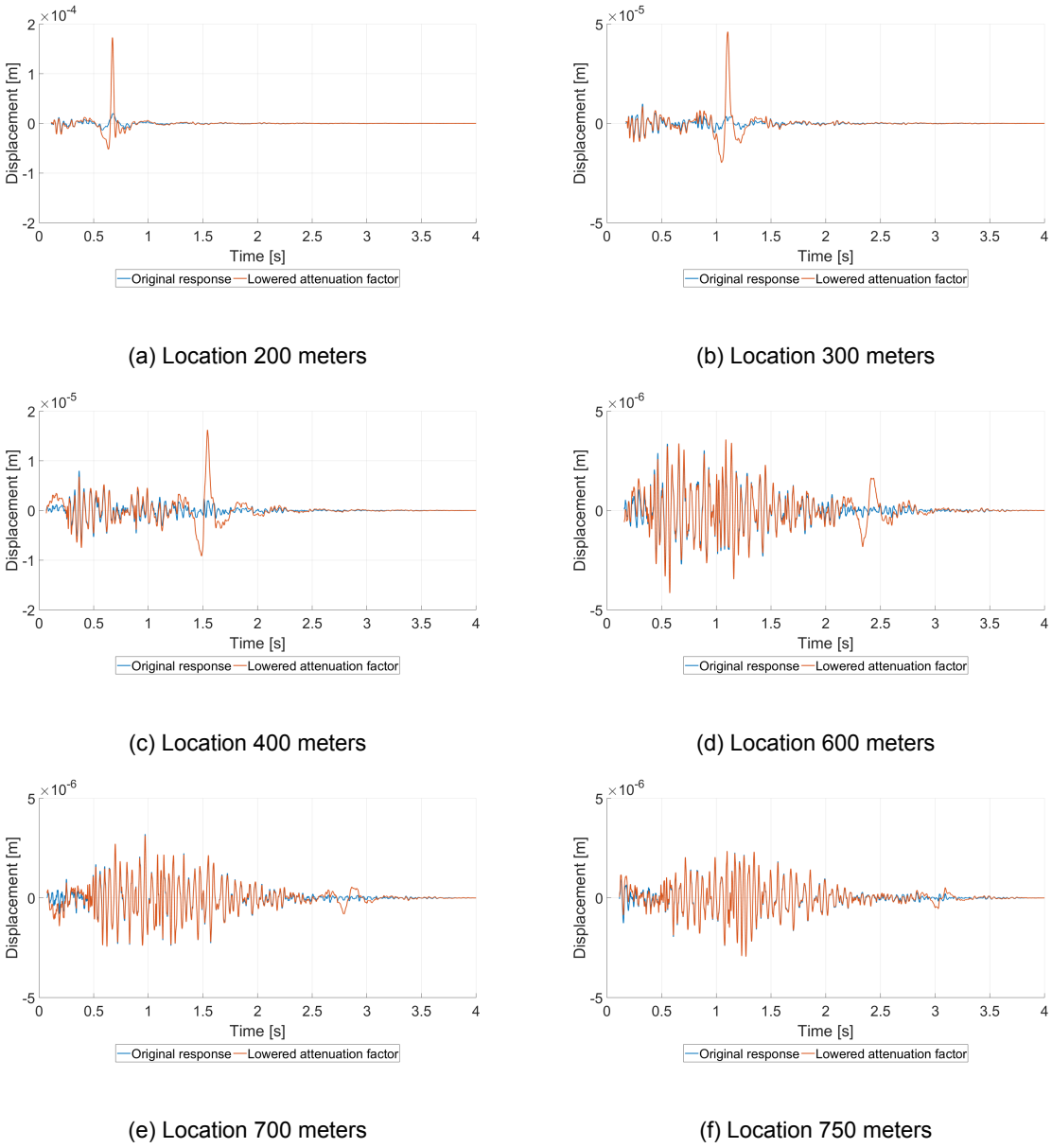

Figure 7.7: The effect of the lowered attenuation factor for the shear waves on the vertical displacement of the soil at the seabed. The Scholte wave is clearly visible and has grown significantly, it can be concluded that the Scholte wave can even travel up to a distance of 750 meters

Figure 7.7 shows that the vertical displacement is significantly influenced. The Scholte waves, identified in section 6.3.3, are confirmed and have grown as the attenuation factor has been lowered. With the large increase of the Scholte wave one would expect it to have a significant impact on the pressure time traces as well, however this is not the case. Its effect is visible but minimal for small range locations as 200 meters, but will certainly not have an influence on the sound levels at locations at large distances from the pile, where the time trace remains exactly the same. Furthermore, the case with the lowered attenuation factor does show that the Scholte wave is capable of traveling up to large distances. Knowing that the soil and its properties are one of the large unknowns in this kind of noise propagation simulations and the fact that this study has only covered a few case studies, further investigation should be done into the properties of the soil and their effect on the Scholte wave, pressure signal and finally the sound levels.

7.4. Scaling the impact force

From section 6.3.4 it was concluded that the sound peak level is fully determined by the primary pressure wave traveling through the water. It was also noted that the difference between the measured and the predicted value were quite large. To gain insight in what the influence of the impact force on this peak level is, it is possible to scale the input force in order to reach the same peak level measured as predicted. This scaling is rather straightforward as the relation between the input force diagram and the pressure time trace is linear, so by scaling the input force with a factor x, the pressure time trace scales with the same factor. When the pressure time trace is redefined, the sound levels will be calculated again and compared to the measured ones from Veja Mate. This factor will be increased until the predicted value of the sound peak level matches the measured one. The results are displayed in table 7.2 below.

Table 7.2: Scaling the impact force to match the predicted sound peak level with the measured one

	Measured	Original	Factor 1.1	Factor 1.25	Factor 1.5	Factor 1.75	Factor 2
L_{peak}	199	192.9	193.8	194.9	196.5	197.8	199.0
SEL	178	175.5	176.3	177.4	179.0	180.3	181.5

From table 7.2, it can be concluded that to match the predicted sound peak level with the measured one, the input force has to be scaled with a factor 2. This is very large and cannot possible be correct. This would result in an input force that is far larger than the one used during the Veja Mate project. Additionally, when doing so, the sound exposure level is overestimated considerably. It is unrealistic that the input force has to be increased so significantly, however the impact diagram that is used, is rather smooth and idealized. In reality the impact diagram of the force can be much coarser, which would excite other frequencies, namely higher ones. These higher frequencies can contribute to the primary pressure wave and as a result enlarge the sound peak level. Instead of using the idealized impact diagram, it would be worth looking into using a measurement of an impact hammer performing the actual installation.

7.5. Conclusions

The parametric study has provided more insight in the pressure time traces that are calculated by the Elastic Medium Model. The physical meaning of the secondary and tertiary wave fronts, identified in previous chapter, has been found. It was concluded that these wave fronts were traveling through the soil and re-radiating into the water region. The lowering of the rigid boundary showed that this delayed their time of arrival and diminished their contribution to the pressure time trace. This led to the conclusion that these waves were reflecting from the rigid boundary, which was, in this configuration of the model, unphysical. However it should be noted that this does indicate the contribution reflecting waves could have when they reflect from, for example, rocks or impermeable layers. Additionally, the lowering of the attenuation factor for the shear wave showed that it is possible for the Scholte wave to travel up to large distances. It was possible to identify it at the reference point of 750 meters, by looking at the vertical displacement on the seabed. Nevertheless, the Scholte wave did not effect the pressure time trace and it remains the question if it is possible to do so. Further study investigating the various soil parameters like soil elasticity and layering of various soil layers should be done to gain more insight in these phenomena. The soil and namely the attenuation factors for the shear waves remain large unknowns. Furthermore, the scaling of the input force showed that it would require the force to increase excessively to match the predicted sound peak level with the measured one, but the idealized impact diagram used, could misrepresent the actual impact force executed by the hammer.

7.6. Computational time

The computational time of the model is of great importance. The computational effort required for acoustic calculations is traditionally very high. With the original setup of the model is was impossible to be able to accurately make predictions for a range of 750 meters. This was mainly due to the large amount of steps (frequencies) that were required to do so. For example to simulate up to 4 seconds with the fine frequency step of $0.25Hz$, a total of 1000 steps are needed. This amount of steps would require a memory allocation that is too high for any standard computer and would need a long computational time to run. The computational time scales exponentially with the increase of the amount of steps. By running the Elastic Medium Model in frequency bins with each 100 frequencies the total computational time was brought down significantly. Each calculation took between the 90 and 150 seconds, adding up to a total less than 24 hours. This is a large improvement to before. Largely due to the fact that frequencies that do not carry energy are no longer calculated.

7.6.1. Response to unit force

The model has an option to simulate the response to a unit force. This unit force is actually a frequency spectrum with the value of 1 for all frequencies, illustrated in figure 7.8. This unit force does not have a physical meaning however it has a significant benefit, because once the response to this unit force is known in the frequency domain, this response spectrum only has to be multiplied with a force spectrum of any force to determine the response to that force. This saves valuable computational effort as it can reduce the amount of simulations to be run to one, when evaluating different impact or vibratory hammers for optimizing the installation method.

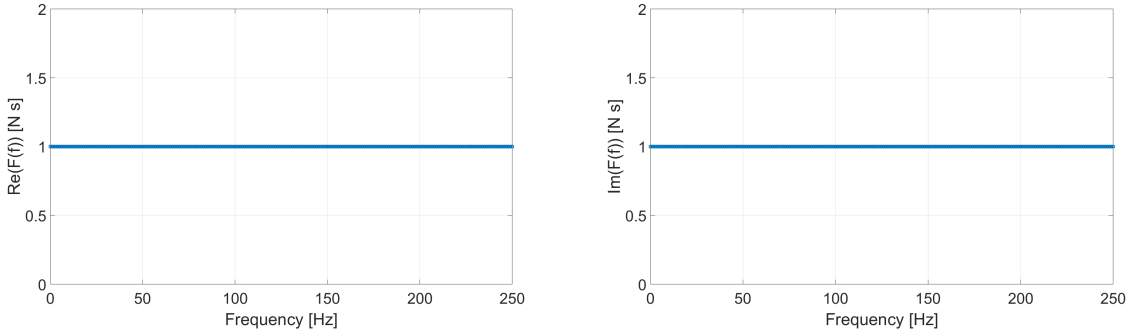

(a) Real part (b) Imaginary part

Figure 7.8: Unit force spectra representation

7.7. Discussion

It became clear in the result analysis that the resolution of the response spectrum has to increase with range to accurately describe the time traces. This range dependency was not anticipated. It was expected that the resolution had to increase and that with higher resolution the output would quickly improve. When the resolution was increased to a step size of $0.25Hz$, the time trace became significantly better. It was not anticipated that even higher resolution would be needed to arrive at a trend for the response spectra like the trend that was seen at the short range location (section 6.3.2). However there still is a spacial factor that introduces scattering of the data of the response spectrum with increasing range. Therefore, the definition for the pressure output will be reevaluated. The pressure output, in the frequency domain, is defined in equation 7.1 (Tsouvalas, 2015).

$$\tilde{p}_f(r,z,\omega) = \sum_{p=1}^{\infty} C_p H_0^{(2)}\left(k_p r\right) \tilde{p}_{f,p}(z) \tag{7.1}$$

The pressure is defined by spacial variables r and z,the angular frequency and the con-

stant C_p. The solution can be split into two main components, namely the pressure component $\tilde{p}_{f,p}(z)$ in the frequency domain varying in vertical position z and the Hankel function $H_0^{(2)}\left(k_p r\right)$ defined by the wave numbers k_p and horizontal position r. The first can be analyzed by looking at the absolute part of the response spectrum and the second will be evaluated by the wave numbers.

$$\tilde{p}_f(r,z,\omega) = \sum_{p=1}^{\infty} C_p H_0^{(2)}\left(k_p r\right) \underbrace{\tilde{p}_{f,p}(z)} \tag{7.2}$$

First the underlined part of equation 7.2 will be discussed. This will be done for all the locations evaluated earlier. This can be done by assessing the absolute frequency response spectra ($|\tilde{p}_f(r,z,\omega)|$) at all these locations. This part of equation 7.1 should not dependent on range.

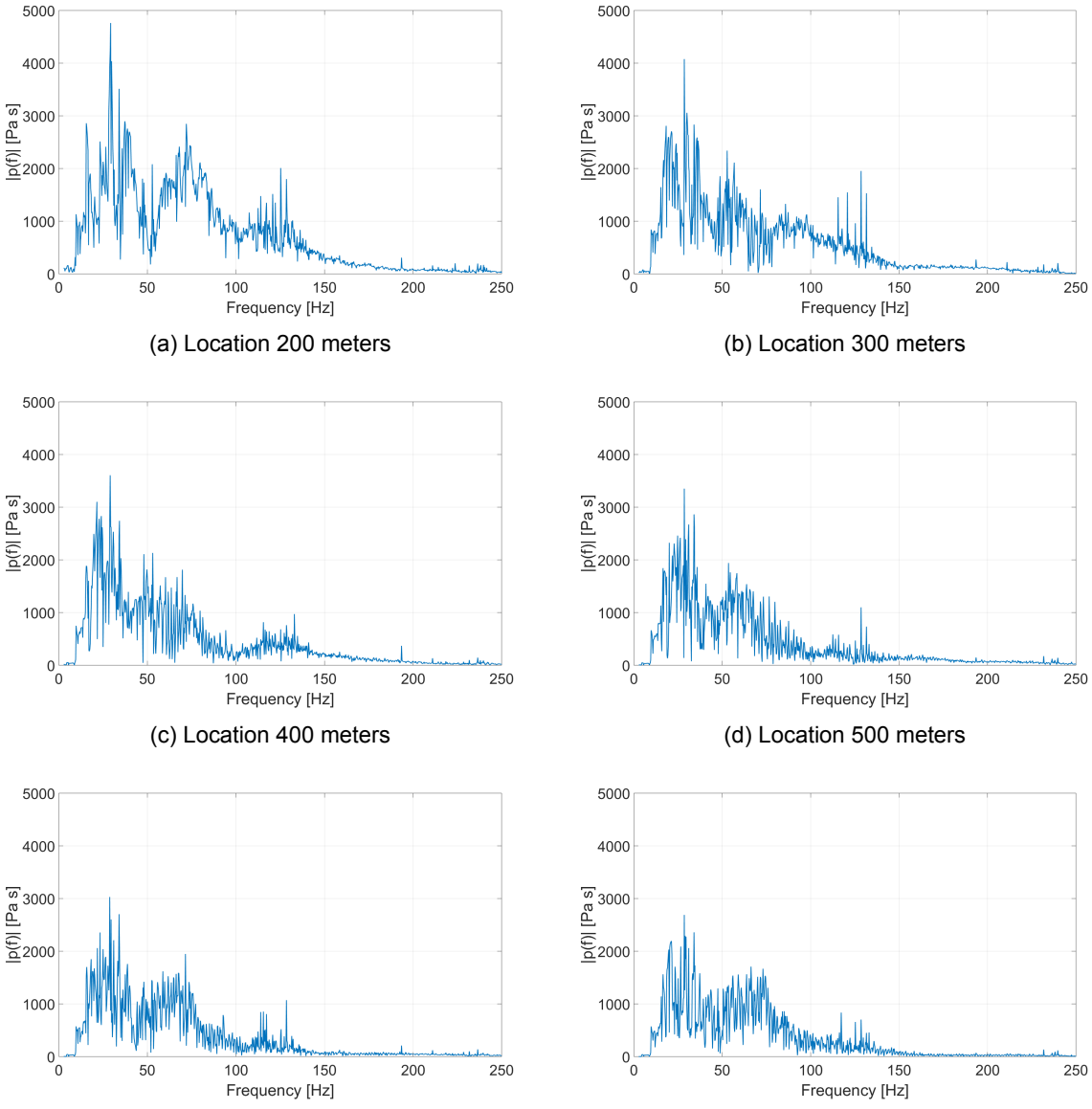

(a) Location 200 meters

(b) Location 300 meters

(c) Location 400 meters

(d) Location 500 meters

(e) Location 600 meters

(f) Location 700 meters

Figure 7.9: Absolute response spectra for various distances
Although it is clear that the spectra aren't equal for all the locations, they do not vary much. It spatial influence on the absolute spectra is present because it is not totally independent of the Hankel function, however it does show that they are similar

Figure 7.9 depicts the absolute pressure response spectra at various locations from the pile. It is striking that the output is still quite scattered. A smooth function independent of range was expected. However it is clear that the absolute part of the pressure response ($|\tilde{p}_f(r,z,\omega)|$) is not range independent. This is due to the fact that the Hankel function is partly contributing to this absolute pressure response.

Next the underlined part displayed in equation 7.3 will be discussed. This part of equation 7.1 is dependent on range.

$$\tilde{p}_f(r,z,\omega) = \sum_{p=1}^{\infty} C_p \underbrace{H_0^{(2)}\left(k_p r\right)} \tilde{p}_{f,p}(z) \tag{7.3}$$

To gain insight in how this part is determined by range, equation 7.4 shows the definition of the zeroth order Hankel function given by Abramowitz et al. (2015).

$$H_0\,(kr) = -\frac{2i}{\pi}\int_0^{\infty} \exp\left(ikr\cosh t\right) dt \tag{7.4}$$

Equation 7.4 clearly show an exponential relation between the Hankel function and the range. One can imagine that with increasing range the value of the Hankel function can increase rapidly, more or less exploding.

The problems that the Hankel function introduces, particularly with increasing range are well known. Tsouvalas (2015) did implement a measure that if the value of the Hankel function becomes too large, the Hankel function is estimated in order to maintain stability. However the response spectra have a highly oscillatory effect as was concluded in section 6.3.1. One of the possible solutions to overcome this issue is proposed by Stange and Friederich (1992). The suggestion is to apply a normalization with the modulus of the imaginary part of the argument to the Hankel function.

$$H_m(kr) \rightarrow \exp\left(|\Im m(kr)|\right) H_m(kr) \tag{7.5}$$

Concluding remarks

Although the absolute part of the pressure response spectra did not display the clear trend that was expected, it does provide a good insight in how the energy is distributed. It should be noted that although it was stated that it was possible to investigate the contribution of the underlined part in equation 7.2 by the absolute part of the pressure response output, the absolute part of the pressure response spectrum is not independent of range as it does include a part of the Hankel function. This explains the scattering effect between consecutive frequencies of the absolute response spectra and the fact that it is not range independent. The instability of the Hankel function is a well know problem and measures to ensure stability were made by Tsouvalas (2015), nonetheless the instability was clearly detected in the response spectra in section 6.3.1. A possible solution was suggested by Stange and Friederich (1992) to normalize the imaginary part of the argument of the Hankel function.

It is unfortunate that it wasn't possible to illustrate that the part of the solution that is independent of range, could be easily predicted and resolution could be added with the initial approach. This is possible as this part of the solution is independent of range and the input force exist of a smooth time trace and an accompanying smooth frequency domain representation. The Hankel function is dependent on range and causes the issues that were experienced applying the proposed interpolation. To further improve the model, the two parts of the solution could be separated within the model and the proposed method could be applied to the part independent of range. This would lead to only the Hankel function requiring exact calculations, further reducing the computational time of the model.

8

Conclusion and Recommendations

This graduation thesis aimed to investigate the possibility to use the Elastic Medium Model of Tsouvalas and Metrikine for accurate noise predictions in the far-field. The original model had some mathematical and computational constraints that made it unable to exactly calculate the noise levels at locations far from the pile. The maximum distance within which the model provided time traces of the various physical quantities was about 150 meters, although this value depends on the soil properties and the location of interest. This resulted in the following research question and subquestions:

"What has to be done to increase the range for which the Elastic Medium Model can predict accurate time traces of the various physical quantities?"

1. What introduces the time window limitation of the original model?
2. How can the limitation be overcome?
3. What are the main phenomena contributing to the sound levels at large distances?

To answer the main and the subquestions above, two different methods were implied to be able to predict sound levels at arbitrary range from the pile. First, a interpolation scheme was applied to the response spectra, calculated by the model, to increase the resolution of the spectra. The increase of the response spectra would lead to longer time traces and therefore enable predictions at locations further from the pile. Alternatively, the resolution was increased by selecting frequencies for which the Elastic Medium Model had to calculate the results and running the model multiple times, adding the results at the end, to create a large data set with high resolution. The model was validated by comparing the calculated sound levels with the data from the Veja Mate project and a parametric study was performed to provide more insight in the output and sensitivity of the model. The conclusions resulting from this research project are discussed and recommendations for further studies are listed in sections 8.1 and 8.2.

8.1. Conclusions

In chapter 3, the uniqueness of the studied phenomenon is highlighted. In contrary to a widespread belief among marine acousticians that the inclusion of the shear rigidity of the seabed is of secondary importance in underwater acoustics, the fact that the shear rigidity is equally important in noise predictions related to marine piling was discussed. Even though fluid approximations of the seabed are commonly favored in computational acoustics and are generally less computationally heavy, in the case of pile driving, more sophisticated models are required. The Elastic Medium Model approximates the seabed as a visco-elastic layer in order to support both compressional and shear waves. Additionally, this allows the Scholte wave to develop and travel along the water-soil interface. These propagate with a

velocity slightly lower than that of the shear waves in the soil medium and experience much less attenuation in comparison to other propagating modes. Concluding that the secondary noise path (re-radiating or leaking from the seabed into the fluid layer) can have a significant contribution to the total noise level production and that the correct modeling of the seabed as a visco-elastic medium is of great importance.

In chapter 5, the first approach was introduced. The application of the Discrete Fourier Transform (DFT) in the original setup of the Elastic Medium Model imposes restrictions to a predefined frequency range and corresponding time duration. Due to the low frequency waves propagating through the soil with a low wave speed, the maximum distance of the propagating waves is limited and therefore the predictable range is also restricted, as these low frequency waves can contribute considerable mentioned above. Therefore, it was suggested to increase the resolution of the frequency spectra by linear interpolation and the same relation between frequency range and time duration would lead to an increase of the time window and consequently the predictable range. This approach was validated with the force diagram and its frequency representation. Using this method led to the following discoveries. The frequency range that the model was calculating included a high amount of frequencies that did not carry any energy, wasting valuable computational effort. Secondly, the result from the suggested approach was able to extend the time window for locations close to the pile, however no value was added as the pressure waves had all passed and only zero-values were added to the time trace. For points located at larger distances, the approach did not work. The resolution increase did not change the time traces and was unable to correct for errors even in the time traces of the locations close to the pile (time traces not starting at 0 for example). It became clear that the suggested approach had its limitations and that higher resolution is needed to accurately describe the time trace responses. This higher resolution can not be created by linear interpolation as the approach suggested.

The alternative approach was discussed in chapter 6, this method solves the lack of resolution in the frequency domain by altering the input of the force diagram in the time domain to the frequency representation of the force in the frequency domain. It is important that the resolution of the frequency spectra of the force is high to make it possible to select the frequencies that the model will calculate. Additionally, to reach response spectra with a very small frequency step and a frequency range that included all contributing frequencies, the model had to run multiple times in bins and all the results of the separate runs had to be combined to create complete data sets. The high resolution spectra drastically improved the time traces for all points.

When overlaying the time traces of the pressure for points increasing in range a interesting phenomenon was identified. The primary pressure wave decayed with increasing range but a secondary pressure wave increased and even became the main pressure wave, showing higher pressures than the primary pressure wave for the same location. This secondary pressure wave is the result of waves traveling through the soil and being re-radiated into the fluid layer. Additionally, a third pressure wave becomes visible from 500 meters and onwards, however this does not manage to develop like the secondary one. The parametric study showed that these wavefronts originate from the soil. However they are actually a result of waves reflecting from the rigid boundary. It is remarkable that these waves have such a large contribution to the pressure in the fluid region. Until now, the physical meaning of these reflections is still up for discussion as the simulations of the model have not yet shown that reflections can be present between two different soil layers. The rigid boundary in the model is not physically present in real life, nonetheless, layers with different densities and orientation are and it could be possible that waves reflect from the interfaces between such layers or from rocks and cause these waves to re-radiate into the water region. Additionally, if the rigid boundary causes unphysical phenomena, the boundary conditions at its depth may have to be redetermined, this could add the potential of absorbing the waves instead of reflecting them for instance.

It was hard to identify the Scholte wave from the pressure time trace and therefore the vertical displacement of the soil at the water-soil interface was studied. For a location of 200 meters from the pile the Scholte wave was definitely present and easily identified. Increasing in range and looking at 300 meters from the pile, it became less obvious if and where the Scholte wave was present. It no longer stood out and had the same magnitude as the rest of the vibrations. When looking at the time traces for points even further from the pile the Scholte wave seemed to loose its contribution to the overall vibrations and at 500 meters from the pile it became impossible to identify the Scholte wave. This led to the conclusion that the Scholte is attenuated for locations of 500 meters or more. However, the parametric study showed that the Scholte wave is able to reach these distances. It could clearly be identified when looking at the vertical displacement at the seabed. Nevertheless, the pressure time trace at large distances was uninfluenced by it and therefore so were the sound levels. Knowing that the soil and its properties are one of the large unknowns in this kind of noise propagation simulations and the fact that this study has only covered a few case studies, further investigation should be done into the properties of the soil and their effect on the Scholte wave, pressure signal and finally the sound levels.

The sound levels predicted by the model and measured at the Veja Mate wind park when installing the foundation pile, were compared and it was determined which pressure waves contribute most to the sound levels. The sound levels decayed with increasing range and this decay can be estimated by a logarithmic function. Comparing the model predictions with the measurements led to the conclusion that the sound exposure level (SEL) was underestimated by 2.5 dB re 1 $\mu Pa^2 s$ and the peak level was underestimated by approximately 6 dB 1 re μPa. Although this seemed like quite a large difference, it should be noted that this is based on only one calculation. A calibration of the soil could lead to better estimates regarding the peak level. A further analysis of the time trace at the 750 meters location resulted in the conclusion that the Scholte wave does not have influence on the sound levels as there is no pressure wave visible around the time it would arrive, nevertheless the influence of the soil remains the large unknown and further study into its sensitivity should be done. By scaling the impact force, its sensitivity on the peak level was examined. The result was that in order to match the model prediction with the measured value of the peak level, the force would have to be scaled with a factor 2. This is very large and cannot possible be correct. This would result in an input force that is far larger than the one used during the Veja Mate project. Additionally, when doing so, the sound exposure level is overestimated considerably. It is unrealistic that the input force has to be increased so significantly, however the impact diagram that is used, is rather smooth and idealized. In reality the impact diagram of the force can be much coarser, which would excite other frequencies, namely higher ones. These higher frequencies can contribute to the primary pressure wave and as a result enlarge the sound peak level. Instead of using the idealized impact diagram, it would be worth looking into using a measurement of an impact hammer applying the force.

The discussion at the end of chapter 7, argued that the resolution of the response spectrum had to increase with range to accurately describe the time traces. This range dependency was not anticipated. It was expected that the resolution had to increase and that with higher resolution the output would quickly improve. When the resolution was increased to a frequency step size of $0.25 Hz$, the time traces became significantly better. It was not anticipated that even higher resolution would be needed to arrive at a trend for the response spectra like the trend that was seen at short range locations. However there still is a spacial factor that introduces scattering of the data of the response spectra with increasing range. This is the Hankel function and evaluating its definition, it became clear that it has a clear range dependency. The Hankel function actually scales to the range exponentially. This clearly explains the scattering effect that the Hankel function introduces, as one can imagine the Hankel function increasing rapidly with growing range, more or less exploding. The instability of the Hankel function is a well know problem and measures to ensure stability were made by Tsouvalas (2015), nonetheless the instability was clearly detected in the response spectra. A possible solution was suggested by Stange and Friederich (1992) to normalize

the imaginary part of the argument of the Hankel function. Additionally, it was unfortunate that it wasn't possible to illustrate that the part of the solution that is independent of range, could be easily predicted and resolution could be added with the initial approach. This is possible as this part of the solution is independent of range and the input force exist of a smooth time trace and an accompanying smooth frequency domain representation. The Hankel function is dependent on range and causes the issues that were experienced when applying the proposed interpolation method. To further improve the model, the two parts of the solution could be separated within the model and the proposed method could be applied to the part independent of range. This would lead to only the Hankel function requiring exact calculations, further reducing the computational time of the model.

8.1.1. Concluding remarks

The aim of this graduation research was to investigate what could lead to an increase of the range for which the Elastic Medium Model could perform accurate predictions. This has been achieved by investigating the limitations of the original model and identifying what caused these. Once the limitations of the discrete fourier transform were identified an alternative method was suggested and applied. This existed of a linear interpolation scheme to increase resolution in the frequency domain. This higher resolution would lead to an increase of the time window and therefore the range the model would be able to perform predictions. However the highly oscillatory effect of the Hankel function made this linear interpolation incorrect. To overcome this issue a different approach was utilized that made smart use of the existing Elastic Medium Model. This made it possible to select the frequencies the model calculated and by running the model multiple time, a large dataset could be created with high resolution. This resulted in acoustic modelling of up to 4 seconds with a reasonable computational time of about 36 hours.

8.2. Recommendations

"To measure is to know. If you can not measure it, you can not improve it."
Lord Kelvin

The quote above illustrates that for accurate noise predictions from acoustic models, measurements are needed to validate the models. Currently, these real life measurements are lacking and for the acoustic models to improve more data has to be generated. Fortunately, there are initiatives like the COMPILE workshop organized by TUHH Hamburg University and participating with these kind of initiatives, to generate a bench mark for models predicting underwater sound generated by offshore piling, is very important.

Further study into the sensitivity of the soil layers and their impact on various physical quantities as the pressure, velocity, displacement and sound levels is highly recommended. The influence of the soil and its parameters remain a couple of the largest unknowns in this kind of acoustic modelling. The soils properties are spatially variable, both in depth and in range, and are therefore hard to approximate with a single or a small number of layers.

The absence of the possibility to incorporate a range of noise mitigation systems into the model, limits the available data that can be used to validate the model. Therefore, an option to implement these into the model, would lead to lots of extra data becoming available for the validation of the model. Additionally, it would be very valuable to see what the effect of various noise mitigations would have during the installation of a large monopile. This would allow for correct selection of noise mitigation systems prior to installation.

The Elastic Medium Model is a valuable tool for predicting underwater piling noise. It can provide insight in the various physical phenomena that take place during the installation process of a monopile. Current study showed that the secondary noise path (waves re-radiating from the soil) contributes little to the overall sound levels. The Scholte wave can travel up to large distances but will not have a significant effect on the sound levels at large distances. Although the fluid approximation of the seabed is known to underestimate the sound levels, modeling the seabed as an elastic medium did not show higher noise levels. It should be noted that the sound levels were calculated with only a few case studies and that the modeling of the case study requires more elaborate calibration.

Bibliography

Milton Abramowitz et al. Handbook of mathematical functions with formulas, graphs, and mathematical tables. 2015.

Allnamics. Geotechnical and pile testing experts, 2017. URL http://allnamics.eu/.

Helen Bailey, Bridget Senior, Dave Simmons, Jan Rusin, Gordon Picken, and Paul M Thompson. Assessing underwater noise levels during pile-driving at an offshore windfarm and its potential effects on marine mammals. *Marine Pollution Bulletin*, 60(6):888–897, 2010.

Mehmet Bilgili, Abdulkadir Yasar, and Erdogan Simsek. Offshore wind power development in europe and its comparison with onshore counterpart. *Renewable and Sustainable Energy Reviews*, 15(2):905–915, 2011.

Michael J Buckingham. Compressional and shear wave properties of marine sediments: Comparisons between theory and data. *The Journal of the Acoustical Society of America*, 117(1):137–152, 2005.

BW Byrne and GT Houlsby. Foundations for offshore wind turbines. *Philosophical Transactions of the Royal Society of London A: Mathematical, Physical and Engineering Sciences*, 361(1813):2909–2930, 2003.

Hans-Peter Damian and Thomas Merck. Cumulative impacts of offshore windfarms. In *Ecological Research at the Offshore Windfarm alpha ventus*, pages 193–198. Springer, 2014.

EIA. International energy outlook 2017. Technical report, U.S. Energy Information Administration, 2017.

Engineering and Physical Sciences Research Council. Screw piles for wind energy foundation systems, 2018. URL https://www.screwpilesforoffshorewind.co.uk/.

Erneuerbare Energien. Eew group produces pipes for beatrice wind farm, 2016. URL https://www.erneuerbareenergien.de.

Fistuca. Blue piling technology, 2016. URL https://fistuca.com/.

Richard G Fizell. Application of high-resolution processing to range and depth estimation using ambiguity function methods. *The Journal of the Acoustical Society of America*, 82(2): 606–613, 1987.

GMBWorks. Gbm works. a new method to silently install monopile foundations offshore, 2018. URL http://www.gbmworks.com/.

George G Goble and Frank Rausche. *Wave equation analysis of pile driving: WEAP program*, volume 1. US Department of Transportation, Federal Highway Administration, Offices of Research and Development, 1976.

GWEC. Global wind 2016 report: Annual market update. *Global Wind Energy Council (GWEC), Brussels, Belgium*, 2017.

Yasser A Hegazy and Paul W Mayne. A global statistical correlation between shear wave velocity and cone penetration data. In *Site and Geomaterial Characterization*, pages 243–248. 2006.

ICE. International construction equipment, 2018. URL http://www.ice-holland.com/.

IEA. World energy outlook 2017. Technical report, International Energy Agency, 2017.

Finn B Jensen, William A Kuperman, Michael B Porter, and Henrik Schmidt. *Computational ocean acoustics*. Springer Science & Business Media, 2011.

Stephan Lippert, Tristan Lippert, Kristof Heitmann, and Otto Von Estorff. Prediction of underwater noise and far field propagation due to pile driving for offshore wind farms. In *Proceedings of Meetings on Acoustics ICA2013*, volume 19, page 070036. ASA, 2013.

Tristan Lippert and Stephan Lippert. Modelling of pile driving noise by means of wavenumber integration. *Acoustics Australia*, 40(3), 2012.

Georg Nehls, Klaus Betke, Stefan Eckelmann, and Martin Ros. Assessment and costs of potential engineering solutions for the mitigation of the impacts of underwater noise arising from the construction of offshore windfarms. *BioConsult SH report, Husum, Germany. On behalf of COWRIE Ltd*, 2007.

Shelby L Peterie, Richard D Miller, and Julian Ivanov. Seismology and its applications in kansas.". 2014.

Per G Reinhall and Peter H Dahl. Underwater mach wave radiation from impact pile driving: Theory and observation. *The Journal of the Acoustical Society of America*, 130(3):1209–1216, 2011.

SW Rienstra and A Hirschberg. An introduction to acoustics. 2017.

SP Robinson, PA Lepper, and RA Hazelwood. Good practice guide for underwater noise measurement. *NPL Good Practice Guide*, (133), 2014.

RoyalHaskoningDHV. Underwater noise. social cost benefit analysis. Technical report, Rijskwaterstaat, 2015.

Zohaib Saleem. Alternatives and modifications of monopile foundation or its installation technique for noise mitigation. *Report by Delft University of Technology for Stichting De Noordzee (the North Sea Foundation)*, 2011.

Stefan Stange and Wolfgang Friederich. Guided wave propagation across sharp lateral heterogeneities: the complete wavefield at a cylindrical inclusion. *Geophysical Journal International*, 111(3):470–482, 1992.

Frank Thomsen, Karin Lüdemann, Rudolf Kafemann, and Werner Piper. Effects of offshore wind farm noise on marine mammals and fish. *Biola, Hamburg, Germany on behalf of COWRIE Ltd*, 62, 2006.

A Tsouvalas and AV Metrikine. A three-dimensional vibroacoustic model for the prediction of underwater noise from offshore pile driving. *Journal of Sound and Vibration*, 333(8): 2283–2311, 2014.

Apostolos Tsouvalas. *Underwater noise generated by offshore pile driving*. PhD thesis, Ph. D. Thesis, Delft University of Technology, Delft, The Netherlands, 2015.

JW Van Rhijn. Reduction of underwater piling noise: An optimization of the impact force to reduce underwater noise during the installation of a large sized monopole. 2017.

WindEurope. Wind in power: 2017 european statistics. *Wind Europe: Brussels, Belgium*, 2018a.

WindEurope. The european offshore wind industry — key trends and statistics 2017. *Wind Europe: Brussels, Belgium*, page 37, 2018b.

Mario Zampolli, Marten JJ Nijhof, Christ AF de Jong, Michael A Ainslie, Erwin HW Jansen, and Benoit AJ Quesson. Validation of finite element computations for the quantitative prediction of underwater noise from impact pile driving. *The Journal of the Acoustical Society of America*, 133(1):72–81, 2013.